

**LIQUID PHASE HYDROGENATION OF CITRAL  
ON ZEOLITE SUPPORTED MONOMETALLIC (Ni,  
Pt) AND BIMETALLIC (Ni-Sn, Pt-Sn) CATALYSTS**

**A Thesis Submitted to  
the Graduate School of Engineering and Science of  
İzmir Institute of Technology  
in Partial Fulfillment of the Requirements for the Degree of**

**MASTER OF SCIENCE**

**in Chemical Engineering**

**by  
Hilal GÜLEÇ**

**August 2005  
İZMİR**

We approve the thesis of **Hilal GÜLEÇ**

**Date of Signature**

.....  
**2005**  
**Assoc. Prof. Dr. Selahattin YILMAZ**  
Supervisor  
Department of Chemical Engineering  
İzmir Institute of Technology

**10 August**

.....  
**2005**  
**Prof. Dr. Levent ARTOK**  
Co-Supervisor  
Department of Chemistry  
İzmir Institute of Technology

**10 August**

.....  
**2005**  
**Prof. Dr. Devrim BALKÖSE**  
Department of Chemical Engineering  
İzmir Institute of Technology

**10 August**

.....  
**2005**  
**Prof. Dr. Gönül GÜNDÜZ**  
Department of Chemical Engineering  
Ege University

**10 August**

.....  
**2005**  
**Asst. Prof. Dr. Fehime ÖZKAN**  
Department of Chemical Engineering  
İzmir Institute of Technology

**10 August**

.....  
**2005**  
**Prof. Dr. Devrim BALKÖSE**  
Head of Department  
İzmir Institute of Technology

**10 August**

.....  
**Assoc. Prof. Dr. Semahat ÖZDEMİR**  
Head of the Graduate School

## ACKNOWLEDGEMENTS

I would like to express my sincere gratitude to my advisors Assoc. Prof. Selahattin Yılmaz and Prof. Levent Artok for their supervision, support, and confidence during my studies. I would like to thank to Prof. Devrim Balköse for her help and encouragement. And special thanks to Prof. Gönül Gündüz for her valuable recommendations, endless support and encouragement through my hardest times.

I also would like to thank to Research Specialists Nesrin Tatlıdil, Özlem Çağlar, Nesrin Gaffaroğulları, Filiz Özmihçı, Evrim Yakut and Gökhan Erdoğan for the characterization studies presented in this study. I would like to thank the technical staff, Şerife Şahin, Burcu Alp, Belgin Tunçel and Tülin Burhanoğlu for their friendship and help during the laboratory works.

I am also grateful to my special friends Öniz Birsoy, Aslı and Özge Can, Işıl Tezel, Senem Yetgin for their friendship, understanding, help and supports.

My special thanks go to my family for their endless support, tolerance and understanding. And finally, to Özgür for his love and patience.

## ABSTRACT

In this study the liquid phase citral hydrogenation reaction over zeolite supported monometallic and bimetallic Ni and Pt catalysts was studied. The zeolite support materials were Na-Y, Na- $\beta$ , Na-Mordenite, MCM-41, and Clinoptilolite. The catalysts were prepared by impregnation and co-impregnation techniques. Catalytic activity and selectivity tests were performed in a semi-batch reactor at 80°C temperature, 6 bar pressure and 600 rpm stirring speed with 0.25 g catalyst.

The characterization studies showed that the structures of support materials were preserved during impregnation and co-impregnation. The Ni and Pt contents of the catalysts was around 8.5 % and 5 %, respectively while the Sn content changed between 0.46 and 4.10 %.

The activity of the catalysts and product distribution were affected by type of active metal and type of support. The major product over monometallic and bimetallic catalysts was citronellal. The Ni/Na-Y catalyst gave the maximum yield of desired products, unsaturated alcohols and citronellal, (93 %) and citral conversion (>99 %) among the monometallic catalysts. The most selective monometallic Pt catalyst to desired products was Pt /MCM-41 with a yield of 40 %.

Addition of Sn increased the unsaturated alcohol formation and decreased the acetal formation. The activity of the Ni catalyst was generally decreased while the activity of the Pt catalyst was improved.

The amount of unsaturated alcohols increased with Sn/Sn+Ni ratio for bimetallic Ni catalysts. The highest yield of desired products was obtained with Ni/Na-Y (93 %) and with Ni-Sn/MCM (80 %) among monometallic and bimetallic catalysts.

## ÖZET

Bu projede zeolit destekli monometalik ve bimetalik Ni ve Pt katalizörler üzerinde sıvı fazda sitral hidrojenasyonu çalışılmıştır. Kullanılan destek malzemeleri Na-Y, Na- $\beta$ , Na-Mordenit, MCM-41 ve Klinoptilolittir. İmpregnasyon (emdirme) ve ko-impregnasyon teknikleriyle hazırlanan 0.25'er g'lık katalizörler, yarı kesikli, karıştırmalı reaktörde 80°C sıcaklık, 6 bar basınç, 600 rpm karıştırma hızıyla sitral hidrojenasyonu reaksiyonunda test edilmiştir.

Karakterizasyon çalışmaları destek malzemelerinin yapılarının metal yükleme işlemleri sırasında bozulmadığını göstermiştir. Katalizörlerin Ni ve Pt miktarlarının sırasıyla % 8.5 ve % 5 olduğu bulunmuştur. Sn miktarı ise % 0.46 ve 4.10 arasında değişmektedir.

Katalizörlerin aktifliği ve ürün dağılımı aktif metal ve destek malzemesine göre değişiklik göstermiştir. Monometalik ve bimetalik katalizörlerle elde edilen ana ürün sitronellaldir. Doymamış alkollere ve sitronellale en yüksek verimi (% 93) ve en yüksek sitral dönüşümünü (>% 99) Ni/Na-Y katalizörü sağlamıştır. En seçici monometalik Pt katalizör ise % 40 verim ile Pt/MCM-41 katalizörüdür.

Katalizörlere Sn eklenmesi, doymamış alkol oluşumunu arttırırken asetal oluşumunu azaltmıştır. Ni katalizörlerin aktivitesi genellikle azalırken Pt katalizörlerin aktifliği artmıştır.

Bimetalik Ni katalizörlerde doymamış alkollerin miktarı Sn/Sn+Ni oranı ile doğru orantılı olarak artmıştır. Değerli ürünlere en yüksek verimi sağlayan monometalik katalizör Ni/Na-Y (% 93) iken bimetalik katalizör % 80 verim ile Ni-Sn/MCM-41 katalizörü olmuştur.

# TABLE OF CONTENTS

LIST OF FIGURES .....	viii
LIST OF TABLES .....	xii
CHAPTER 1. INTRODUCTION.....	1
CHAPTER 2. CITRAL HYDROGENATION .....	3
2.1. Hydrogenation of Aldehydes .....	3
2.2. Citral Hydrogenation Mechanism.....	5
2.3. Previous Studies on Citral Hydrogenation.....	6
2.3.1. Homogeneous Catalysis .....	6
2.3.2. Heterogeneous Catalysis .....	7
2.3.2.1. Citral Hydrogenation over Monometallic Catalysts .....	7
2.3.2.2. Citral Hydrogenation over Bimetallic Catalysts .....	11
CHAPTER 3. CATALYSTS .....	15
3.1. Heterogeneous Catalysts.....	15
3.1.1. Active Component .....	15
3.1.2. Support.....	15
3.1.3. Promoter.....	16
3.2. Zeolites.....	16
3.2.1. Composition and Structure .....	17
3.2.2. Zeolite Y .....	19
3.2.3. Zeolite Beta.....	20
3.2.4. Mordenite.....	20
3.2.5. Clinoptilolite .....	22
3.2.2. MCM-41 .....	23
3.3. Catalyst Preparation Methods.....	24
3.3.1. Impregnation .....	24
3.3.2. Incipient Wetness.....	25
3.3.3. Ion Exchange .....	25
CHAPTER 4. EXPERIMENTAL STUDY .....	26
4.1. Materials .....	26
4.2. Methods .....	27
4.2.1. Catalyst Preparation .....	27
4.2.1.1. Preparation of Supports .....	27
4.2.1.2. Preparation of Monometallic Catalysts.....	28
4.2.1.3. Preparation of Bimetallic Catalysts .....	28
4.2.2. Catalyst Characterization.....	29
4.2.3. Catalyst Testing .....	30
CHAPTER 5. RESULTS AND DISCUSSIONS .....	32
5.1. Catalyst Characterization.....	32
5.1.1. Na-Y Zeolite .....	32
5.1.2. Na- $\beta$ Zeolite .....	37

5.1.3. Na-Mordenite Zeolite .....	41
5.1.4. MCM-41 Zeolite .....	46
5.1.5. Clinoptilolite .....	50
5.2. Catalyst Testing .....	54
5.2.1. Ni/Na-Y & Ni-Sn/Na-Y Catalysts .....	55
5.2.2. Ni/Na- $\beta$ & Ni-Sn/Na- $\beta$ Catalysts.....	61
5.2.3. Ni/Mordenite & Ni-Sn/Na-Mordenite Catalysts.....	64
5.2.4. Ni/MCM-41 & Ni-Sn/MCM-41 Catalysts.....	70
5.2.5. Ni/Clinoptilolite & Ni-Sn/Clinoptilolite Catalysts .....	73
5.2.6. Pt/Na-Y & Pt-Sn/Na-Y Catalysts .....	75
5.2.7. Pt/MCM-41 & Pt-Sn/MCM-41 Catalysts .....	78
5.2.8. Pt/Clinoptilolite & Pt-Sn/Clinoptilolite Catalysts.....	80
5.2.9. Comparison of Different Supports.....	83
5.2.10. Comparison of Active Metals .....	85
5.2.11. Comparison of Bimetallic Catalysts .....	87
CHAPTER 6. CONCLUSIONS .....	90
REFERENCES .....	92
APPENDIX A. GC-MS Chromatograms of Products.....	95

## LIST OF FIGURES

<u>Figure</u>		<u>Page</u>
Figure 2.1.	Reaction pathways for the hydrogenation of $\alpha$ - $\beta$ unsaturated aldehydes	4
Figure 2.2.	A reaction schema for the hydrogenation of citral .....	5
Figure 3.1.	Primary building blocks of zeolites .....	17
Figure 3.2.	Secondary building units .....	18
Figure 3.3.	Framework structure of zeolite Y .....	19
Figure 3.4.	Tetrahedral framework structure of mordenite with unit-cell outlines ...	21
Figure 3.5.	(a) Orientation of clinoptilolite channel axes (b) Model framework for the structure of clinoptilolite .....	22
Figure 3.6.	Proposed structures of MCM-41 .....	23
Figure 4.1.	Simplified Schematic Representation of Experimental Set-up .....	31
Figure 5.1.	SEM micrographs of Na-Y support (a) and Ni/Na-Y (b) catalyst .....	34
Figure 5.2.	XRD spectra of Na-Y support, monometallic and bimetallic Ni catalysts .....	35
Figure 5.3.	XRD spectra of monometallic and bimetallic Pt catalysts .....	36
Figure 5.4.	N <sub>2</sub> adsorption isotherms of Na-Y and Ni/Na-Y catalyst.....	36
Figure 5.5.	SEM micrographs of Na- $\beta$ support (a) and Ni/ Na- $\beta$ catalyst (b) .....	39

Figure 5.6	XRD diagram of Na- $\beta$ supported monometallic and bimetallic Ni catalysts .....	40
Figure 5.7.	N <sub>2</sub> adsorption isotherms of Na- $\beta$ and Ni/Na- $\beta$ and Ni-Sn/Na- $\beta$ catalysts	40
Figure 5.8.	SEM micrographs of Na-Mordenite support (a) and Ni/Na-Mordenite catalyst (b) .....	43
Figure 5.9.	XRD diagram of Na-Mordenite supported monometallic and bimetallic Ni catalysts .....	44
Figure 5.10.	N <sub>2</sub> adsorption isotherms of Na-Mordenite and Ni-Sn/Na-Mordenite(0.2) catalysts.....	45
Figure 5.11.	SEM picture of synthesized MCM-41 .....	47
Figure 5.12.	XRD diagram of synthesized MCM-41 .....	47
Figure 5.13.	XRD diagram of MCM-41 Supported Pt catalysts .....	48
Figure 5.14.	N <sub>2</sub> adsorption isotherms of MCM-41, Ni/MCM-41 and Ni-Sn/MCM-41(0.033) catalysts.....	49
Figure 5.15.	SEM micrographs of clinoptilolite support .....	51
Figure 5.16.	XRD spectra of clinoptilolite support, monometallic and bimetallic Ni and Pt catalysts .....	52
Figure 5.17.	N <sub>2</sub> adsorption isotherms of Clinoptilolite, Ni/ Clinoptilolite and Ni-Sn/ Clinoptilolite (0.2) catalysts.....	53
Figure 5.18.	GC chromatogram of citral hydrogenation products.....	55
Figure 5.19.	Product distribution of citral over Ni/Na-Y catalyst.....	56
Figure 5.20.	Product distribution of citral over Ni-Sn/Na-Y (0.02) (a), Ni-Sn/Na-Y (0.05) (b) and Ni-Sn/Na-Y (0.1) (c).and Ni-Sn/Na-Y(0. 2) (d) .....	59
Figure 5.21.	Change of acetal formation with respect to reaction time over Ni-Sn/Na-Y(0.05) catalyst. ....	60

Figure 5.22.	Selectivity to unsaturated alcohols as a function of Sn/Sn+Ni ratio .....	61
Figure 5.23.	Product distribution of citral hydrogenation over monometallic Ni/Na- $\beta$ catalyst .....	62
Figure 5.24.	Product distribution of citral hydrogenation over bimetallic Ni-Sn/Na- $\beta$ (0.2) catalyst .....	63
Figure 5.25	Change of acetal formation with respect to reaction time over Ni-Sn/Na- $\beta$ (0.2) catalyst. ....	63
Figure 5.26.	Product distribution of citral hydrogenation over monometallic Ni/Mordenite catalyst .....	65
Figure 5.27.	Product distribution of citral hydrogenation reaction over Ni-Sn/Mordenite (0.02) (a), Ni-Sn/Mordenite (0.06) (b) Ni-Sn/Mordenite. ....	67
Figure 5.28	Change of acetal formation with respect to reaction time over Ni-Sn/Na-Mordenite catalyst.....	68
Figure 5.29	Selectivity to unsaturated alcohols as a function of Sn/Sn+Ni ratio .....	69
Figure 5.30	Product distribution of citral hydrogenation over monometallic Ni/MCM-41 catalyst .....	70
Figure 5.31	Product distribution of citral hydrogenation over bimetallic Ni-Sn/MCM-41(0.033) (a) and Ni-Sn/ MCM-41(0.042) (b) .....	71
Figure 5.32	Change of acetal formation with respect to reaction time over Ni-Sn/MCM-41 catalyst.....	72
Figure 5.33	Product distribution of citral hydrogenation over monometallic Ni/Clinoptilolite catalyst .....	74
Figure 5.34	Product distribution of citral hydrogenation over bimetallic Ni-Sn/Clinoptilolite(0.2) catalyst .....	75
Figure 5.35	Product distribution of citral hydrogenation over monometallic Pt/Na-Y catalyst .....	76
Figure 5.36	Product distribution of citral hydrogenation over bimetallic Pt-Sn/NaY(0.02) catalyst .....	77
Figure 5.37	Product distribution of citral hydrogenation over Pt/MCM-41 catalyst .....	78

Figure 5.38	Product distribution of citral hydrogenation over Pt-Sn/MCM-41(0.02) catalyst .....	79
Figure 5.39	Product distribution of citral hydrogenation over Pt/Clinoptilolite catalyst.....	80
Figure 5.40	Product distribution of citral hydrogenation over Pt-Sn/Clinoptilolite(0.02) catalyst.....	81
Figure 5.41	Change of acetal formation with respect to reaction time over Ni-Sn/Na-Y(0.02) catalyst.....	82
Figure 5.42	Conversion and Yield vs. Time for zeolite supported Ni catalysts.....	84
Figure 5.43	Conversion and Yield vs. Time for zeolite supported Pt catalysts.....	84
Figure 5.44	Conversion and Yield vs. Time for Na-Y (a), MCM-41 (b) and Clinoptilolite (c) supported Pt and Ni catalysts.....	86
Figure 5.45	Conversion and Yield vs. Time for Na-Y (a) and MCM-41 (b) supported Pt-Sn and Ni-Sn bimetallic catalysts.....	88
Figure A. 1	GC-MS chromatogram(a) and spectrum(b) of citronellal.....	95
Figure A.2	GC-MS chromatogram(a) and spectrum(b) of citronellol.....	96
Figure A.3	GC-MS spectrum (a) and chromatogram (b) of geraniol.....	97
Figure A.4	GC-MS chromatogram (a) and spectrum (b) of nerol.....	98
Figure A.5	GC-MS chromatogram (a) and spectrum (b) of isopulegol.....	99
Figure A.6	GC-MS chromatogram (a) and spectrum (b) of 3,7 Dimethyl-1-octanol.....	100
Figure A.7	GC-MS spectrum (a) and chromatogram (b) of menthol.....	101
Figure A.8	GC-MS spectrum (a) and chromatograms (b), (c), (d) of citral.....	103

## LIST OF TABLES

<b><u>Table</u></b>		<b><u>Page</u></b>
Table 4.1.	Properties of chemicals used in experiments .....	26
Table 4.2.	Properties of supports used in experiments .....	27
Table 5.1.	Chemical compositions of Na-Y zeolite.....	32
Table 5.2.	Metal contents of Na-Y supported catalysts .....	33
Table 5.3.	Physico-chemical properties of Na-Y and Ni/Na-Y catalysts.....	37
Table 5.4.	Chemical compositions of Na- $\beta$ zeolite .....	38
Table 5.5.	Metal contents of Na- $\beta$ supported catalysts.....	38
Table 5.6.	Physico-chemical properties of Na- $\beta$ and Na- $\beta$ supported catalysts....	41
Table 5.7.	Chemical compositions of Na-Mordenite zeolite .....	41
Table 5.8.	Metal contents of Na-Mordenite supported catalysts .....	42
Table 5.9.	Physico-chemical properties of Na-Mordenite and Na-Mordenite supported catalysts.....	45
Table 5.10.	Chemical compositions of MCM-41 zeolite .....	46
Table 5.11.	Metal contents of MCM-41 supported catalysts .....	46
Table 5.12.	Physico-chemical properties of MCM-41, Ni/MCM-41, Ni-Sn/MCM 41(0.033) catalysts.....	49

Table 5.13.	Chemical compositions of clinoptilolite.....	50
Table 5.14.	Metal contents of clinoptilolite supported catalysts .....	50
Table 5.15.	Physico-chemical properties of Clinoptilolite, Ni/Clinoptilolite, Ni-Sn/Clinoptilolite, Pt/Clinoptilolite catalysts.....	53
Table 5.16.	Conversion, selectivity and yield values with Ni/Na-Y and Ni-Sn/Na-Y catalysts (t=300 min.) .....	60
Table 5.17.	Conversion, selectivity and yield values with different catalysts (t=300 min.) .....	64
Table 5.18.	Conversion, selectivity and yield values with Ni/MCM-41 and Ni-Sn/MCM-41 catalysts (t=300 min.) .....	69
Table 5.19.	Conversion, selectivity and yield values with Ni/MCM-41 and Ni-Sn/MCM-41 catalysts (t=300 min.) .....	73
Table 5.20.	Conversion, selectivity and yield values with Ni/Clinoptilolite and Ni-Sn/Clinoptilolite catalysts (t=300 min.) .....	75
Table 5.21.	Conversion, selectivity and yield values with Pt/Na-Y and Pt-Sn/Na-Y catalysts (t=300 min.) .....	77
Table 5.22.	Conversion, selectivity and yield values with different catalysts (t=300 min.) .....	80
Table 5.23.	Conversion, selectivity and yield values with Pt/Clinoptilolite and Pt-Sn/Clinoptilolite catalysts (t=300 min.) .....	82
Table 5.24.	Physico-chemical properties, citral conversion, product distribution and yield to desired products obtained all catalysts tested.....	89

# CHAPTER 1

## INTRODUCTION

In the organic synthesis of fine chemicals,  $\alpha$ - $\beta$  unsaturated alcohols are important intermediates in several industries, such as flavor, fragrance and pharmaceutical industry. However the selective hydrogenation of  $\alpha$ - $\beta$  unsaturated aldehydes is a difficult challenge since the C=C bond is much easily attacked than the C=O bond when a conventional heterogeneous catalysts used. Therefore, many efforts have been made to develop a suitable industrial catalyst that would be able to lead to the hydrogenation of C=O bond to get desired products.

Much works have been done to develop heterogeneous catalysts applicable to these reactions. The usage of these heterogeneous catalysts prevents the production of residues and waste obtained in homogeneously catalyzed systems. Besides, the difficulties associated with the separation and recycling homogeneous catalysts is eliminated by heterogeneous catalysts (Baeza et al. 2001).

In the catalyst selection there are several important issues, which can affect on the product selectivity. These are active metal, specific metal surface area, support material, catalyst preparation method, catalyst precursor, promoter (Arvela 2003). Suitable heterogeneous catalysts for the selective hydrogenation of  $\alpha$ - $\beta$  unsaturated aldehydes are mostly based on supported noble metals, Pt, Ru, Rh, Pd. The effectiveness of supported noble metals for the selective hydrogenation of the C=O bond can be enhanced by combining them with promoters (Sn, Ge, Fe) (Silva 2003).

Citral is a very attractive model molecule as unsaturated aldehydes both from scientific and industrial point of view. It has conjugated double bonds, an isolated double bond, furthermore there are possibilities for cis-trans isomerization and for several types of side reactions (cyclisation, acetalization, decarbonylation and dehydrogenation) (Arvela et al. 2003).

Catalysts having different supports have been prepared for citral hydrogenation (Section 2). Some of these supports are inert (e.g., SiO<sub>2</sub>, Al<sub>2</sub>O<sub>3</sub>) and some others show metal support interactions (e.g., Zeolite-Y and TiO<sub>2</sub>). Recently, there are many studies concerning the use of zeolites as catalyst support in many organic reactions. Zeolites are known for a variety of defined cage/channel structures and offer significant advantages

over conventional inorganic oxides, either for the stabilization of small metallic particles induced by geometrical constraints or for the fine control of acid properties by exchange of the balancing cations against protons (Recchia et al. 1999). In addition, shape selectivity, high surface area and high thermal stability of zeolites make them suitable materials to be catalysts or catalyst supports. However, zeolite supports are hardly tested in citral hydrogenation.

Thus, the use of Na-Y, Na-Beta, Mordenite, Clinoptilolite and MCM-41 zeolites were investigated in this study. Their pore size ranged from micropore to mesopore. They have different unit cells, morphologies and Si/Al ratio.

It was aimed to prepare catalysts that provided higher selectivity to unsaturated alcohols. For this, the activity and product distribution for different monometallic (Ni and Pt) and bimetallic (Ni-Sn and Pt-Sn) catalysts prepared by impregnation and co-impregnation methods were determined. An attempt was made to explain product distribution based on catalyst characterisation data.

## CHAPTER 2

### CITRAL HYDROGENATION

Hydrogenation is a chemical reaction between molecular hydrogen and an element or compound, ordinarily in the presence of a catalyst. The reaction may be one in which hydrogen simply adds to a double or triple bond connecting two atoms in the structure of the molecule or one in which the addition of hydrogen results in dissociation (breaking up) of the molecule (called hydrogenolysis, or destructive hydrogenation). Hydrogenation typically uses hydrogen gas as a reactant and a heterogeneous metal catalyst, such as nickel, palladium or platinum. Otherwise, the homogeneous rhodium-based catalyst known as Wilkinson's catalyst is often used. The reaction is usually carried out at elevated temperature and pressure. (Ponec 1997).

Hydrogenation reactions are widely used in chemical and petrochemical industry (removal of benzene from fuels, oils, etc.), the food processing industry (fat hardening), fine chemicals and pharmaceutical industries and in many laboratory-scale operations (Ponec 1997).

#### 2.1. Hydrogenation of Aldehydes

The selective hydrogenation of unsaturated carbonyl intermediates such as  $\alpha$ - $\beta$  unsaturated aldehydes to its unsaturated alcohol is a critical step in fine chemical manufacturing particularly in respect of fragrances, flavorings and the pharmaceutical industry (Baeza et al. 2001). Although the hydrogenation of unsaturated compounds is a reaction with important applications in industrial processes, it is very complex to be fulfilled. This hydrogenation is a consequence of different reaction pathways as it is given schematically in Figure 2.1 for an R-HC=CH-CHO aldehydes.

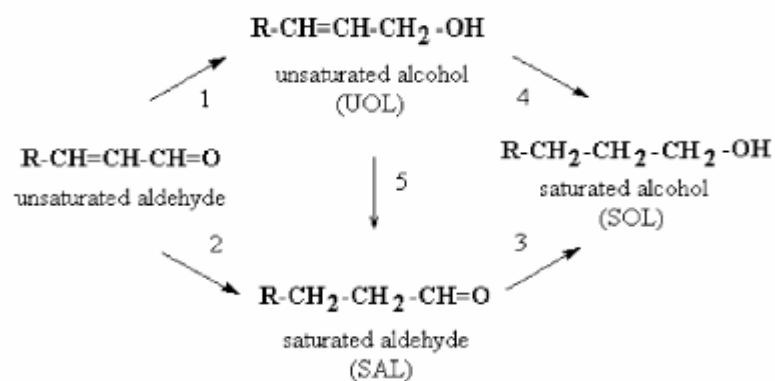


Figure 2.1. Reaction pathways for the hydrogenation of  $\alpha$ - $\beta$  unsaturated aldehydes.

(Source: Santori et al. 2002)

The double C=O bond can react giving an unsaturated alcohol UOL (1), the double C=C bond can be hydrogenated giving a saturated aldehyde SAL (2), and also the UOL-SAL isomerization can be produced (5). Finally, the subsequent SAL or UOL hydrogenation leads to the saturated alcohol SOL (3 and 4).

The most important product from the industrial point of view is, in most of the cases, the unsaturated alcohol (UOL), however this product is also the most difficult to be obtained. The reduction of C=C bond is thermodynamically favored in comparison with that of the C=O bond due to the fact that the bond energy of the C=C bond (615 kJ/mol) is much less than that of the C=O bond (715 kJ/mol) (Noller et al. 1984), which makes the C=C bond more reactive than C=O bond.

The hydrogenation of  $\alpha$ - $\beta$  unsaturated aldehydes has been extensively studied using different monometallic and bimetallic systems and also different supports. According to literature the nature of the metallic phase of the catalyst and also the support have an important influence on the activity and selectivity. Suitable heterogeneous catalysts for selective hydrogenation are generally supported noble metals such as Pt, Ru, Rh, and Pd. The activity can be modified and selectivity to unsaturated alcohols can be improved by combining the noble metals with promoters such as Sn, Ge, and Fe (Noller et al. 1984).



The hydrogenation products of citral have all important uses not only in the synthesis of flavors but also in pharmaceutical and cosmetic industries (Vilella et al. 2004). Citronellal and citronellol are especially interesting to the perfume industry because of their highly pleasant odors. The presence of 3,7-Dimethyl octanol and 3,7-Dimethyl octanal detracts from this valuable quality (Aramendia et al. 1997).

As a result, for a catalytic process to have the desired results, it should reduce the conjugated C=C bond first and then the C=O bond, without altering the isolated C=C bond.

### **2.3. Previous Studies on Citral Hydrogenation**

The catalytic reactions are classified as heterogeneous and homogeneous in industrial and academic fields. There are many studies investigating the use of homogeneous and heterogeneous catalysts in citral hydrogenation reaction (Aramendia et al. 1997).

#### **2.3.1. Homogeneous Catalysis**

In homogeneous catalysis reactants, products and the catalyst are in the same phase. Homogeneous catalysts were commonly used ones for the synthesis of pharmaceuticals and other fine chemicals. The homogeneous rhodium-based catalyst known as Wilkinson's catalyst is an example that often used in hydrogenation of alkenes and selective 1,4-reduction of  $\alpha$ ,  $\beta$ -unsaturated carbonyl compounds reactions (Jones 1973; Birch et al. 1976). These types of catalysts are very flexible where the choice of active metal, ligands and reaction conditions can lead to highly selective hydrogenations (Chen et al. 2004). Homogeneously catalyzed reactions can be very specific with high yields of desired products. These reactions are easily studied in laboratories since the mechanism involve readily identified species. However it is difficult to operate commercially. Liquid phase operation places restrictions on temperature and pressure, so the equipment is complicated. The catalyst must be separated from the products, imposing additional difficulties. For these reasons, homogeneous catalysis is found only in limited industrial use, such as manufacture of drugs and food (Bhatia 1990). A possible solution to these problems is to separate the catalyst and the product into two

individual and immiscible phases by development of heterogeneous catalysts which are preferred due to their reusability and being environmental friendly.

### **2.3.2. Heterogeneous Catalysis**

Heterogeneous catalysts are in different phase with the reactants and products. The French chemist Poul Sabatier discovered the heterogeneous catalysts for addition of hydrogen to unsaturated bonds and then hydrogenations were intensively studied and applied in all sectors of chemical industry (van Druten et al. 2000).

There are many studies in literature reported on the hydrogenation of aldehydes mostly crotonaldehyde, cinnamaldehyde and citral on single and two-metal catalysts supported on various materials such as carbon, zeolite, sepiolite. They have also pointed out some parameters that influence the catalytic performance such as nature of the active metal, support, the addition of promoters, reaction conditions, and metal particle size and catalyst preparation methods. These parameters are studied on citral hydrogenation reactions catalyzed by monometallic and bimetallic catalysts.

#### **2.3.2.1. Citral Hydrogenation over Monometallic Catalysts**

Uçar et al. (2002) and Yılmaz et al. (2005) studied the liquid phase citral hydrogenation over clinoptilolite rich natural zeolite supported Pd and Ni catalysts. The effect of reaction temperature (80, 100 and 120°C) and catalyst amount on the product distribution was investigated. The catalysts were prepared by impregnation and ion exchange methods to get Pd loadings 0.72, 2.42 and 5.63 %. Catalytic activity increased with reaction temperature following an Arrhenius behavior, while selectivity remained constant for a given conversion. However, selectivity increased with the amount of catalyst in the reaction solution (150-400 mg/100mL). High selectivity to citronellal (90 %) was obtained at complete conversion of citral. The product distribution changed with different metal loading. Pd catalyst prepared by ion exchange and Ni impregnated catalysts gave different products. Pd catalyst had the lowest selectivity while Ni catalyst had lower activity for a given conversion. This was attributed to the metal and the support interactions. The spent catalyst regained its fresh activity and selectivity upon regeneration.

Malathi et al (2001) studied the selective hydrogenation of citral over supported Pt systems. The catalysts used were prepared by the wet impregnation of Pt (5 %) onto the titania, ceria and mixed oxide supports. Reaction was carried out at atmospheric pressure and a temperature of 45°C. All supported Pt systems (Pt/TiO<sub>2</sub>, Pt/CeO<sub>2</sub> and Pt/T-A mixed oxide) selectively produced the unsaturated alcohols rather than the saturated aldehydes. The selectivity towards geraniol was 100 % for all catalysts. This was attributed to the influence of the SMSI (strong metal-support interaction) state in these supported Pt catalysts. They have also found that the titania and mixed oxide supported Pt catalysts indicated the maximum conversion (25 %) and higher activities. This activity was explained with the migration of the reduced TiO<sub>2</sub> species on the surface of the metal and enhancing the preferential hydrogenation of C=O bond to give an unsaturated alcohol geraniol, which has been observed as the sole product for all of the catalysts.

Aramendia et al. (1997) studied the liquid phase hydrogenation of citral in a low-pressure hydrogenator using Pd supported SiO<sub>2</sub>/AlPO<sub>4</sub> and sepiolite catalysts. They examined the influence of reaction variables such as temperature (20-50°C), hydrogen pressure (20-80 psi) and type of solvent (Methanol, CHA, DIO, THF) on the reaction sequence. They have also investigated the effect of Lewis acid type by the addition of FeCl<sub>2</sub> to the reaction mixture on the reaction sequence and selectivity to unsaturated alcohols. Pd (3 %) loaded catalysts were prepared by using incipient wetness method. It was observed that single metal Pd catalyst led to the formation of saturated aldehydes citronellal. The highest selectivity (94-97 % at 10 % citral conversion) was obtained at low temperatures and pressures (20°C, 1.5 bar). Type of solvent markedly affected the hydrogenation rate and the nonpolar solvents led to greater rate. It was concluded that the use of alcohol gives rise to the formation of acetals between solvent and citral, and also side reactions. Finally the presence of Lewis acid additives (FeCl<sub>2</sub>) induces an electron transfer between the two metals (Fe and Pd) arising from their differential electro negativity. This effect favors the adsorption of citral with the C=O group to give geraniol and nerol.

Singh et al. (2000) studied the citral hydrogenation over Pt/SiO<sub>2</sub> catalyst. The aim of the study was to investigate the temperature effect on activity and selectivity. For this purpose the reaction was performed in the pressure and temperature range 7-21 atm and 25-150°C respectively. They have observed that the product distribution was strongly depended on reaction temperature. It was seen that reaction at 100 and 150°C

gave high selectivities to the primary products geraniol and nerol, (78 % at 50 % conversion) with 1.44 % Pt/SiO<sub>2</sub> catalyst whereas hydrogenation at 25°C yielded secondary products like citronellol due to readsorption and further reaction of primary products. The effect of pretreatment procedure of catalysts was also investigated in this study. Catalysts were reduced in situ and ex situ at 400°C in flowing hydrogen then cooled to reaction temperature in hydrogen. It was shown that pretreatment procedure could have a pronounced effect on reaction rate because the catalyst reduced ex situ exhibited a TOF (the initial rate of disappearance of citral) (0.007 s<sup>-1</sup>) that was only one third of that for the catalyst reduced in situ (0.020 s<sup>-1</sup>). However the two different pretreatment procedures did not influence the product distribution. This result suggests either that the catalyst may not be completely activated on ex situ reduction procedure or that low concentrations of water can affect the kinetics.

Salmi et al. (2000) used nickel impregnated silica fibers in the gas phase hydrogenation of citral in a tubular glass reactor. Catalysts were calcined at three different temperatures (700, 800 and 900°C). Formation of citronellal was favored as primary and secondary products in fiber catalysts. The most active catalyst was 5 wt % Ni on silica fiber calcined at 700°C with 92 % selectivity to citronellol. This was the catalyst with lower Ni content and calcined at lower temperature. The XRD results showed that nickel particle size increased with increasing nickel content. The nitrogen adsorption analysis showed that BET surface area decreased with increase in calcinations temperature. This was reported to be the reason of decrease in activity of catalysts at higher calcination temperatures.

Arvela et al. (2003) studied the selective hydrogenation of citral to citronellol. The aim of the study was to compare different catalyst preparation techniques and different supports. The catalysts tested in citral hydrogenation reaction were prepared by incipient wetness and atomic layer epitaxy (ALE) methods. Supports used were Al<sub>2</sub>O<sub>3</sub>, SiO<sub>2</sub>, Y zeolites in H and NH<sub>4</sub> forms. The hydrogenation experiment was carried out under hydrogen pressure varied between 2.3 and 40 bar and reaction temperature was 70 or 100°C. The highest maximum selectivity to citronellol (83 %) at 2.3 bar H<sub>2</sub> was obtained with Ni/Al<sub>2</sub>O<sub>3</sub> (8.8 wt % Ni) catalyst prepared by ALE method. It was concluded that the main advantage with an ALE catalyst is the more equal metal distribution, thus giving higher specific metal surface area and higher hydrogenation rates. When the Ni loaded alumina and zeolite Y catalysts were compared it was seen that zeolite Y catalysts did not exhibit high activity in citral hydrogenation in spite of

high BET surface area (635 m<sup>2</sup>/g for NH<sub>4</sub>-Y and 574 m<sup>2</sup>/g for H-Y). Selectivity towards citronellol was lower over Ni/NH<sub>4</sub>-Y (5 %) and Ni/H-Y (0 %) catalysts than over Ni/Al<sub>2</sub>O<sub>3</sub> catalyst (42 %) at 70°C and 20 bar H<sub>2</sub> in 2-pentanol as a solvent. Zeolites exhibiting strong acid sites preferred other types of reactions like cracking, dehydrogenation. In this study the optimum catalyst reduction temperature was also investigated over Ni/Al<sub>2</sub>O<sub>3</sub> (16.7 wt % Ni) catalyst. The catalyst was reduced at 400, 450, 480°C, maximum selectivities to citronellol were 82 %, 79 % 80 % respectively. The highest maximum selectivity to citronellol (82 %) was obtained in ethanol at 70°C and 5.3 bar H<sub>2</sub> with the catalyst reduced at 400°C. According to literature sintering of Ni begins at 450°C. That is why the selectivities were low with catalysts reduced at 450 and 480°C in spite of high specific metal surface area (100 m<sup>2</sup>/g<sub>Ni</sub> for 480°C, 87m<sup>2</sup>/g<sub>Ni</sub> for 400°C).

Blackmond et al. (1991) studied the hydrogenation of two  $\alpha$ - $\beta$  unsaturated aldehydes, cinnamaldehyde and 3-methylcrotonaldehyde over Ru, Pt, Rh loaded activated carbon, Na-Y and K-Y zeolites. The aim of the study was to compare the zeolites with activated carbon as an inert amorphous support and the effect of different metals on product distribution. Catalysts were prepared by ion exchange method to get the metal loading of 3 wt %. For cinnamaldehyde hydrogenation selectivity to unsaturated alcohols over Ru loaded catalysts was greatly enhanced when the zeolite supports were used (63 % for Na-Y, 67 % for K-Y at 25 % conversion) compared to the active carbon (30 %). Similar result was obtained with the catalysts loaded with Pt and Rh metals. The little difference between the two types of zeolites for unsaturated alcohol (UOL) selectivity suggested that the zeolite pore structure was the important factor for high UOL selectivity with cinnamaldehyde as the organic substrate. In 3-methylcrotonaldehyde hydrogenation, Ru/K-Y produced UOL three times as selectively as Ru/NaY (35 % for Ru/K-Y and 10 % for Ru/Na-Y at 25 % conversion). For the other metals, Pt and Rh, results were the same demonstrating the effect of the type of zeolite cation on UOL selectivity depend on the organic substrate employed in the reaction.

Singh et al. (2000) studied the kinetics of citral hydrogenation on Pt/TiO<sub>2</sub> catalysts and compared to those reported earlier for Pt/SiO<sub>2</sub> catalyst. Catalysts were prepared by incipient wetness method with the loadings of 0.61, 1.24, 1.78 and 1.92 wt % Pt. Reactions were carried out at the temperature of between 25 and 150 °C and 7-21 atm H<sub>2</sub> pressure. They observed marked changes in product distribution with Pt/TiO<sub>2</sub>

compared to Pt/SiO<sub>2</sub>. Pt/TiO<sub>2</sub> catalyst exhibited selectivity of 90 % to unsaturated alcohols at 10 % citral conversion. At the same reaction conditions 1.44 % Pt/SiO<sub>2</sub> catalyst exhibited an increase in selectivity from 40 % initially to 80 % after 50 % conversion. Metal-support interaction (MSI) resulted in a dramatic enhancement in specific activity at 100°C, 20 atm H<sub>2</sub> as Pt/TiO<sub>2</sub>-HTR exhibited a TOF of 1.0 compared to 0.02 s<sup>-1</sup> for Pt/TiO<sub>2</sub>-LTR and 0.004 s<sup>-1</sup> for Pt/SiO<sub>2</sub>. It was concluded that MSI can affect not only reaction rates, but also kinetic parameters in the rate expression.

### **2.3.2.2. Citral Hydrogenation over Bimetallic Catalysts**

Silva et al (2003) studied the combined effects of support and promoter on the citral hydrogenation over ruthenium-tin catalysts. They used Al<sub>2</sub>O<sub>3</sub> and TiO<sub>2</sub> as supports and Sn as a promoter. The monometallic and bimetallic catalysts were prepared by impregnation and coimpregnation techniques respectively. All catalysts were produced to obtain a Ru content of 2 wt % while the tin content was varied in order to obtain different (Sn/Ru+Sn) atomic ratios between 0.1 and 1. Titania supported catalysts were reduced at temperatures of 205°C (LTR) and 400°C (HTR) while the alumina supported catalyst was reduced at 400°C. The reaction was carried out at constant hydrogen pressure of 50 bar and at 126°C in the presence of 600 mg catalyst. For the monometallic catalysts it was seen that HTR Ru/TiO<sub>2</sub> was less active and more selective to the unsaturated alcohols than Ru/Al<sub>2</sub>O<sub>3</sub> and LTR Ru/TiO<sub>2</sub>. This was explained by the presence of Strong Metal-Support Interaction (SMSI) effect induced by the high temperature reduction of Ru loaded titania catalyst with the simultaneous formation of special metal-support sites active for the selective hydrogenation of C=O bond. On the other hand, LTR Ru/TiO<sub>2</sub> was less selective to unsaturated alcohols than Ru/Al<sub>2</sub>O<sub>3</sub>. This result was clarified by the fact that reduction temperature (250°C) of LTR Ru/TiO<sub>2</sub> was not effective for the Ru-titania interaction. The addition of tin to the TiO<sub>2</sub> supported Ru catalyst led considerable changes in their performances. Selectivity to unsaturated alcohols increased from 41.5 % to 87.8 % for LTR Ru/TiO<sub>2</sub> and from 73.4 % to 85.6 % for HTR Ru/TiO<sub>2</sub> at the end of 6 h. The selectivity to geraniol and nerol increased for Ru-Sn catalyst as Sn/Ru atomic ratio increased, reaching a maximum (96 %) at Sn/Ru = 0.25. It was also concluded that the nature of support and

addition of tin have a profound influence on the production of isopulegol in hydrogenation of citral over Ru-Sn catalysts.

Lafaye et al. (2002) prepared bimetallic Rh-Ge/SiO<sub>2</sub> and Rh-Ge/Al<sub>2</sub>O<sub>3</sub> catalysts and investigated their catalytic performances in liquid phase citral hydrogenation reaction. The monometallic 1 wt % Rh/Al<sub>2</sub>O<sub>3</sub> and 1 wt % Rh/SiO<sub>2</sub> were prepared by ion exchange method while the bimetallic catalysts were prepared by surface redox reaction between hydrogen activated on rhodium particles and the germanium salt dissolved in water. For the bimetallic catalysts Ge content was varied between 0.07 and 2.5 wt %. Reactions were performed at a constant hydrogen pressure of 70 bar and at 70°C with 800 mg catalyst. It was seen that the addition of small amounts of Ge to Rh induces a drop of citral conversion, but the activity increases at higher Ge contents. Regarding the hydrogenation of conjugated C=O and C=C double bonds of citral, the selectivity towards unsaturated alcohols geraniol and nerol progressively increased with Ge content. For Rh-Ge/SiO<sub>2</sub> catalyst, selectivity to unsaturated alcohols increased from 10 % to 44 % when the Ge content changed from 0 to 4 wt %. For Rh-Ge/Al<sub>2</sub>O<sub>3</sub> catalyst, selectivity increased from 2 % to 75 % as the Ge content varied from 0 to 4 %. The opposite behavior was observed for the hydrogenation of C=C bond leading to citronellal formation. Selectivity towards citronellal decreased from 50 % to 10 % for the silica supported catalyst and from 90 % to 10 % for the alumina supported catalyst. However for the selectivity toward unsaturated alcohol, citronellol was slightly dependent on the Ge loading of catalyst. For the liquid phase hydrogenation of citral, the main effect of Ge addition to Rh catalyst was to improve the reaction selectivity toward unsaturated alcohols. This effect was being more obvious on alumina supported catalyst.

Sordelli et al. (1999) studied the citral hydrogenation over catalysts produced by coimpregnation technique with the aim of clarifying the relationship between structure and catalytic properties of tin promoted silica supported rhodium catalysts. The rhodium loading of the catalysts was 4 wt % with Sn/Rh molar ratio was 0.5. The monometallic Rh/SiO<sub>2</sub> catalyst showed a high activity with a 100 % conversion but a very low selectivity to the unsaturated alcohols (5.2 %) with citronellal and citronellol as the main products. Addition of tin decreased the catalytic activity (57 % conversion) with a corresponding increase in the selectivity (70 %) to unsaturated alcohols. It was concluded that the production of unsaturated alcohols need an initial induction period during which the conjugated double bond is predominantly attacked. Once unsaturated

alcohols start to form, the conjugated C=C bond hydrogenation rate rapidly decreases with time. It was found that the selectivity depends on the Sn content where the optimum Sn/Rh molar ratio was 0.5.

Reyes et al. (2002) also studied the effect of the addition of a second metal on the activity and selectivity for the hydrogenation of citral in liquid phase. For this purpose Iridium catalysts supported on SiO<sub>2</sub> and TiO<sub>2</sub> with the addition of cationic promoters Fe or Ge prepared by impregnation were compared. Ir loading of the catalysts was 1 wt % while the atomic ratio of Ir:Ge or Ir:Fe was 1:1. The creation of new active sites due to the addition of Fe or Ge as promoters led to an enhancement in selectivity to unsaturated alcohols. The selectivity to geraniol and nerol were 0 % and 100, respectively for Ir/TiO<sub>2</sub> catalyst. After the addition of Ge, selectivities were 82 % and 16 % for geraniol and nerol respectively. Nearly the same effect was seen in the case of silica-supported catalyst after the Fe and Ge addition. This shows that the Ir-supported catalysts can be very selective toward the hydrogenation of carbonyl bonds.

Coupe et al. (2000) studied the hydrogenation of citral on bimetallic Rh-Sn/SiO<sub>2</sub> catalysts. In this study, the effect of different preparation techniques on the product distribution were investigated. Catalysts were prepared by coimpregnation, successive impregnation and an organometallic route methods in order to get 1 wt % Rh content and to keep a molar ratio Rh/Sn of 0.92. Reaction was carried out at 50 bar H<sub>2</sub> and 126 °C. Results showed that all catalysts were active as well as selective to geraniol and nerol. There were small differences in product distributions. Catalyst produced by organometallic route. (Rh-Sn-OM) gave 98 % selectivity to unsaturated alcohols at 50 % conversion with some citronellal formation. The selectivity over catalyst prepared by coimpregnation (Rh-Sn-CI) was as high as that over (Rh-Sn-OM) (96 %) with small amounts of citronellal and citronellol. Catalyst produced by impregnation method gave some traces of by products. It was concluded that coimpregnation method appears as a potential method to obtain bimetallic Rh-Sn catalysts for selective hydrogenation of citral. Because the intimate interaction between Rh and Sn on bimetallic sites was sufficient to promote C=O bond reduction. The extension of this interaction differs according to the preparation method and seems to be stronger in the coimpregnation method.

Baeza et al. (2001(a)) performed citral hydrogenation over Ru-Fe catalysts supported on activated carbon (AC) and on high surface area graphite (G). Monometallic catalysts were prepared by incipient wetness and bimetallic ones were

prepared by coimpregnation methods. Ru contents of tested catalysts were between 1.4 and 1.9 wt % and the Fe/Ru ratios were 0.4 and 2.0. Selectivity to nerol and geraniol over Ru/AC and Ru/G catalysts were 39 and 38 %, respectively and it follows same trend in the whole range of conversion. For AC supported catalyst selectivity increased from 39 to 52 % and 69 % for the 0.4 and 2.0 Fe/Ru ratios, respectively. For the graphite supported catalyst, the selectivity increased from 38 to 66 and 73 % for two different Fe/Ru ratios. In this study, two mechanisms were proposed for the promoting effect in bimetallic catalysts. (i) The promoter acts as an electrophilic or Lewis site activating the C=O bond and favoring its hydrogenation. (ii) The promoter acts as electron-donor ligand, increasing the electron density of the active metal, which reduces the adsorption of C=C bond and its hydrogenation.

Baeza et al. (2001(b)) used Ce and Mg as promoters in Ru based catalysts supported on Al<sub>2</sub>O<sub>3</sub> and activated carbon (AC). Monometallic catalysts were prepared by incipient wetness and the bimetallic ones prepared by coimpregnation methods. Ru content of alumina -supported catalyst was 2 wt % and for activated carbon supported catalyst 1.6 % while the atomic ratio of Ru to promoter was 1:2 for bimetallic catalysts. The use of Ce increased the selectivity to unsaturated alcohols in citral hydrogenation. The selectivities were 54 % and 68 % for Ru/Al<sub>2</sub>O<sub>3</sub> and Ru-Ce/Al<sub>2</sub>O<sub>3</sub>, respectively. In AC supported catalysts, selectivities were 38 and 82 % for monometallic and bimetallic catalysts at 70 % of conversion. However no effect was found due to Mg addition. It was suggested that the positive effect of Ce is related to the presence of new surface sites on the promoter, which activate the C=O bond of aldehyde and favor its hydrogenation.

## CHAPTER 3

### CATALYSTS

A catalyst is a substance that accelerates the rate of a chemical reaction without itself appearing in the products. Thermodynamic factors cannot be modified by the presence of a catalyst. Kinetic factors, such as reaction rate, activation energy, nature of the transition state and so on, are the reaction characteristics that can be affected by a catalyst.

The term “catalysis” was first introduced by Jakob Berzelius in 1835. He defined that “the phenomenon whereby the chemical reaction rate may be significantly increased by the presence of a substance that is not a part of the reactants and hence can continue to exist and accelerate the reaction for infinitely long periods (Augustine 1996).

#### **3.1. Heterogeneous Catalysts**

Many practical heterogeneous catalysts are consists of three components namely active component, support and promoter.

##### **3.1.1. Active Component**

Active component is the phase that is principally responsible for the catalytic activity. The active phase usually constitutes between 0.1 and 20 % of the total catalyst and is normally in the form of very small crystallites (1-50 nm). Active components can be either oxides or metals (Moulijn et al. 1993). In this study, Ni and Pt were used as active components.

##### **3.1.2. Support**

Support is the vehicle for the active phase. It exercises several functions, among which are the maximization of the surface area of the active phase by providing a large

area over which it may be spread and allowing the active phase to be cast into the form of coarse particles suitable for use in technical reactors. The support is usually supposed to be catalytically inactive by itself; however in partnership with the active phase it can participate in the total reaction in important ways (Moulijn et al. 1993).

The main purpose of using a support is to achieve an optimal dispersion of the catalytically active component and to stabilize it against sintering. However, in a number of reactions, the support is not inert and the overall process actually a combination of two catalytic functions: that of the active component and that of the support (G. Ertl et al. 1999). In the present study, various types of zeolites were used as catalyst support.

### **3.1.3. Promoter**

Promoter is deliberately or inadvertently added to a metal catalyst may have an influence on the activity of the catalyst and the selectivity of the reaction. These changes are brought about when the added material is adsorbed on the surface of the catalyst. A promoter can also influence catalyst activity and/or selectivity by modifying the electronic character of the active sites. This can result in either an increase or decrease in activity. Promoter can also change the rate of a reaction by interacting with the substrate to alter its mode of adsorption. There are number of different classes of catalyst modifiers such as acids and bases, metal cations, nucleophilic species and compound with multiple bounds, which are strongly chemisorbed (Robert L. Augustine et al. 1996). In this study, Sn was chosen as promoter.

### **3.2. Zeolites**

The word “Zeolite” has Greek roots and means “boiling stones”, an allusion to the visible loss of water noted when the natural zeolites are heated. Zeolites are crystalline aluminosilicates with a tetrahedral framework structure enclosing cavities occupied by cations and water molecules, both of which have enough freedom of movement to permit cation exchange and reversible dehydration (J. V. Smith 1976).

### 3.2.1. Composition and Structure

The fundamental building block of the zeolites consists of a small silicon or aluminum ion surrounded by a tetrahedron of four oxygen anions. Each of the four oxygen anions in this tetrahedral is shared in turn with another silica or alumina tetrahedron. The crystal lattice extends in three-dimension and the -2 oxidation state of each oxygen is accounted for. Each silicon ion has its +4 charge balanced by the four tetrahedral oxygen and the silica tetrahedral are therefore electrically neutral. Each alumina tetrahedron has a residual charge of -1 since the trivalent aluminum is bounded to four oxygen anions. Therefore, each alumina tetrahedron requires a +1 charge from a cation in the structure to maintain electrical neutrality. These cations are usually sodium in the zeolites as it is initially prepared, but they can be replaced by ion exchange. Figure 3.1 shows the primary building blocks of zeolites.

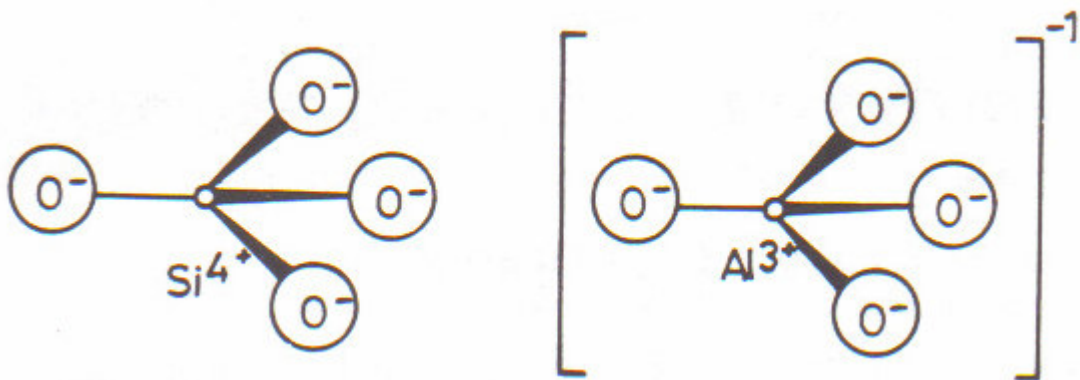
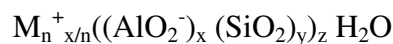


Figure 3.1. Primary building blocks of zeolites.

(Source: Bhatia 1990)

The building blocks of the framework zeolite crystal structures are formed by the secondary units, which are the combination of silica and alumina tetrahedral. The unit cell formula is usually written as



where  $M_n^{+}$  is the cation, which balances the negative charge associated with the framework aluminum ions.  $z$  is the numbers of water molecules fill the remaining volume in the interstices of the zeolite.

Zeolites have an open framework structure, which defines a pore structure with a high surface area. The chemistry of the zeolite surface is determined uniquely by the properties of the crystalline solids, which is a major advantage in elucidating the catalytic chemistry.

Secondary building units of some common zeolites are given in Figure 3.2.

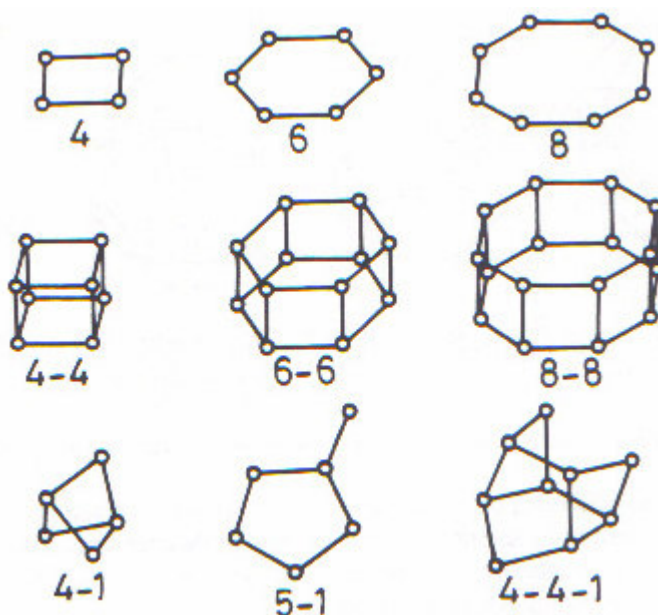


Figure 3.2. Secondary building units.

(Source: Bhatia 1990)

A large numbers of zeolites are known, 45 known different frameworks are naturally occurring and nearly 150 types are prepared synthetically (Breck 1974). These natural and synthetic zeolites are very usable materials as heterogeneous catalysts due to their superior properties such as:

- They have exchangeable cations allowing the introduction of cations with various catalytic properties.
- If these cationic sites are exchanged to  $H^+$ , they can have high number of very strong acid sites.
- Their pore diameters are less than  $10 \text{ \AA}$ .
- They have pores with one or more discrete sizes (Subhash Bhatia 1990).

Brief information about the supports used in our study (Zeolite-Y, Zeolite-Beta, Mordenite, MCM-41 and Clinoptilolite) is given below.

### 3.2.2. Zeolite Y

Zeolite Y is a synthetic form of faujasite. Faujasite is a natural crystalline aluminosilicate zeolite with a chemical composition of



The structure of faujasite is the most open of all zeolites. The channels have a minimum diameter of 9 Å. The unit cells have a dimension of nearly 25 Å. Figure 3.3 shows the framework structure of zeolite Y.

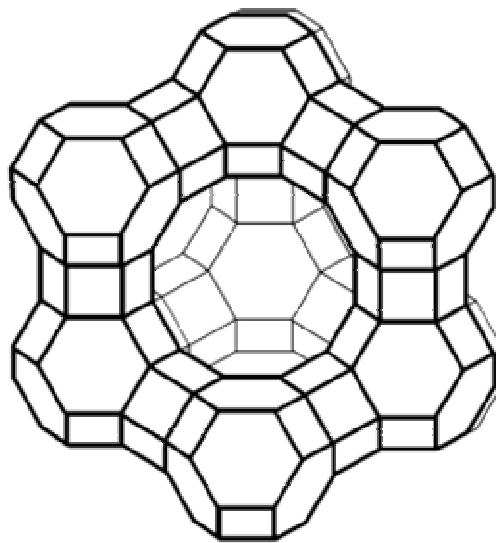


Figure 3.3. Framework structure of zeolite Y.

(Source: Bhatia 1990)

The crystals of zeolite Y are basically three-dimensional frameworks of  $\text{SiO}_4$  tetrahedrons cross-linked by the sharing of oxygen atoms. The electrovalence of each tetrahedron containing aluminum is balanced by the presence in the aluminosilicate framework of a cation such as an alkali metal ion. Water molecules occupy the void spaces in the framework. Dehydration to affect the loss of the water of hydration results in a crystal interlaced with channels of molecular dimensions that offer very high surface areas for the adsorption of foreign molecules. The chemical formula for zeolite Y expressed in terms of moles of oxides may be written as



wherein  $w$  is a value greater than 3 up to 6 and  $x$  may be a value up to about 9 (Michiels et al. 1987).

Since faujasite has very large pore openings, which are accessible for isoparaffines, cyclohexane and aromatics, it is very suitable as a catalyst for the cracking of petroleum or in combination with hydrogenating metals for hydrocracking reactions. The most important use of zeolite Y is as a cracking catalyst. It is used in acidic form in petroleum refinery catalytic cracking units to increase the yield of gasoline and diesel fuel from crude oil feedstock by cracking heavy paraffins into gasoline grade naphthas. Zeolite Y has superseded zeolite X in this use because it is both more active and more stable at high temperatures due to the higher Si/Al ratio. It is also used in the hydrocracking units as a platinum/palladium support to increase aromatic content of reformulated refinery products (Bhatia 1990; Ribeiro et al. 1984).

### **3.2.3. Zeolite Beta**

Beta zeolite is an old zeolite discovered before Mobil began the "ZSM" naming sequence. As the name implies, it was the second in an earlier sequence. The structure of zeolite beta was only recently determined because the structure is very complex and interest was not high until the material became important for some dewaxing operations. It has tetragonal crystal structure with straight 12-membered ring channels ( $7.6 \times 6.4 \text{ \AA}$ ) and crossed 10-membered ring channels ( $5.5 \times 6.5 \text{ \AA}$ ).

Zeolite beta consists of an intergrowth of two distinct structures termed Polymorphs A and B. The polymorphs grow as two-dimensional sheets and the sheets randomly alternate between the two. Both polymorphs have a three dimensional network of 12-ring pores. The intergrowth of the polymorphs does not significantly affect the pores in two of the dimensions, but in the direction of the faulting, the pore becomes tortuous, but not blocked (Michiels et al. 1987).

### **3.2.4. Mordenite**

Mordenite is a natural aluminosilicate, which is orthorhombic and has the general formula:



The aluminosilicate framework involves a chain containing 5-membered rings of tetrahedral. They are interspersed with 4-membered rings. Together they form twisted 12 rings, which form a system of channels parallel to (001), nearly cylindrical and having a free diameter of 6.6 Å. The walls of these cylinders are formed by 5, 6 and 8-membered rings, forming interconnecting channels with diameter of 2.8 Å. Generally used Mordenite zeolites have silica to alumina ratio between 9 and 20, preferably 9-11. They have effective pore diameters of about 6 to 10 Å.

The structure of mordenite can be described as built by edge-sharing 5-membered rings of tetrahedral (secondary building unit 5-1, Figure 3.2) forming chains along the c-axis (Simoncic et al. 2005).

These chains are interlinked by four-membered rings (Figure 3.4) in a way that large, ellipsoidal 12-membered (12MRc: aperture 7 - 6.5 Å) and strongly compressed 8-membered rings (8MRc: aperture 5.7 - 2.6 Å) channels parallel to the c-axis. Another set of compressed 8-membered rings (8MRb: aperture 3.4 - 4.8 Å) connects the wide channels with the strongly compressed channels parallel to the b axis.

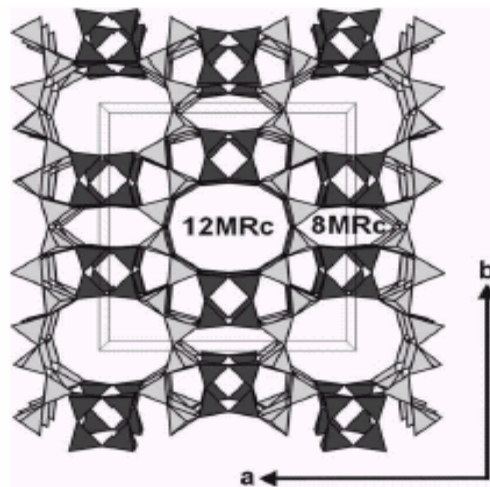


Figure 3.4. Tetrahedral framework structure of mordenite with unit-cell outlines.

(Source: Simoncic et al. 2005)

The structure can be envisioned as built by pucker sheets (light gray shading) parallel to (100) formed by six-membered rings of tetrahedra. These sheets are connected along a by 4-membered ring pillars (dark gray shading) in a way that 12-

membered ring channels (12MRc) and compressed 8-membered ring channels (8MRc) are formed, both extending along c (Simoncic et al. 2005).

### 3.2.5. Clinoptilolite

Clinoptilolite is a mineral from the heulandite group of natural zeolites with the Si/Al ratio between 4.25 and 5.25. In Clinoptilolite structure (Si, Al)O<sub>4</sub><sup>-</sup> tetrahedral are bound in layers. These layers are in turn bound by oxygen atoms in the symmetry plane and form a three dimensional framework. Pseudo layers of structure are also noticeable and cause the characteristic perfect cleavage to the mineral. Figure 3.5 presents the clinoptilolite channel axis and a model framework for the structure of clinoptilolite (Hernandez 2000).

The channel system is two-dimensional, consisting of 10-membered channel A (diameter 0.44 0.72 nm) and 8-membered channel B (0.40×0.55 nm) parallel to each other and the c axis of the unit cell. The 8-membered channel C lies along a axis of the unit cell, intersecting channels A and B.

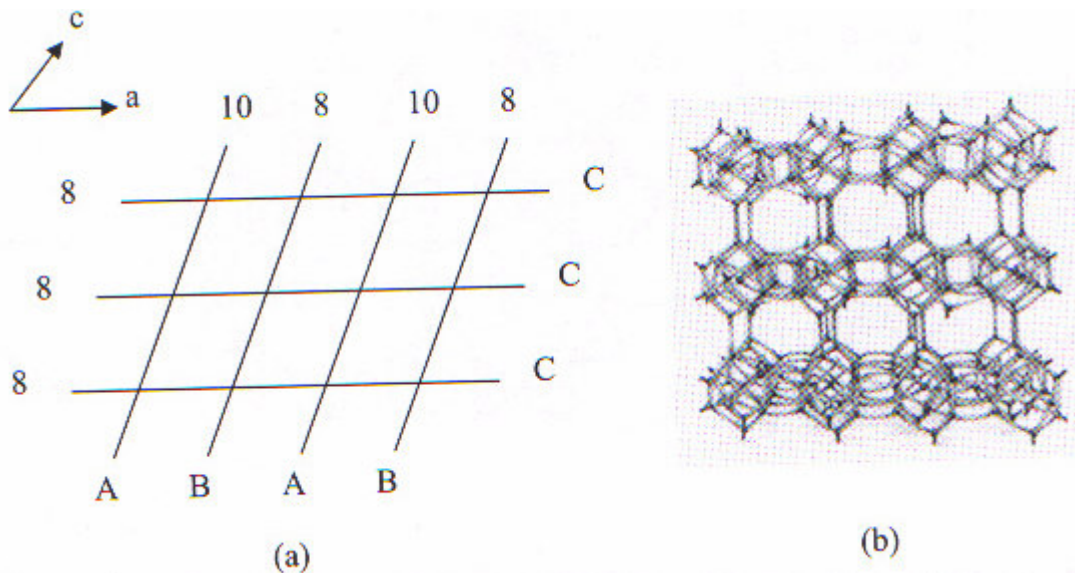


Figure 3.5. (a) Orientation of clinoptilolite channel axes, (b) Model framework for the structure of clinoptilolite.

(Source: Hernandez 2000)

Calcium and sodium ions both occupy two sites in channels A and B. There are also two sites occupied by potassium and magnesium ions (J. V. Smith 1976).

Typical oxide formula of clinoptilolite is expressed as:



The typical unit cell content of clinoptilolite is as follows:

$\text{Na}_6 ((\text{AlO}_2)_6(\text{SiO}_2)_{30}) \cdot 24\text{H}_2\text{O}$ , Ca, K, Mg are also present;  $\text{Na}, \text{K} \gg \text{Ca}$ . (Breck 1974).

Studies of the catalytic activity of clinoptilolite and its modifications have shown that it can promote many chemical reactions. Natural clinoptilolite and its modifications can be used as a carrier of noble and transition metals. Such metal-clinoptilolite catalysts are prospective with respect to acceleration of isomerizations, alkylations, hydrogenation and hydrodesulfonation (Smith 1976).

### 3.2.6. MCM-41

The M41S family of mesoporous molecular sieves, especially MCM-41 has attracted considerable attention since their discovery.

Mesoporous molecular sieves of the MCM-41 has a one dimensional, hexagonally-ordered pore structure due to the ordered hexagonal array of parallel silica tubes with narrow pore size distributions as it is seen in Figure 3.6.



Figure 3.6. Proposed structure of MCM-41

(Source: Vartuli et al. 2001)

Physical properties of MCM-41 materials including regular pore structure, pore shape, tunable dimensions (15-100 Å), a highly specific surface of up to 1000 m<sup>2</sup>/g, a specific pore volume of up to 1.3 ml/g and high thermal stability make them very useable materials as heterogeneous catalysts. MCM-41 type materials are used as acid

catalysts, redox catalysts, films and membranes. The large surface areas of M41S materials make these materials very attractive as supports for active phases (Eimer et al. 2003).

### **3.3. Catalyst Preparation Methods**

There are two main steps in catalyst preparation. The first step is loading the active component precursor on the support and the second one is transforming this precursor into the required active component, which can be found in the oxide sulfide or metallic form depending on the reaction to be catalyzed.

The methods used for the loading of the active component precursor are impregnation, ion exchange, anchoring, grafting, spreading and wetting, heterogenization of complexes, deposition-precipitation (homogeneous and redox) and adapted methods in the case of supported bimetallic catalysts. The most widely used methods are impregnation, incipient wetness and ion exchange (Ertl et al. 1999).

#### **3.3.1. Impregnation**

In impregnation process, an excess of an aqueous solution of a metal salt is brought in contact with a porous support. The solution fills the pores, and some of the metal salt may be adsorbed, with the adsorption depending on the polarization of the support surface, which is influenced by the solution pH. When the solution is decanted and the remainder of the solvent is evaporated, the metal salt is left dispersed on the surface. This process is sometimes referred to as “wet impregnation” since the pores of the support are filled with solvent before coming in contact with the precursor salt. It is also referred to as “diffusional impregnation” since the impregnation of the support is accomplished by the diffusion of the salt inside these solvent filled pores.

A typical procedure for impregnation includes stirring a suspension of the support in the salt solution for a prescribed length of time followed by the separation of the modified support by filtration or centrifugation. The supported salt is then dried and calcined before the salt is reduced to the metal (Augustine et al. 1996).

### **3.3.2. Incipient Wetness**

This method is also referred to as “dry impregnation or capillary impregnation”, involves contacting a dry support with only enough solution of the impregnant to fill the pores of the support. The required amount of liquid to reach the stage of incipient wetness is usually determined by slowly adding small quantities of the solvent to a well stirred weight amount of support until the mixture turns slightly liquid. The volume ratio is used to prepare a solution of precursor salt having the appropriate concentration to give the desired metal loading. Drying, calcinations and reduction processes are performed after loading of the active component to the support (Augustine et al. 1996).

### **3.3.3. Ion Exchange**

To give a higher initial dispersion of the metal species on the support ion exchange process may be used. Ion exchange consists of replacing an ion in an electrostatic interaction with the surface of a support by another ion species. The support containing ion A is plunged into an excess volume (compared to the pore volume) of a solution containing ion B that is to be introduced. Ion B gradually penetrates into the pore space of support and takes the place of ion A, which passes into the solution, until equilibrium is established corresponding to a given distribution of the two ions between the solid and the solution (Ertl et al. 1999).

Two conditions must be met for exchange on a support. First one is the fact that the pH of the impregnating solution must be either sufficiently high or low to provide the appropriate surface potential. Second one is that the adsorbent must have the proper charge (Augustine et al. 1996).

## CHAPTER 4

### EXPERIMENTAL STUDY

Synthetic and natural zeolite supports, namely Na-Mordenite, NaY, Na- $\beta$ , MCM-41 and clinoptilolite were loaded with Pt, Ni and Sn metals to prepare monometallic and bimetallic catalysts. Catalysts were loaded through impregnation and coimpregnation. Prepared catalysts were characterized and then tested in citral hydrogenation reaction.

#### 4.1. Materials

Table 4.1 shows the chemicals and Table 4.2 shows supports used during the experiments and their properties.

Table 4.1. Properties of chemicals used in experiments

Chemicals	Properties
Citral	Fluka, 97 %
Cyclohexanone	Sigma, 99 %
Nickel(II)nitrate hexahydrate	Aldrich, 97 %
Platinum(II) acetyl-acetonate	Aldrich, 97 %
Tin(II)-chloride Dihydrate	Fluka, 98 %
Cetyl tetramethyl ammonium bromide	Adrich, 99 %
Sodium silicate	Aldrich, 27 % SiO <sub>2</sub> , 14 % NaOH
Sulfuric acid	Merck, 95-98 %
Ethanol	J.T.Baker, 99.5%
Toluene	Merck, 99.5 %

Table 4.2 Properties of supports used in experiments.

<b>Supports</b>	<b>Properties</b>
MCM-41	Synthesized, pure silica
Na- $\beta$ Zeolite	SüdChemie, BEA powder, Si/Al=12.4
Na-Mordenite	SüdChemie, MOR powder, Si/Al=9
Clinoptilolite	From Gördes Doğu, 38-150 $\mu$ m, Si/Al=5.1
Na-Y Zeolite	Zeolyst, CBV100, Si/Al=2.6

## 4.2. Methods

### 4.2.1. Catalyst Preparation

#### 4.2.1.1. Preparation of Supports

Clinoptilolite rich natural zeolites, were the same with that used in the study by Uçar et al. (2002) were crushed with a hammer and sieved with stainless steel sieves to the desired particle size ranging between 38 and 150 $\mu$ . Clinoptilolite samples were washed with deionized water in a shaking water bath at a temperature of 80°C for 2 h. This procedure was repeated twice to remove the water soluble impurities. Washed zeolites were dried at 120°C overnight and then calcined at 500°C under N<sub>2</sub> flow of 100ml/min for 5h.

For the synthesis of pure-silica MCM-41 material, a synthesis procedure given in literature was applied (Lin et al. 2001). Firstly the template solution was prepared by mixing 3.825 g cetyl tetramethyl ammonium bromide (CTMABr) and 29.3 ml water and stirring for 20 min. Then 14.2 ml sodium silicate (water glass) was added to the solution and stirred 20 min more at room temperature. After preparing the gel mixture, 1.10 M sulfuric acid solution was added to the mixture drop wise to adjust the pH value to 10.1. The molar ratio of resultant gel composition was 1SiO<sub>2</sub>/0.25Na<sub>2</sub>O/0.11CTMABr/0.26H<sub>2</sub>SO<sub>4</sub>/38.18H<sub>2</sub>O. The gel was then aged at 100°C for 48 h in a Teflon lined autoclave. Finally, the gel was quenched to ambient temperature, filtered and washed with 2 L of deionized water. The product was dried at

room temperature for 2 days and calcined at 560°C with 1.5°C/min heating rate for 6 h and used as support.

Na-Mordenite, Na-Y, Na-β synthetic zeolites were commercially available. They were calcined at 500°C under N<sub>2</sub> flow (100 ml/min) for 5 h in a tubular reactor and used as support.

#### **4.2.1.2. Preparation of Monometallic Catalysts**

Monometallic Ni catalysts were prepared by impregnation method. For this Ni loaded catalysts, 0.01M ethanolic solution of Nickel(II)nitrate hexahydrate salt was prepared by mixing 0.5 g of Nickel(II)nitrate hexahydrate with 172 ml of ethanol for 10 min. Zeolite support weighing 0.9 g was contacted with the solution by mixing them for 16 h with a magnetic stirrer at room temperature. This gave 10 % Ni loading when all Ni in the solution was loaded. Then the ethanol was evaporated in a rotary evaporator at 45°C and 50 rpm for 1h. The impregnated catalyst was dried at 120°C overnight and then it was calcined at 500°C under dry air (100 ml/min) for 5 h.

Monometallic Pt catalysts were also prepared with the same method. In order to prepare 5 wt % Pt loaded catalysts, 0.01 M Platinum(II)Acetyl Acetonate solution was prepared by mixing 0.1 g Platinum(II)Acetyl Acetonate with 25.5 ml of toluene for 10 min. Zeolite support weighing 0.9 g was contacted with the solution by mixing them for 16 h with a magnetic stirrer at room temperature. Then the ethanol was evaporated in a rotary evaporator at 45°C and 50 rpm for 1h. The impregnated catalyst was dried at 120°C overnight and then it was calcined at 500°C under dry air (100 ml/min) for 5 h.

#### **4.2.1.3. Preparation of Bimetallic Catalysts**

Bimetallic catalysts were prepared by coimpregnation method. The Ni loading of the catalysts were kept constant (10 wt %) while the Sn/(Sn+Ni) mole ratio were changed between 0.02 and 0.2. For the catalyst, which has Sn/(Sn+Ni) ratio of 0.2, 0.5 g Ni(NO<sub>3</sub>)<sub>2</sub>.6H<sub>2</sub>O salt was dissolved in 25 ml ethanol by mixing in a magnetic stirrer for 10 minutes. After all of the Ni salt was dissolved in ethanol, 0.095 g Cl<sub>2</sub>Sn.2H<sub>2</sub>O was added to the mixture and mixed for 10 minutes more. Finally 0.85 g of support was contacted with the solution and they were mixed together for 16 h at room temperature.

The solvent was evaporated in a rotary evaporator at 45°C and 50 rpm for 1h. The Ni and Sn loaded samples were dried at 120°C overnight and then calcined at 500°C under dry air flow (100 ml/min) for 5 h.

The same method was applied for the preparation of bimetallic Pt-Sn catalysts. The Pt content of the bimetallic catalysts were the same as monometallic catalysts (5 %). The Sn/(Pt+Sn) mole ratio was 0.02 for all bimetallic Pt catalysts. After 0.076 g Pt salt was dissolved in 25.5 ml toluene, 0.001 g tin(II)-chloride dihydrate was added to the mixture and mixed 10 minutes more. Finally 0.07 g of support was contacted with the solution and they were mixed together for 16 h at room temperature. The solvent was evaporated in a rotary evaporator at 45°C and 50 rpm for 1 h. The Pt and Sn loaded samples were dried at 120°C overnight and then calcined at 500°C under dry air flow (100 ml/min) for 5 h.

#### **4.2.2. Catalyst Characterization**

Prepared catalysts were characterized by using different instrumental techniques.

The morphology of the catalysts was investigated by Philips SFEG 30S scanning electron microscopy (SEM).

Metal contents (Ni, Sn) and Si/Al ratios of the zeolite supports were determined by using Varian model Liberty II ICP-AES. For the ICP analysis, samples were dissolved by fusion method. 0.1 g of sample was mixed with 1 g of lithium tetraborate and mixed in a platinum crucible and then kept at 1000°C for 1 h. The mixture was cooled and then dissolved in a aqueous solution of 1.6 M HNO<sub>3</sub>.

The Si/Al ratio for each sample was also calculated using Energy Dispersive X-Ray System (EDX) attached to the SEM. In the EDX analysis, the average of analysis of 10 points was taken.

The crystalline structures of catalysts, after calcination at 500°C and reduction under H<sub>2</sub>, were determined by Philips X'Pert diffractometer (XRD) with CuK $\alpha$  radiation. The scattering angle 2 $\theta$  was varied from 5° to 50° with a step length of 0.02. The XRD diagram of MCM-41 support was obtained with grading angle attachment in the range of 2 $\theta$  1.8 - 6°.

The surface area and adsorption isotherms of the samples were determined by using the nitrogen adsorption technique over a Micromeritics ASAP 2010 model static

volumetric adsorption instrument. Degassing was performed at 400°C for 24 h under 5  $\mu\text{mHg}$  vacuum.

The thermal properties of the samples were analyzed by the Thermogravimetric Analyzer (TGA-51, Shimadzu). TGA gives information about the thermal stability and dehydration properties of the samples due to the weight loss of the sample as it is heated to elevated temperatures. The water contents of the supports were determined by this technique. For TGA analysis 10 mg of sample was heated to 1000°C with 10°C/min under 40 ml/min  $\text{N}_2$  stream.

### 4.2.3. Catalyst Testing

A stirred, semibatch reactor (500 ml, 4574 model, Parr Instrument Co.) equipped with an electrical heater and temperature controller (4842 model, Parr Instrument Co.) was used in the citral hydrogenation experiments. The system had a high-pressure Oxytrap (Altech) and a bubbling unit, in which the dissolved oxygen was removed. The reaction temperature was controlled with a thermocouple probe inside the reactor. Figure 4.1 presents the experimental set-up.

Before the reaction, the catalysts were reduced in situ. For this purpose, the reactor was loaded with 0.25 g of catalyst, sealed and leak tested at 6 bar with Helium. Temperature was set to 200°C and He was filled to the reactor and released three times. After the temperature reached to 200°C, He was fed to the reactor with a flow rate of 80-100 ml/min for 1 h at 4 bar to purge air content from the reactor. After 1 h, gas flow was switched to  $\text{H}_2$ , temperature was set to 400°C. The reactor was filled with 4 bar of  $\text{H}_2$  and discharged three times. Finally catalyst was activated at 400°C for 2 h under the flow of 4 bar  $\text{H}_2$  then the reactor was cooled to reaction temperature of 80°C and stored overnight under 2 bar of  $\text{H}_2$ .

Reactant mixture was prepared as 0.1 M citral and 0.025 M cyclohexanone in ethanol with a total reaction volume of 200 ml. Firstly, 100 ml of ethanol was injected to the bubbling unit to remove the dissolved oxygen. Ethanol was then injected into the reactor and contacted with the catalysts. After 30 minutes of mixing the catalysts and ethanol, reactants were injected into the bubbling unit and then into the reactor. Citral was hydrogenated at 80°C under 6 bar  $\text{H}_2$  with a stirring rate of 600 rpm. The liquid samples were withdrawn from the reactor at the 0, 2, 5, 10, 20, 60, 90, 120, 150, 180,

300 and 360 minutes reaction durations. Preliminary tests showed that the reaction was kinetically controlled under the condition studied (Uçar et al. 2002; Yılmaz et al. 2005).

Samples taken from the reactor were analyzed with Agilent Technologies 6890N Network GC System Gas Chromatograph equipped with a flame ionization detector and a capillary column DB-225 (J&W, 30m, 0.53mm i.d.). The temperature program of analysis was as follows: Heating from 80°C to 100°C at 2°C/min, heating from 100°C to 180°C at 3°C/min and holding at 180°C for 1 min. Injector and detector temperatures were 190°C and 200°C, respectively while the velocity of carrier gas He was 21 cm/s.

Hydrogenation products of citral were identified by GC-MS technique (Varian Saturn 2000). The compositions of components in the reaction mixture were determined by internal standardization method. The commercially available citral hydrogenation products were citronellal (Fluka, ≥80 %), citronellol (Fluka, 90-95 %), nerol (Fluka, 90 %), geraniol (Fluka, 99.5 %), isopulegol (Fluka, 99 %), menthol (Fluka, 95 %), 3, 7-Dimethyl-1-octanol (Aldrich, 99 %).

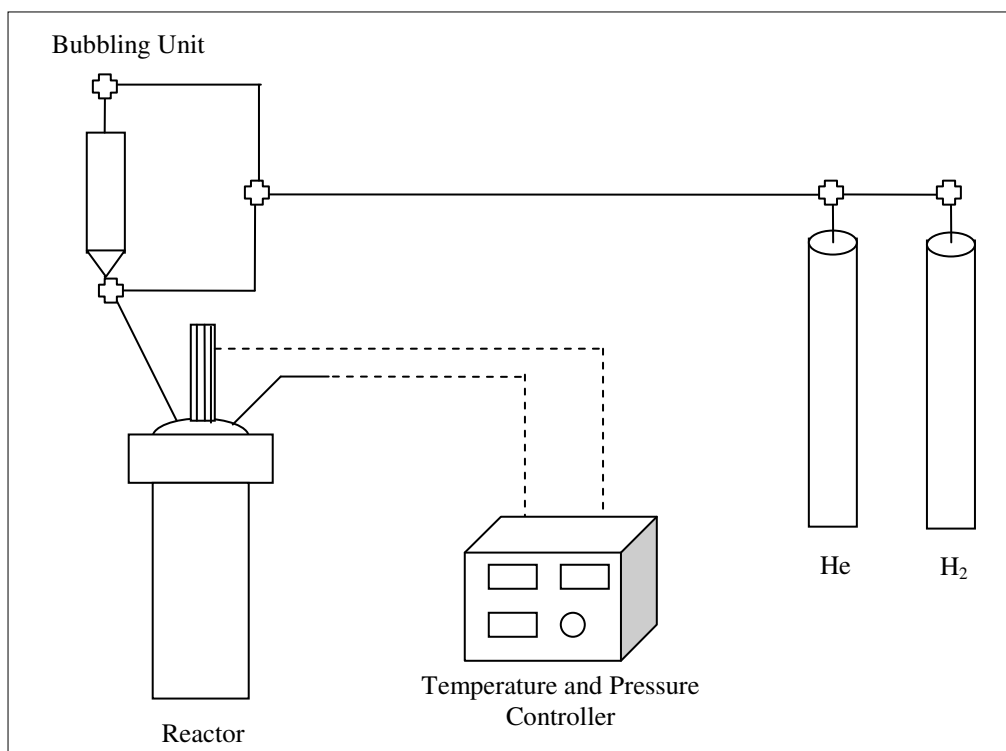


Figure 4.1. Simplified Schematic Representation of Experimental Set-up.

## CHAPTER 5

### RESULTS AND DISCUSSION

#### 5.1. Catalyst Characterization

##### 5.1.1. Na-Y Zeolite

Metal contents (Ni, Sn) of monometallic and bimetallic Na-Y supported catalysts and the chemical composition of the Na-Y zeolite support were determined. Table 5.1 shows the chemical compositions of Na-Y zeolite in oxide forms. This composition obtained from ICP analysis gave Si/Al ratio of 2.6. For Zeolite-Y the ratio is reported to change between 1.5 and 3. (Michiels et. al. 1987).

Table 5.1. Chemical compositions of Na-Y zeolite.

Compounds	Weight %
Al <sub>2</sub> O <sub>3</sub>	14.60
CaO	0.73
Fe <sub>2</sub> O <sub>3</sub>	0.05
K <sub>2</sub> O	0.08
MgO	0.04
Na <sub>2</sub> O	8.50
SiO <sub>2</sub>	53.30
H <sub>2</sub> O	22.70
<b>Total</b>	<b>100.00</b>

The metal loadings of monometallic and bimetallic Na-Y supported catalysts are given in Table 5.2. The Sn/Sn+M (M: Metal) mol ratio of bimetallic catalysts are given in brackets. Ni content was found to change between 8.1 % and 8.8 %. This variation in composition could be due to the experimental errors namely sample preparation and

analysis. The Sn contents of bimetallic catalysts were found to vary between 0.45 % and 4.1 % as the Sn/Sn+M mol ratio varied between 0.025 and 0.2.

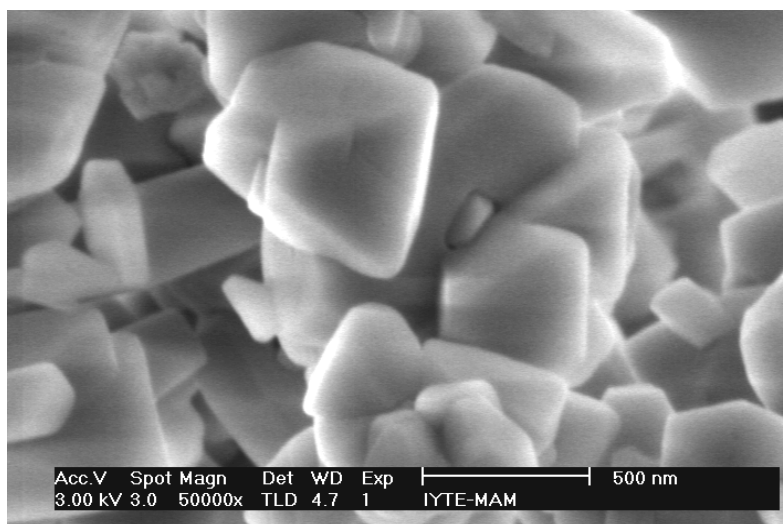
The elements determined by the ICP analysis were quantitatively analyzed also by EDX technique. The average of 10 EDX analysis showed that their compositions were close to that obtained by ICP analysis. The difference was smaller than 3 %. The Si/Al mol ratios of all monometallic and bimetallic catalysts were calculated by the help of EDX analysis. The ratio was found as 2.7 ( $\pm 0.1$ ) for Na-Y supported catalysts. This result confirmed the experimental measurements.

Table 5.2. Metal contents of Na-Y supported catalysts.

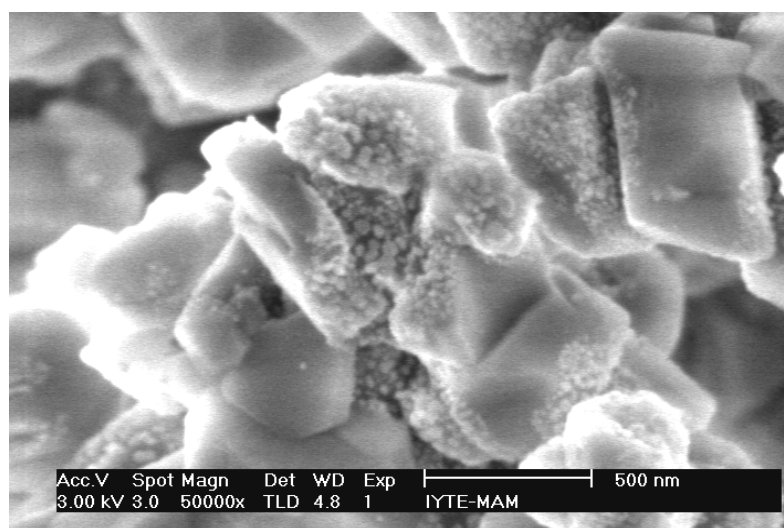
Catalysts	Metal Content (wt %)	Sn content (wt%)
Ni/Na-Y	8.2	-
Ni-Sn/Na-Y(0.025)	8.8	0.46
Ni-Sn/Na-Y(0.053)	8.1	0.93
Ni-Sn/Na-Y(0.1)	8.1	2.0
Ni-Sn/Na-Y(0.2)	8.1	4.1
Pt/Na-Y*	5.0	-
Pt-Sn/Na-Y(0.02)*	5.0	0.45

\* The content was calculated from initial solution composition.

Figure 5.1 shows the SEM micrographs of Na-Y and a typical Ni/Na-Y catalyst. The Zeolite-Y crystalline morphology can be seen in Figure 5.1 (a). In Figure 5.1 (b) agglomerates of Ni particles are observed on the surfaces of Zeolite-Y crystals. SEM images also showed that the crystallite size of Zeolite-Y samples was around 400 nm.



(a)



(b)

Figure 5.1. SEM micrographs of Na-Y support (a) and Ni/Na-Y catalyst (b).

The XRD diagram of Na-Y supported monometallic and bimetallic Ni catalysts are given in Figure 5.2. The XRD patterns of monometallic and bimetallic catalysts showed the characteristic peaks of the support. This suggested that the structure of Na-Y was preserved. Ni peak was observed for all of the catalysts at  $2\theta = 44.5^\circ$ . Since the Sn content of the catalysts was lower than 4 wt %, Sn peak could not be observed by XRD. The peak of Nickel Tin Alloy ( $\text{Ni}_4\text{Sn}$ ) around  $2\theta = 44.8^\circ$  was observed. The reason than  $\text{Ni}_4\text{Sn}$  alloy peak was not observed with the other bimetallic catalysts could be due to low Sn loadings.

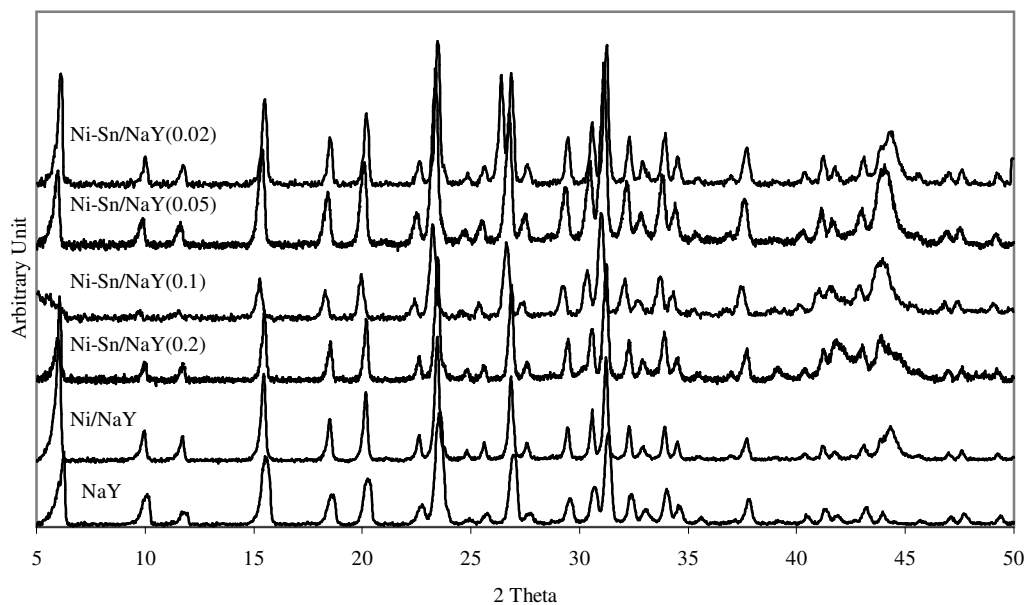


Figure 5.2. XRD diagram of Na-Y support, monometallic and bimetallic Ni catalysts.

The XRD patterns of Na-Y, Na-Y supported monometallic and bimetallic Pt catalysts are given in Figure 5.3. The characteristic peaks of Na-Y support were observed in XRD diagram of monometallic and bimetallic Pt catalysts. This showed that the structure of Na-Y was not destroyed. After the addition of Sn metal to the monometallic catalyst, the peak intensities of Na-Y support was reduced. This might be due to the coverage of the crystal surface by metal loading. The Pt peaks were observed at  $2\theta = 39.83^\circ$  and  $46.3^\circ$  in monometallic catalyst. In the XRD spectra of Pt-Sn/Na-Y(0.02) catalyst, the peaks of PtSn<sub>2</sub> alloy were observed at  $2\theta = 40.5^\circ$  and  $46.8^\circ$ . The addition of Sn reduced the intensities of Pt peaks and led to the formation of PtSn<sub>2</sub> alloy.

The N<sub>2</sub> adsorption isotherms of Na-Y support and Ni/Na-Y catalysts are shown in Figure 5.4. In the figure isotherm showed a long plateau. This is the main feature of Type I isotherm, which is indicative of a relatively small amount of multilayer adsorption on the open surface. This result indicated that Na-Y support is a microporous material

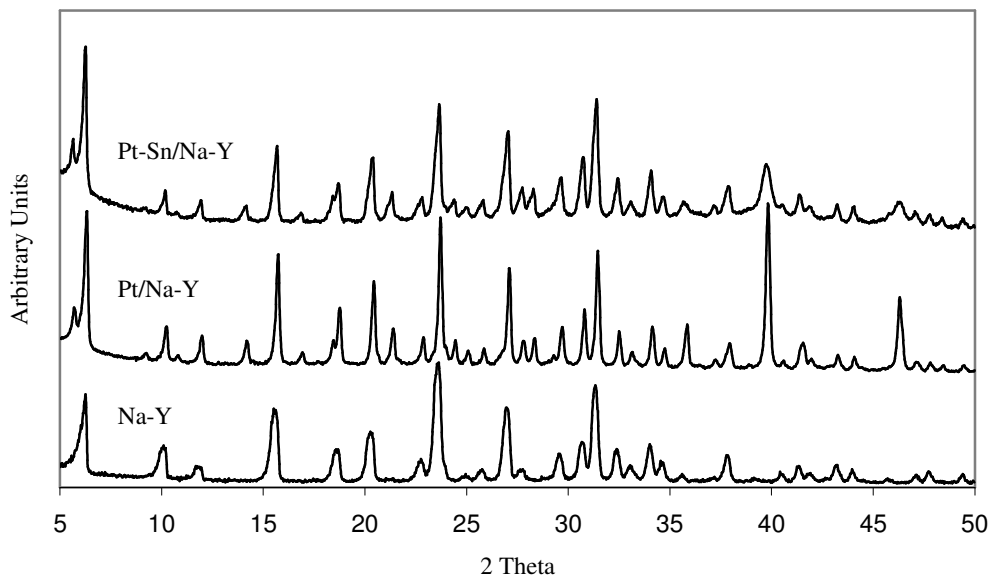


Figure 5.3. XRD diagram of monometallic and bimetallic Pt catalysts.

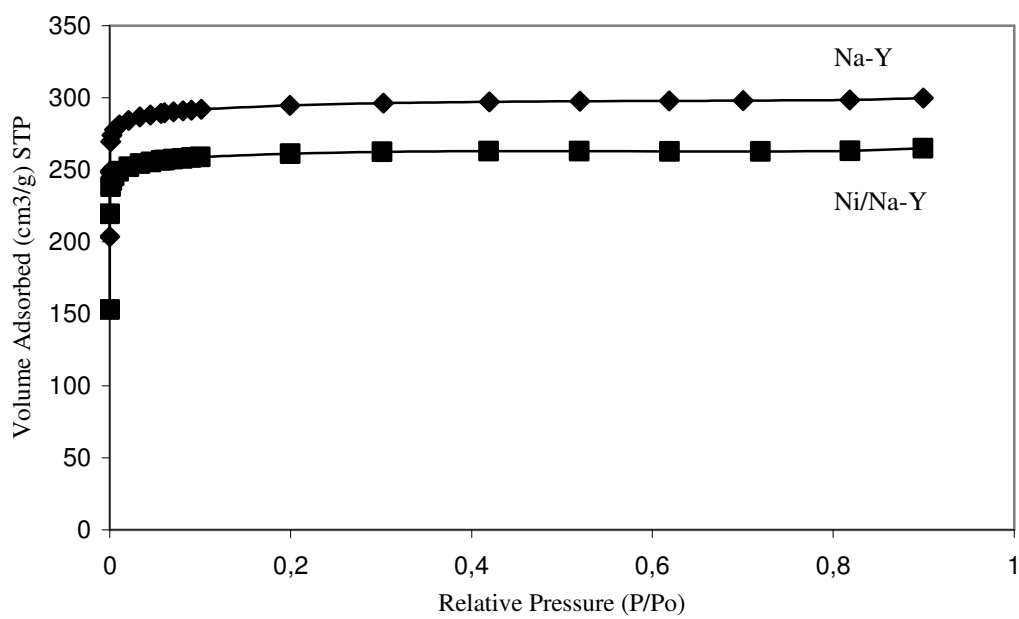


Figure 5.4. N<sub>2</sub> adsorption isotherms of Na-Y and Ni/Na-Y catalyst.

The surface area, pore volume and pore diameter measurements with Horvath-Kawazoe method for Na-Y support and monometallic catalysts are given in Table 5.3.

Table 5.3. Physico-chemical properties of Na-Y and Ni/Na-Y catalysts.

<b>Catalysts</b>	<b>BET Surface Area (m<sup>2</sup>/g)</b>	<b>Langmuir Surface Area (m<sup>2</sup>/g)</b>	<b>Micropore Area (m<sup>2</sup>/g)</b>	<b>Micropore Volume (cm<sup>3</sup>/g)</b>	<b>Median Pore Diameter (Å)</b>
Na-Y Zeolite	886.1	1292.4	818.3	0.426	5.6
Ni/Na-Y	785.7	1144.8	729.1	0.379	5.5

It was found that the catalyst surface areas and pore sizes changed due to metal loadings. For the catalyst Ni/Na-Y, BET surface area decreased with the metal loading. The blockage and/or narrowing of some of the pores due to the loadings can be the reason of the decrease in surface areas. This can be seen by reduction of micropore volumes of the catalysts.

### 5.1.2. Na-β Zeolite

The composition of Na-β support is given in Table 5.4. The metal loadings of monometallic and bimetallic catalysts are given in Table 5.5. The Si/Al ratio for Na-β zeolite was calculated as 12.4.

The Ni contents of monometallic and bimetallic catalysts were found as 8.2 % and 8.1 % respectively. The Sn content of bimetallic catalyst was 4.2 % and the Sn/Ni+Sn mol ratio of bimetallic catalyst was given in brackets.

The average of 10 EDX analyses gave similar Ni/Na-β composition. The difference between two analysis methods was around 3.3 %. The Si/Al ratios of monometallic and bimetallic catalyst supports were calculated as 12.0, which was very close to the value calculated from the ICP results.

Table 5.4. Chemical compositions of Na- $\beta$  zeolite.

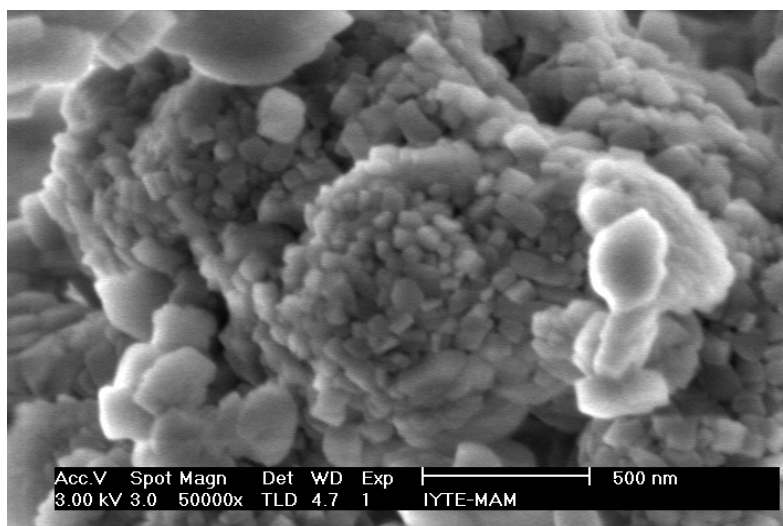
Compounds	Weight %
Al <sub>2</sub> O <sub>3</sub>	6.02
CaO	0.46
Fe <sub>2</sub> O <sub>3</sub>	0.09
K <sub>2</sub> O	0.99
MgO	0.11
Na <sub>2</sub> O	1.12
SiO <sub>2</sub>	87.63
H <sub>2</sub> O	3.58
<b>Total</b>	<b>100.00</b>

Table 5.5. Metal contents of Na- $\beta$  supported catalysts.

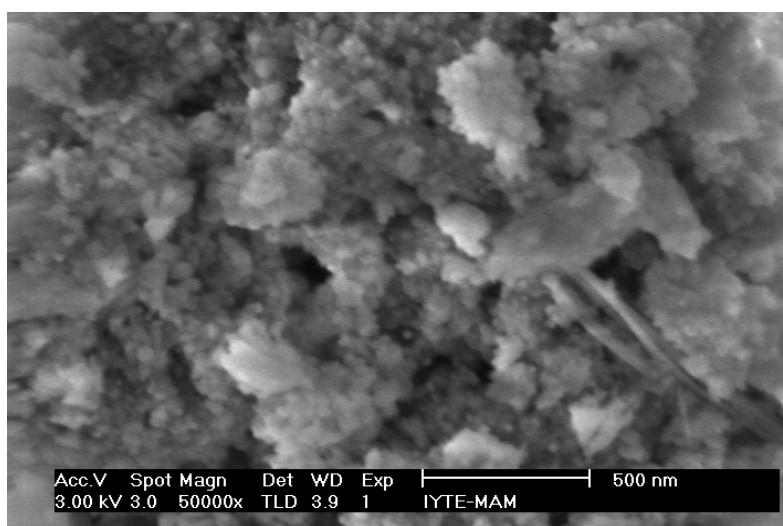
Catalysts	Metal Content (wt %)	Sn Content (wt %)
Ni/Na- $\beta$	8.2	-
Ni-Sn/ Na- $\beta$ (0.2)	8.1	4.2

Figure 5.5 shows the SEM images of Na- $\beta$  and Ni/ Na- $\beta$  catalysts. Na- $\beta$  had crystals smaller than 100 nm. The crystals were covered with Ni particles (Figure 5.5 (b)).

The XRD pattern of Na- $\beta$  supported monometallic and bimetallic catalysts are given in Figure 5.6. It was observed for the monometallic and bimetallic catalysts that the intensity of the main peaks of the support were significantly decreased by addition of metals on the support. The reduction of peak intensities could be due to coverage of crystal by loaded metals. As it is seen in the spectra, addition of Sn shifted the Ni peak to the left and lowered the  $2\theta$  value from  $44.5^\circ$  to  $43.5^\circ$ . The addition of Sn reduced the intensity of Ni peak in bimetallic catalyst. This could result from the coverage of Ni metal particles by Sn particles. Nickel-Tin alloy formation was not observed in the Ni-Sn/Na- $\beta$  bimetallic catalyst.



(a)



(b)

Figure 5.5. SEM micrographs of Na-β support (a) and Ni/ Na-β catalyst (b).

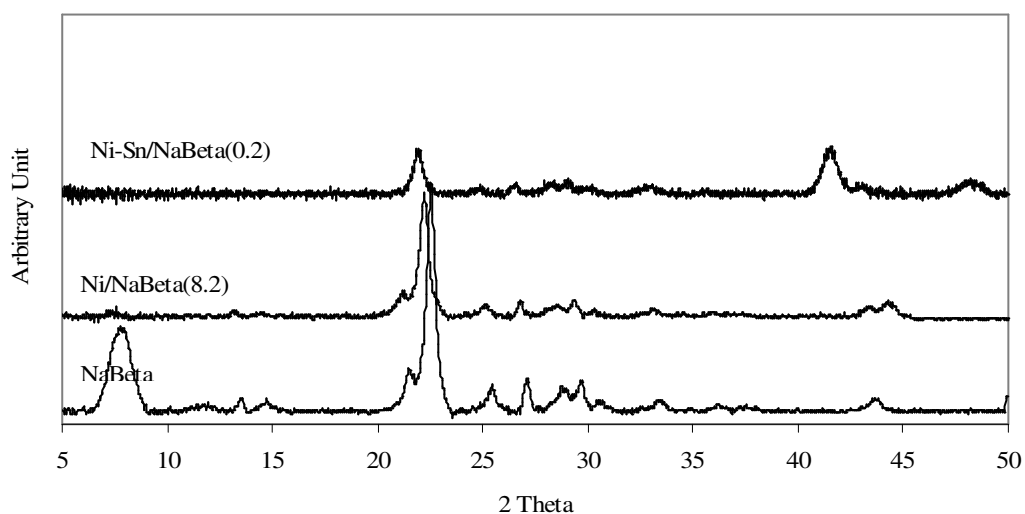


Figure 5.6. XRD diagram of Na- $\beta$  supported monometallic and bimetallic Ni catalysts.

Figure 5.7 shows the adsorption isotherms of Na- $\beta$ , Ni/Na- $\beta$  and Ni-Sn/Na- $\beta$ (0.2) catalysts. This support also showed Type I isotherm features, which indicates it is a microporous material. The surface area, pore volume and pore diameter measurements of Na- $\beta$ , Na- $\beta$  supported monometallic and bimetallic catalysts are given in Table 5.6. Pore size and pore volumes were determined using Horvath-Kawazoe method. The surface areas of monometallic and bimetallic catalysts were lower than that of the parent catalyst. Bimetallic catalysts had the lowest surface area. On the contrary it had the highest micropore volume. These changes could be attributed to the blockage and narrowing of some of the pores due to metal loading.

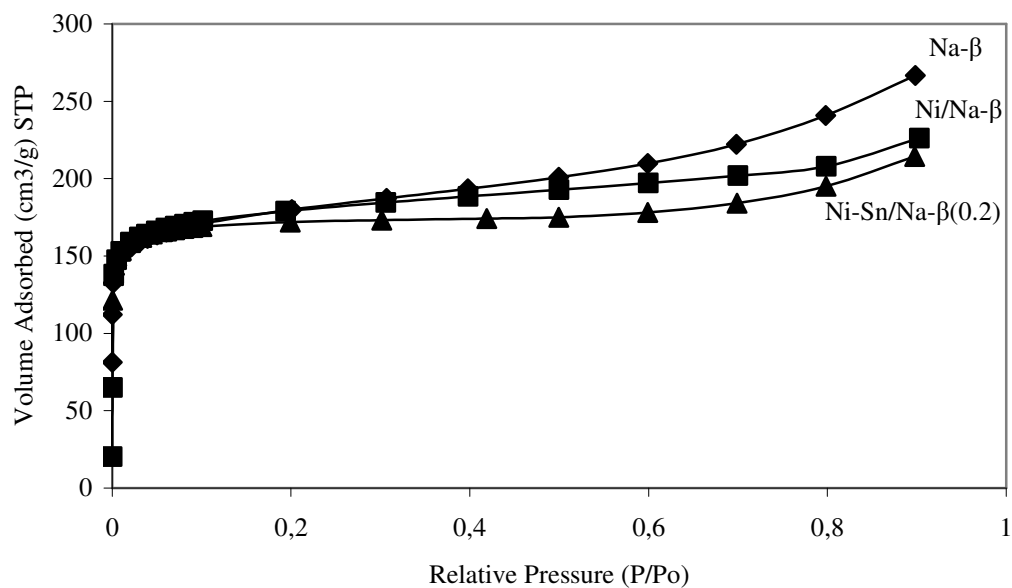


Figure 5.7. N<sub>2</sub> adsorption isotherms of Na-β and Ni/Na-β and Ni-Sn/Na-β catalysts.

Table 5.6. Physico-chemical properties of Na-β and Na-β supported catalysts.

Catalysts	BET Surface Area (m <sup>2</sup> /g)	Langmuir Surface Area (m <sup>2</sup> /g)	Micropore Area (m <sup>2</sup> /g)	Micropore Volume (cm <sup>3</sup> /g)	Median Pore Diameter (Å)
Na-β Zeolite	558.8	839.0	354.7	0.189	5.7
Ni/Na-β	549.2	802.1	390.7	0.208	7.1
Ni-Sn/Na-β (0.2)	515.8	759.4	445.2	0.235	6.6

### 5.1.3. Na-Mordenite Zeolite

Table 5.7 represents the composition of Na-Mordenite support. The metal loadings of monometallic and bimetallic catalysts are given in Table 5.8. Si/Al ratio for Mordenite was calculated as 9. This ratio was reported to change between 4.5 and 10 (Simoncic et al. 2005).

Table.5.7. Chemical compositions of Na-Mordenite zeolite.

Compounds	Weight %
Al <sub>2</sub> O <sub>3</sub>	7.60
CaO	0.08
Fe <sub>2</sub> O <sub>3</sub>	0.20
K <sub>2</sub> O	0.06
MgO	0.02
Na <sub>2</sub> O	6.14
SiO <sub>2</sub>	78.70
H <sub>2</sub> O	7.20
<b>Total</b>	<b>100.00</b>

Table 5.8. Metal contents of Na-Mordenite supported catalysts.

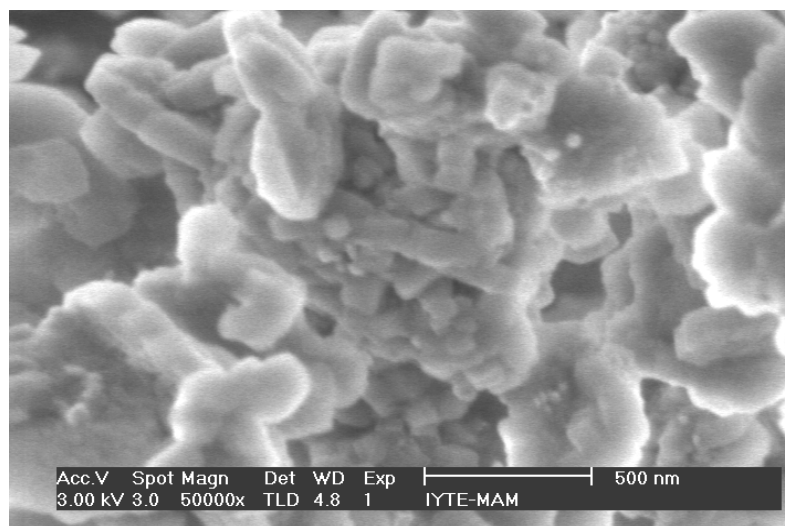
Catalysts	Metal Content (wt %)	Sn Content (wt %)
Ni/Na-Mordenite	8.80	-
Ni-Sn/Na-Mordenite(0.02)	8.30	0.4
Ni-Sn/Na-Mordenite(0.06)	8.20	1.2
Ni-Sn/Na-Mordenite(0.1)	8.30	2.2
Ni-Sn/ Na-Mordenite(0.2)	8.10	3.87

The catalysts Ni content was found to change between 8.1 % and 8.8 %. The errors in the preparation and/or analysis steps could cause these differences. Sn contents of the bimetallic catalysts were found in the range of 0.4-3.87 %. The molar Sn/Sn+Ni ratios of the catalysts are given in the brackets.

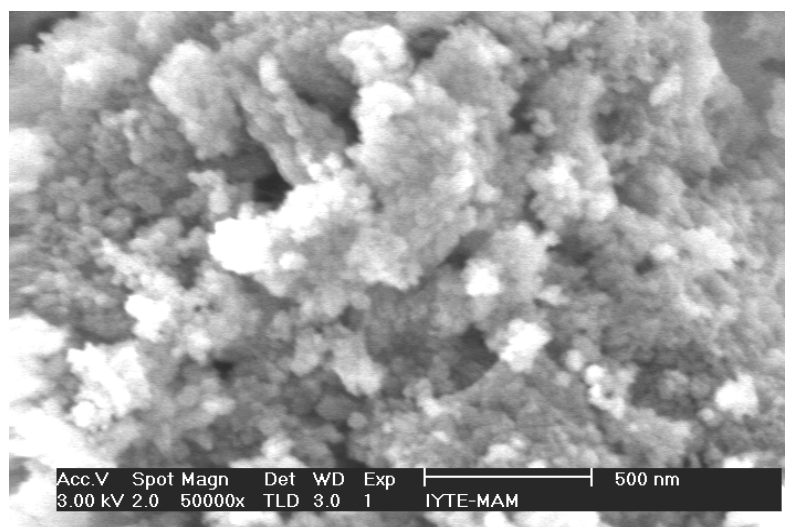
EDX analyses were performed for all monometallic and bimetallic catalysts. Si/Al ratio was calculated from the average of 10 EDX analysis as 8.3, which was so close to the value calculated from ICP analysis as 9. Also other element percentages were found to be close to that of obtained by ICP results. The difference between the results of two analysis techniques was calculated as 6.5 %.

Figure 5.8 shows the SEM micrographs of Na-Mordenite and Na-Mordenite supported Ni catalyst. Figure 5.8 (a) represents the irregular crystal structure of Na-

Mordenite sample with the crystal size ranging between 100-200 nm. The crystal surfaces of the catalysts were covered by the agglomerates of Ni particles (Figure 5.8(b)).



(a)



(b)

Figure 5.8. SEM micrographs of Na-Mordenite support (a) and Ni/Na-Mordenite catalyst (b).

Figure 5.9 shows the XRD patterns of Na-Mordenite, Na-Mordenite supported monometallic and bimetallic Ni catalysts. There were no significant changes in the position of the peaks of the Mordenite after Ni and Sn loading. In the monometallic and bimetallic samples Ni peak was observed at  $2\theta = 44.5^\circ$ . At  $2\theta = 44.8^\circ$  nickel tin alloy

was detected for the catalysts Ni-Sn/Na-Mordenite(0.2) and Ni-Sn/Na-Mordenite(0.1). For the other bimetallic catalysts, Ni-Sn alloy were not detected. This could be due to their low Sn content.

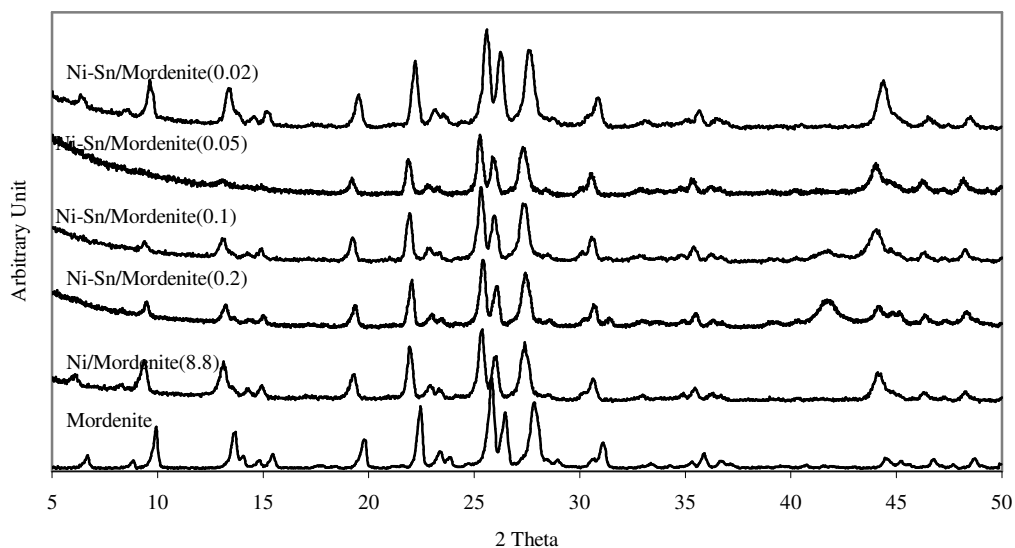


Figure 5.9. XRD diagram of Na-Mordenite supported monometallic and bimetallic Ni catalysts.

Figure 5.10 shows the N<sub>2</sub> adsorption isotherms of Na-Mordenite and Ni-Sn/Na-Mordenite(0.2) catalysts. Na-Mordenite support has microporous structure since it showed a Type I isotherm. The surface area, pore volume and pore diameter measurements with Horvath-Kawazoe method are given in Table 5.9. The surface area of the bimetallic catalyst decreased with metal loading. These findings showed that the metal loading caused the pore blockage and/or narrowing of the bimetallic catalysts differently. Average pore diameter of bimetallic catalyst Ni-Sn/Na-Mordenite(0.2) was lower than that of the support.

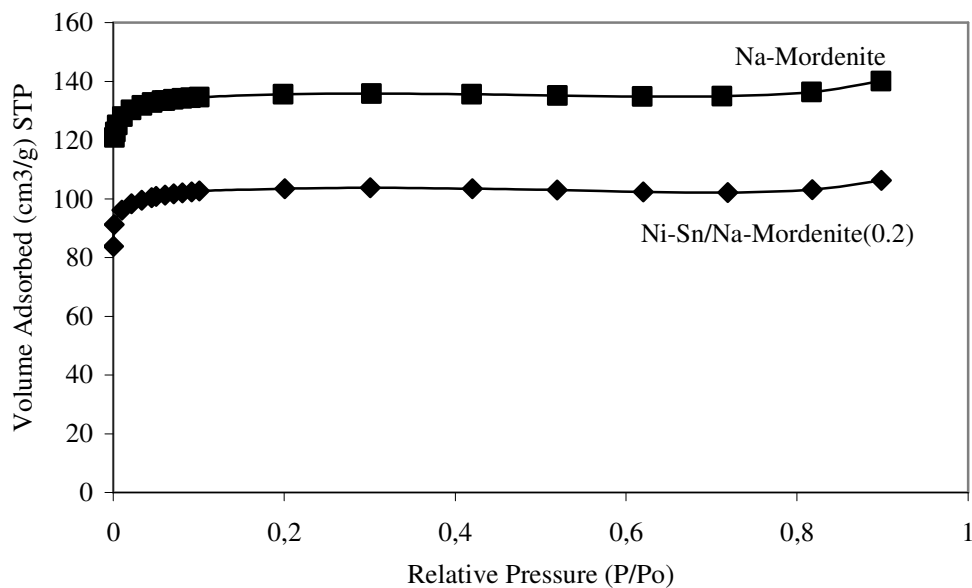


Figure 5.10. N<sub>2</sub> adsorption isotherms of Na-Mordenite and Ni-Sn/Na-Mordenite(0.2) catalysts.

Table 5.9. Physico-chemical properties of Na-Mordenite and Na-Mordenite supported catalysts.

Catalysts	BET Surface Area (m <sup>2</sup> /g)	Langmuir Surface Area (m <sup>2</sup> /g)	Micropore Area (m <sup>2</sup> /g)	Micropore Volume (cm <sup>3</sup> /g)	Median Pore Diameter (Å)
Na-Mordenite Zeolite	390.2	596.8	431.0	0.230	8.0
Ni-Sn/Mordenite(0.2)	348.2	531.4	420.1	0.223	8.5

#### 5.1.4. MCM-41 Zeolite

The elemental composition of pure silica MCM-41 support is given in Table 5.10. The metal loadings of monometallic and bimetallic catalysts are given in Table 5.11.

Table 5.10. Chemical composition of MCM-41 zeolite.

Compounds	% Weight
Al <sub>2</sub> O <sub>3</sub>	0.07
CaO	0.05
Fe <sub>2</sub> O <sub>3</sub>	0.08
K <sub>2</sub> O	0.04
MgO	0.01
Na <sub>2</sub> O	0.60
SiO <sub>2</sub>	95.05
H <sub>2</sub> O	4.10
<b>Total</b>	<b>100.00</b>

Table 5.11. Metal contents of MCM-41 supported catalysts

Catalysts	Metal Content (wt %)	Sn Content (wt %)
Ni/MCM-41	8.5	-
Ni-Sn/ MCM-41(0.033)	9.1	0.40
Ni-Sn/ MCM-41(0.042)	9.2	0.83
Pt/MCM-41*	5.0	-
Pt-Sn/ MCM-41(0.02) *	5.0	0.38

\*The content was calculated from initial solution composition.

The Ni contents of the monometallic and bimetallic catalyst varied between 8.5 % and 9.1 %. Sn contents of bimetallic Ni catalysts were found as 0.4 % and 0.83 %. The bimetallic Pt catalyst contained 0.38 % Sn and approximately 5 % Pt metal.

The SEM micrograph of synthesized MCM-41 support is given in Figure 5.11. The spherical particles with a size of around 0.5 μm could be easily observed. Besides, the hollow tubular structure with coaxial cylindrical nanometer channels of MCM-41 material could be marked. The gradual acidification process provides such a structure as it was indicated in the study of Lin et al. (1997).

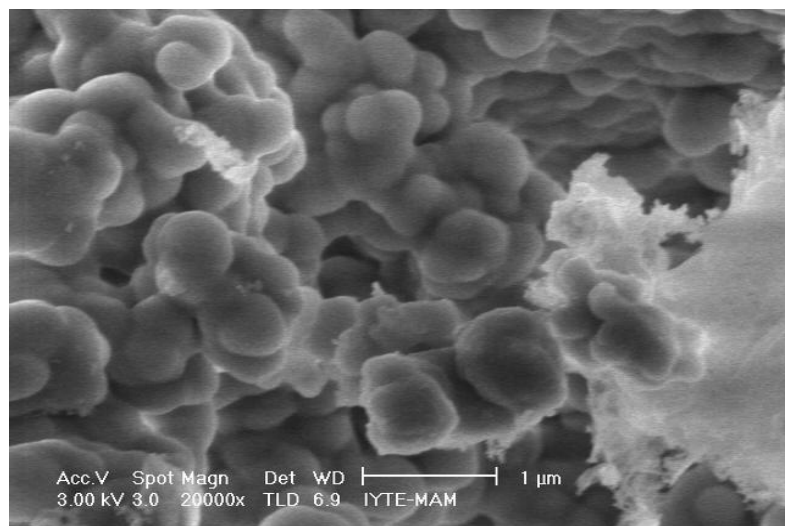


Figure 5.11. SEM picture of synthesized MCM-41.

Figure 5.12 shows the XRD pattern of the MCM-41. The XRD pattern had three reflections between  $2\theta = 2^\circ$  and  $6^\circ$ , which was in accordance with those found in literature (Ciesla et al. 1999).

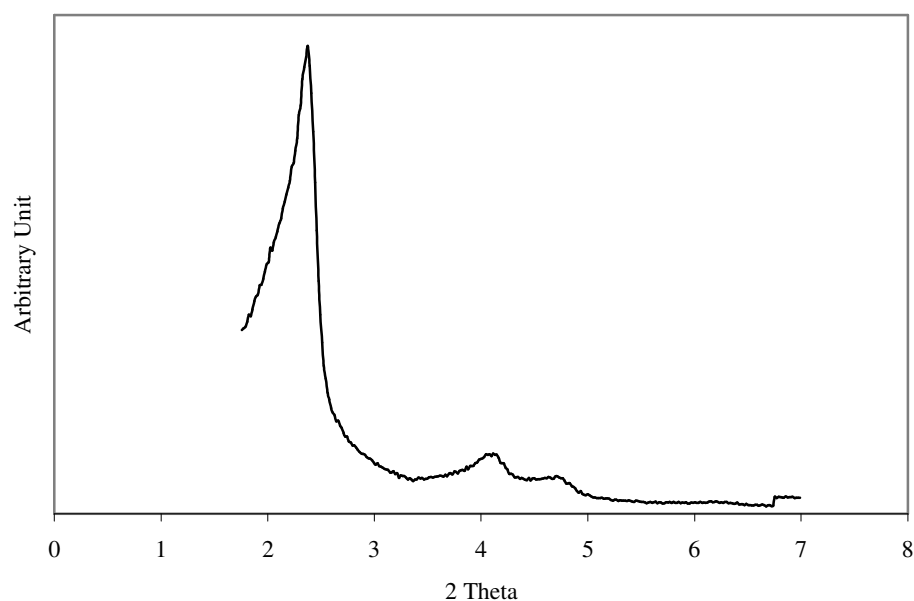


Figure 5.12. XRD diagram of synthesized MCM-41.

The XRD patterns of MCM-41 supported monometallic and bimetallic Pt catalysts are given in Figure 5.13. Although no reflections were observed at higher angles for the MCM-41 material, the XRD spectra of monometallic and bimetallic catalysts were taken between  $2\theta = 5^\circ$  and  $50^\circ$  in order to observe the peaks of metals loaded. The main Pt peaks were observed at  $2\theta = 39.83^\circ$  and  $46.3^\circ$  for both

monometallic and bimetallic catalysts. In the bimetallic catalyst the peak intensities were reduced by the addition of Sn metal. This could result from the coverage of some Pt metal surfaces by Sn metal particles. The search-match analysis showed that the peaks of PtSn<sub>2</sub> alloy were at  $2\theta = 40.5^\circ$  and  $46.8^\circ$ , which were very close to the Ni peaks.

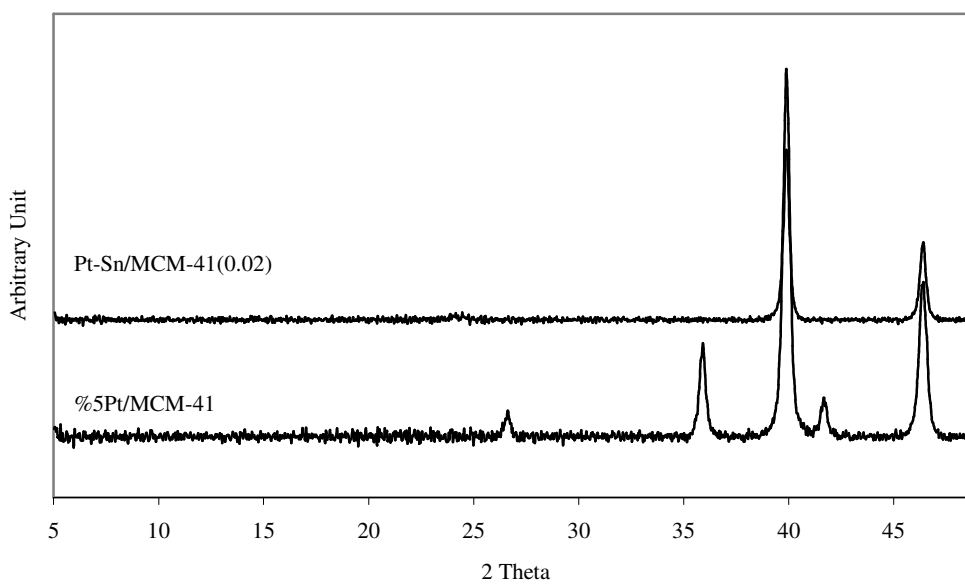


Figure 5.13. XRD diagram of MCM-41 Supported Pt catalysts.

Figure 5.14 shows the N<sub>2</sub> adsorption isotherms of MCM-41, Ni/MCM-41 and Ni-Sn/MCM-41(0.033) catalysts. MCM-41 support showed a plateau after the point around  $(P/P_0)=0.4$  indicating that it has a mesoporous structure. The surface area, pore volume and pore diameter measurements of MCM-41 support, monometallic and bimetallic catalysts with BJH method are given in Table 5.12.

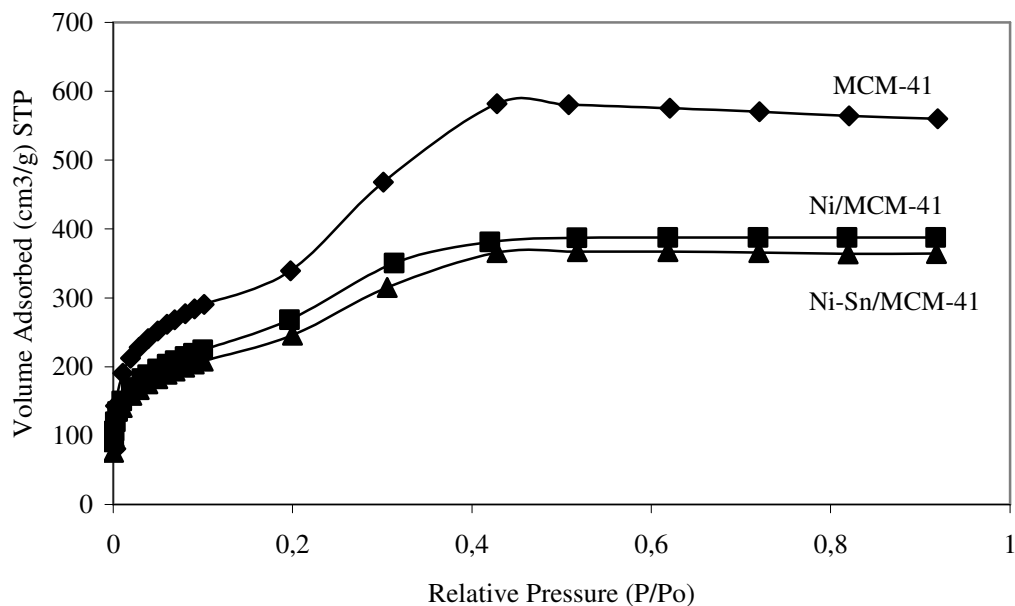


Figure 5.14. N<sub>2</sub> adsorption isotherms of MCM-41, Ni/MCM-41 and Ni-Sn/MCM-41(0.033) catalysts.

Table 5.12. Physico-chemical properties of MCM-41, Ni/MCM-41, Ni-Sn/MCM 41(0.033) catalysts.

Catalysts	BET Surface Area (m <sup>2</sup> /g)	Langmuir Surface Area (m <sup>2</sup> /g)	Micropore Area (m <sup>2</sup> /g)	Micropore Volume (cm <sup>3</sup> /g)	Average Pore Diameter (Å)
MCM-41	1449.0	1692.3	298.2	0.024	20.7
Ni/MCM-41	1074.2	1352.2	72.5	0.020	21.5
Ni-Sn/ MCM-41(0.033)	984.3	1387.1	59.2	0.023	21.3

The BET surface areas of monometallic and bimetallic catalysts are smaller than that of the parent catalyst. The metal loading decreased the micropore volumes of the supports due to the blockage and/or narrowing of the pores.

### 5.1.5. Clinoptilolite

The chemical compositions of clinoptilolite is given in Table 5.13 and Table 5.14 shows the metal contents (Pt, Ni, Sn) of monometallic and bimetallic clinoptilolite supported catalysts. The Si/Al ratio of clinoptilolite sample was found as 5.3, which was reported to be in the range of 4.25-5.25 (Breck 1974).

Table 5.13. Chemical compositions of clinoptilolite.

Compounds	Weight %
Al <sub>2</sub> O <sub>3</sub>	12.30
CaO	1.80
Fe <sub>2</sub> O <sub>3</sub>	1.10
K <sub>2</sub> O	4.80
MgO	0.90
Na <sub>2</sub> O	1.60
SiO <sub>2</sub>	67.30
H <sub>2</sub> O	10.20
<b>Total</b>	100.00

Table 5.14. Metal Contents of Clinoptilolite Supported Catalysts.

Catalysts	Metal Content (wt %)	Sn Content (wt %)
Ni/Clinoptilolite	9.00	-
Ni-Sn/Clinoptilolite (0.2)	8.50	4.6
Pt/Clinoptilolite*	5	-
Pt-Sn/Clinoptilolite*	5	4.4

- The content was calculated from initial solution composition.

The Ni content of monometallic and bimetallic catalysts were 9 % and 8.5 % respectively. The Pt content was calculated from the initial solution composition. The bimetallic Ni catalyst contained 4.6 % and bimetallic Pt catalyst contained 4.4 % Sn.

EDX analysis of monometallic and bimetallic Pt and Ni catalysts gave similar composition to that obtained by ICP analysis. The difference between the two methods was calculated as 8.8 %. The Si/Al ratio of clinoptilolite catalysts were calculated as around 5.1. This ratio was also calculated as 5.34 by Uçar et al. (2002).

Figure 5.15 shows the SEM micrograph of clinoptilolite support. The crystals were regular and platelike. Since the clinoptilolite used was a natural zeolite, the impurities were also observed.

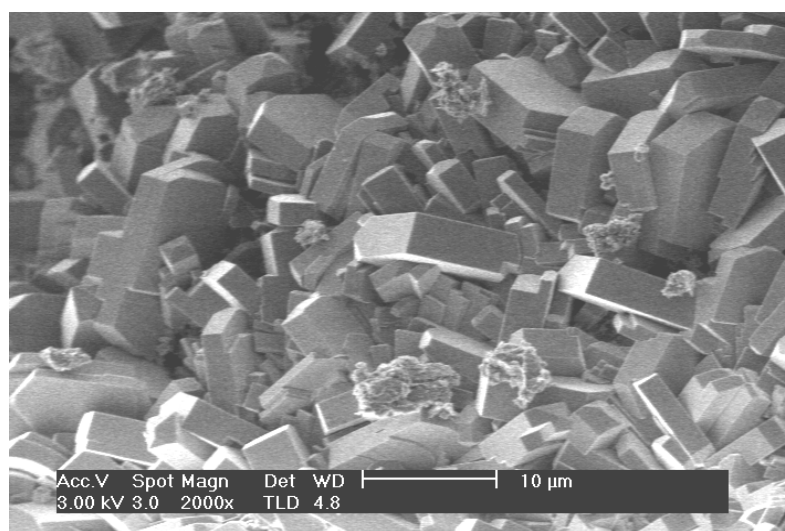


Figure 5.15. SEM micrographs of clinoptilolite support.

The XRD patterns of clinoptilolite support, monometallic and bimetallic catalysts are given in Figure 5.16. The characteristic peaks of clinoptilolite were observed in this spectra at  $2\theta = 9.93^\circ$ ,  $22.48^\circ$  and  $30.18^\circ$ . Significant changes were detected in the spectra of Ni/Clinoptilolite sample compared to the clinoptilolite and the bimetallic Ni-Sn/Clinoptilolite (0.2) samples. The reason of these changes could be the coverage of the crystal surfaces by metal agglomerates due to the impregnation processes. On the other hand for the monometallic and bimetallic catalyst Ni peak could be seen clearly at  $2\theta = 44.5^\circ$ . Sn or  $\text{Ni}_4\text{Sn}$  peaks were not detected. In the spectrum of the bimetallic Pt catalyst, it was possible to see the Pt peaks at  $2\theta = 39.83^\circ$  and  $46.3^\circ$ . The search-match analysis showed that there was a  $\text{PtSn}_2$  alloy formation, which was observed at  $2\theta = 40.5^\circ$  and  $46.8^\circ$  near the Pt peaks.

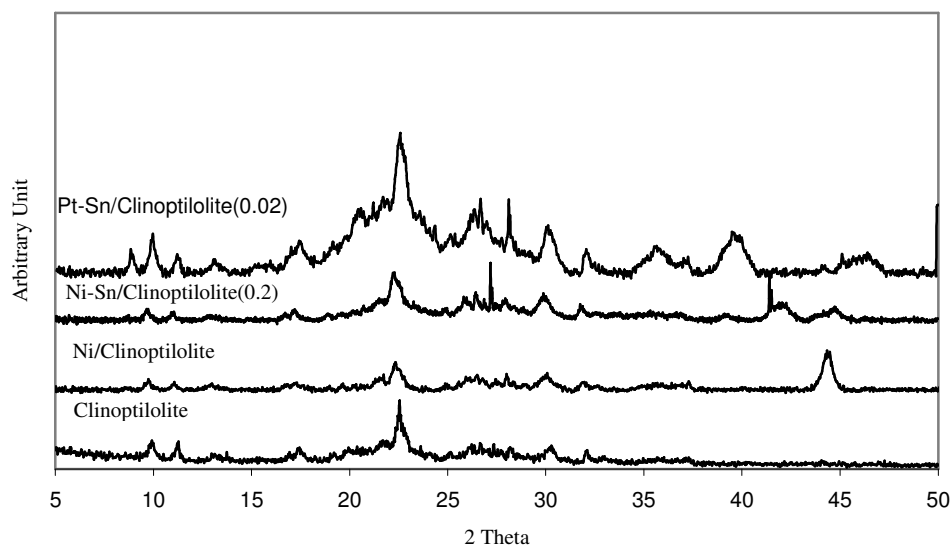


Figure 5.16. XRD diagram of clinoptilolite support, monometallic and bimetallic Ni and Pt catalysts.

Figure 5.17 shows the  $N_2$  adsorption isotherms of Clinoptilolite, Ni/Clinoptilolite and Ni-Sn/ Clinoptilolite (0.2) catalysts. This support showed a Type II isotherm. This type of isotherm is normally associated with monolayer-multilayer adsorption on an open and stable external surface of a powder, which may be non-porous, macroporous or even to a limited extent microporous.

The surface area, pore volume and pore diameter measurements of clinoptilolite support, monometallic and bimetallic catalysts by Horvath-Kawazoe method are given in Table 5.15. The measured surface area were too small for clinoptilolite, as only the surface area of the pores accessible by  $N_2$  molecule were determined. The data was used for comparison proposes. Surface areas of clinoptilolite decreased by metal loading. Average pore diameters also decreased while the micropore volumes are similar to each other. The decreases in surface areas and pore diameters could be explained by the fact that metal loading blocked and/or narrowed some pores.

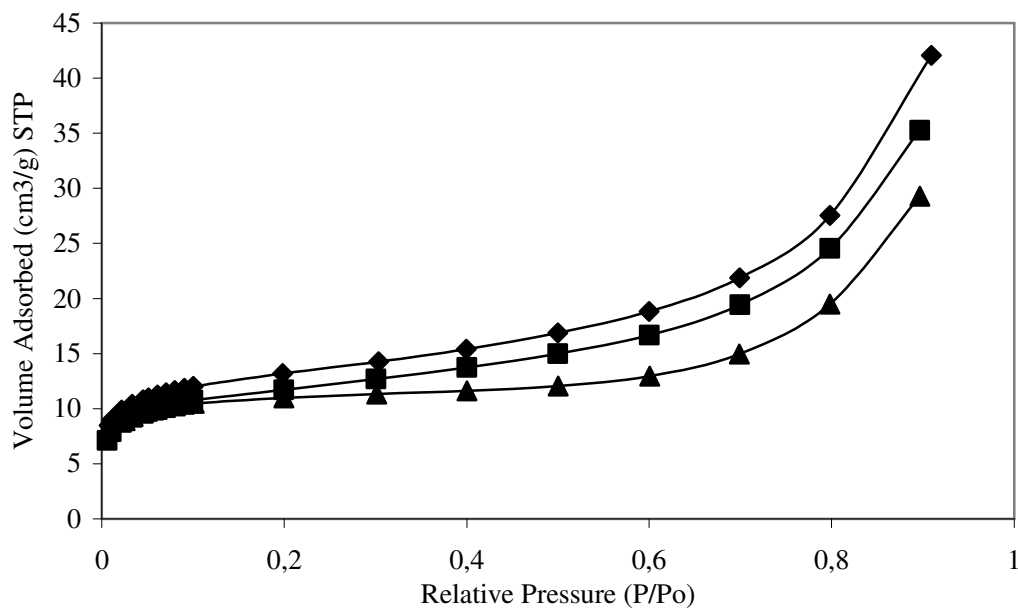


Figure 5.17. N<sub>2</sub> adsorption isotherms of Clinoptilolite, Ni/ Clinoptilolite and Ni-Sn/ Clinoptilolite (0.2) catalysts (♦) Clinoptilolite, (■) Ni/Clinoptilolite, (▲)Ni-Sn/Clinoptilolite(0.2).

Table 5.15. Physico-chemical properties of Clinoptilolite, Ni/Clinoptilolite, Ni-Sn/Clinoptilolite, Pt/Clinoptilolite catalysts.

Catalysts	BET Surface Area (m <sup>2</sup> /g)	Langmuir Surface Area (m <sup>2</sup> /g)	Micropore Area (m <sup>2</sup> /g)	Micropore Volume (cm <sup>3</sup> /g)	Median Pore Diameter (Å)
Clinoptilolite	43.3	62.1	15.5	0.008	9.8
Ni/Clinoptilolite	38.6	55.0	15.6	0.008	9.4
Ni-Sn/Clinoptilolite(0.2)	34.1	50.1	21.5	0.011	12.1

## 5.2. Catalyst Testing

The prepared catalysts were tested in citral hydrogenation reaction. Reactions were carried out at 80°C temperature, 6 bar pressure and 600 rpm stirring speed with 250 mg of catalysts.

The citral conversion was calculated as the mole percent of reactant consumed as follows:

$$\text{Conversion (mole \%)} = \frac{(\text{citral})_{in} - (\text{citral})_{out}}{(\text{citral})_{in}} \times 100$$

The selectivities to desired products were defined as the ratio of the number of moles of product to the number of moles of the reactant consumed. The yields of desired products were defined as the ratio of number of moles of desired product to the reactant. Calculations were done as follows:

$$\text{Selectivity to Desired Product (mole \%)} = \frac{(\text{Product})_{out}}{(\text{citral})_{in} - (\text{citral})_{out}} \times 100$$

$$\text{Yield of Desired product (mole \%)} = \frac{(\text{Product})_{out}}{(\text{citral})_{in}} \times 100$$

The relationship between conversion, yield and selectivity is as follows:

$$\text{Yield} = \text{conversion} \times \text{selectivity}$$

The calculations showed that the mass input of reactants at the beginning of the reaction was recovered during and at the end of the reaction with a difference of 5 %. This difference in the mass balance was attributed to the presence of products, which formed in very small amounts.

The citral hydrogenation reaction gives variety of products that are citronellal, citronellol, nerol, geraniol, isopulegol, 3,7-Dimethyl-1-octanol, menthols and acetals (Section 2.2, Figure 2.2). Three different acetal peaks were observed in GC chromatograms. These peaks might belong to the citral or citronellal acetals. Figure 5.18 shows a typical GC chromatogram that contained the characteristic peaks of citral hydrogenation products obtained during this study. The GC-MS chromatograms of each product were given in Appendices section.

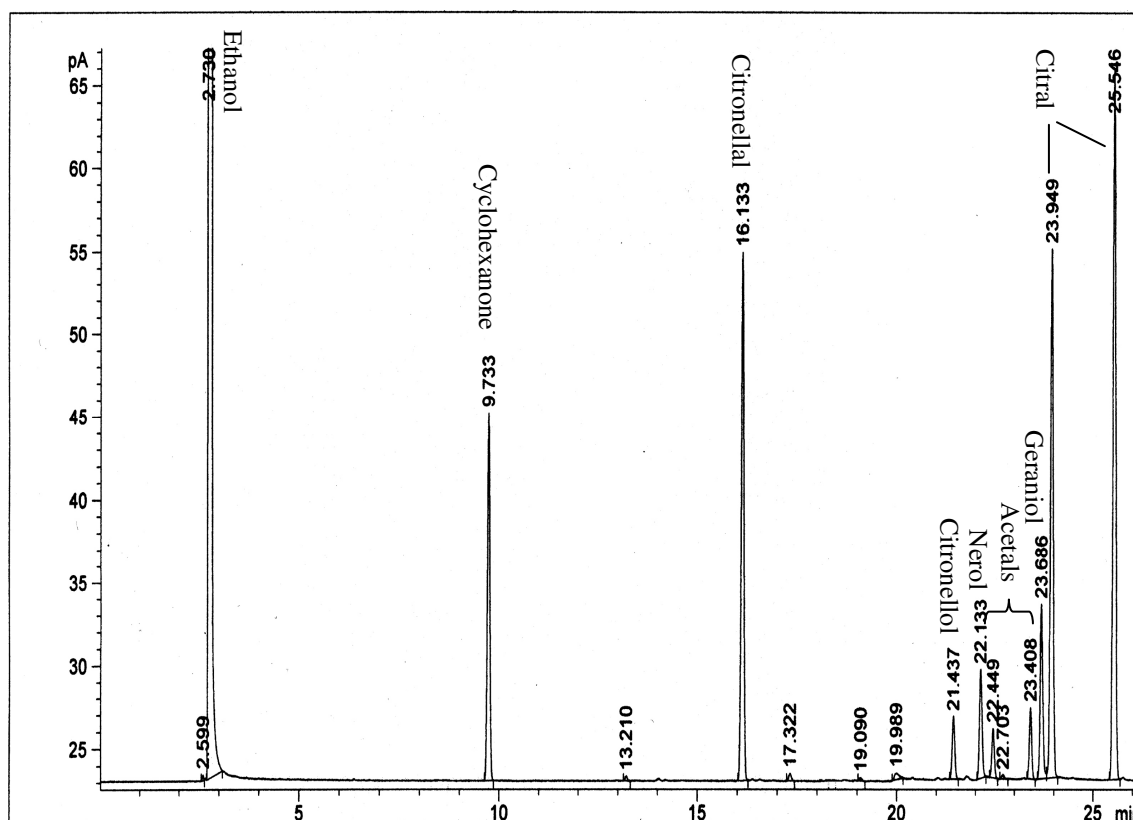


Figure 5.18. Characteristic peaks of citral hydrogenation products.

### 5.2.1. Ni/Na-Y & Ni-Sn/Na-Y Catalysts

The Na-Y supported catalysts were Ni/Na-Y, Ni-Sn/Na-Y(0.02), Ni-Sn/Na-Y(0.05), Ni-Sn/Na-Y(0.1) and Ni-Sn/Na-Y(0.2). The product distribution over monometallic Ni/Na-Y catalyst up to the reaction time of 300 minutes is shown in Figure 5.19.

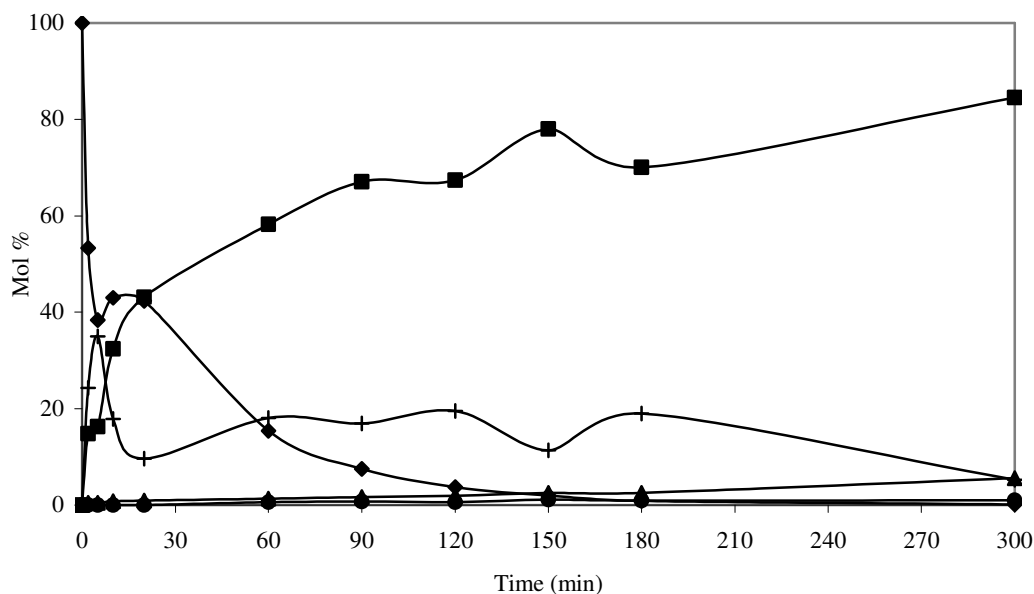


Figure 5.19. Product distribution of citral hydrogenation over Ni/Na-Y catalyst: (◆) Citral; (■) Citronellal; (▲) Citronellol; (●) Isopulegol; (+) Acetals.

It was observed that citral was mainly converted to citronellal and acetal over the monometallic Ni/Na-Y catalyst. After the complete conversion of citral at 180 min, most of the acetal formed was converted to citronellal. This suggested that acetal formed could be citronellal acetal. At the end of the reaction time of 300 min large amount of citronellal (84.5 %), small amounts of citronellol (5 %), acetal (5.5 %) and isopulegol (<1 %) were obtained. Monometallic Ni/Na-Y catalyst was found to be the most active and more selective to citronellal. This result is opposite of the results of Arvela et al. (p.g. 9). The differences between these studies are types of supports and the preparation techniques. They used the H and NH<sub>4</sub> forms of the Y zeolite, which had very strong acid sites. These acid sites prefer the side reactions and give undesired products. The importance of the form of the Y zeolite was also shown by the study of Blackmond et al. (1991). Also the preparation method can cause differences in the product distribution.

The product distribution over bimetallic catalysts for different Ni/Ni+Sn ratio is shown in Figure 5.20. The product distribution changed with Sn/Ni+Sn ratio. The main product for all the bimetallic catalysts was again citronellal. Its amount changed differently for different catalysts. Acetal formation was also observed. The striking

difference between monometallic and bimetallic catalysts was that nerol formation was observed with bimetallic catalysts. However its amount was low. This showed that Sn addition had modified active Ni metal properties. This was in agreement with the literature finding that unsaturated alcohol formation increased by bimetallic Sn catalysts (Section 3.2.2).

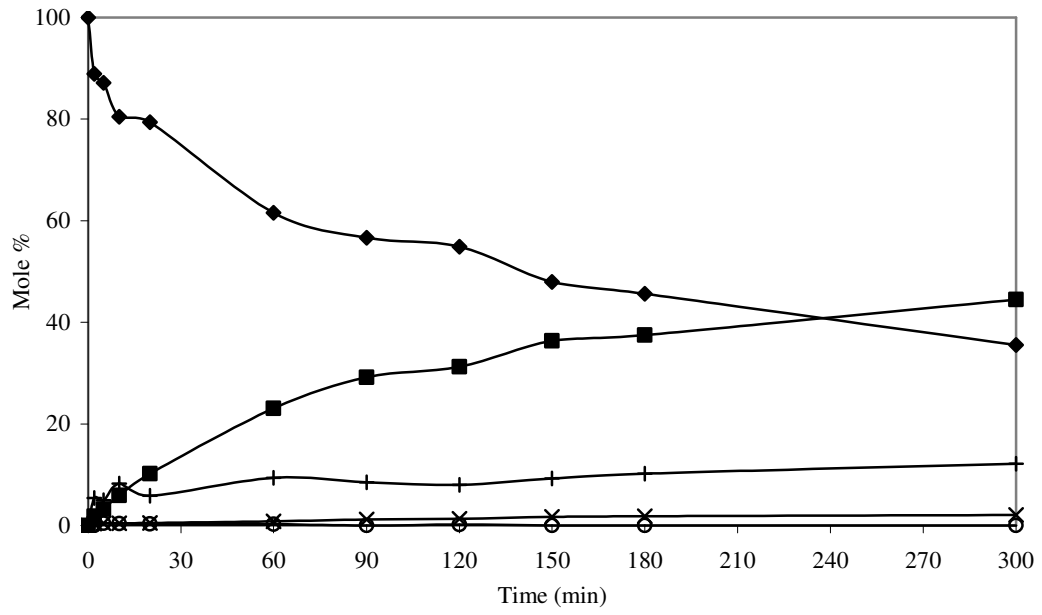
For the catalyst Ni-Sn/Na-Y(0.02), citral was transformed to citronellal and acetal during 300 min. The amount of citronellal was 45 %, the amount of acetal was 12 %, nerol composition was 2 % and geraniol composition was smaller than 1 % at the end of the reaction.

Catalyst Ni-Sn/Na-Y(0.05) led to an increase in the composition of citronellal from 45.5 to 59 %. Acetal formed during 90 min of the reaction was then converted to citronellal. The increase in the Sn content of the bimetallic catalyst increased the formation of nerol (4.5 %) and decreased the production of acetal (6 %).

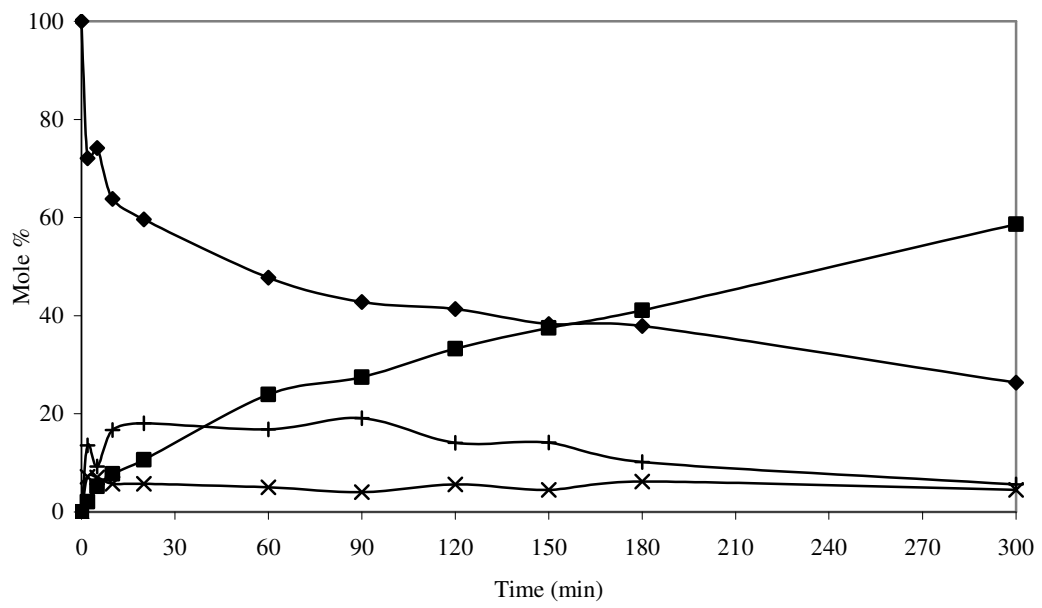
With the catalyst Ni-Sn/Na-Y(0.1), there was a small increase in the concentration of nerol (5 %) and acetal (8 %) while the amount of citronellal decreased to 47 %.

When the Sn/Ni+Sn ratio increased to 0.2, less acetal was formed. In the first 15 min of reaction some acetals were formed and then they transformed to citronellal. Between the reaction time of 90 and 180 min acetal formation was also observed. The amount of nerol increased to the value of 6.2 % and the citronellal amount was decreased to 33.5 %. Small amount of citronellol (<1 %) was also produced.

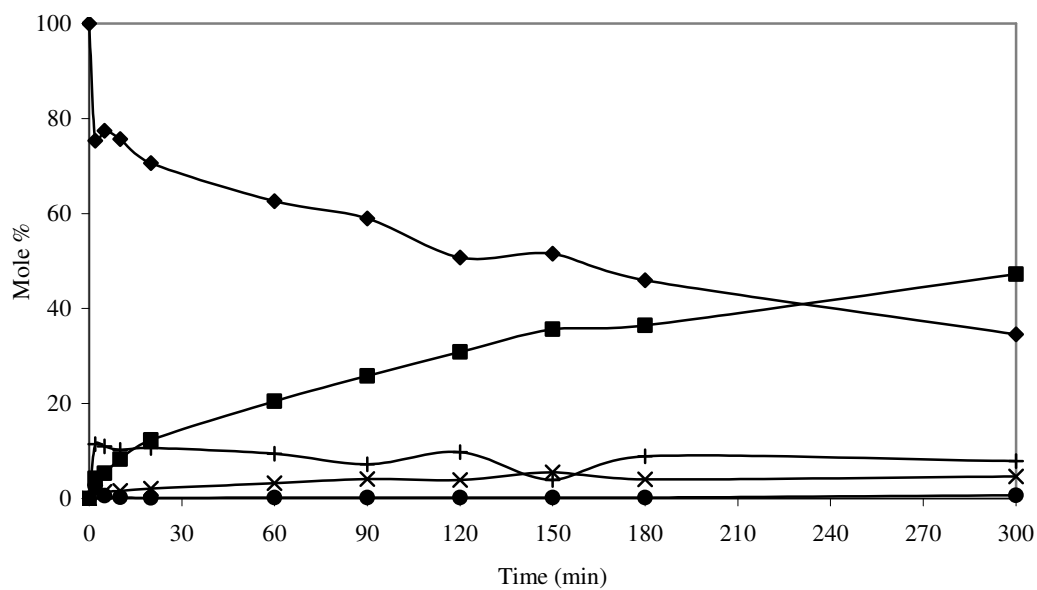
Sn loading decreased the monometallic catalyst activity. This showed that some of the active Ni sites were blocked by Sn particles. This can also be attributed to decrease of surface area by higher metal loading. Lower amounts of acetal were formed by bimetallic catalysts compared to monometallic catalyst.



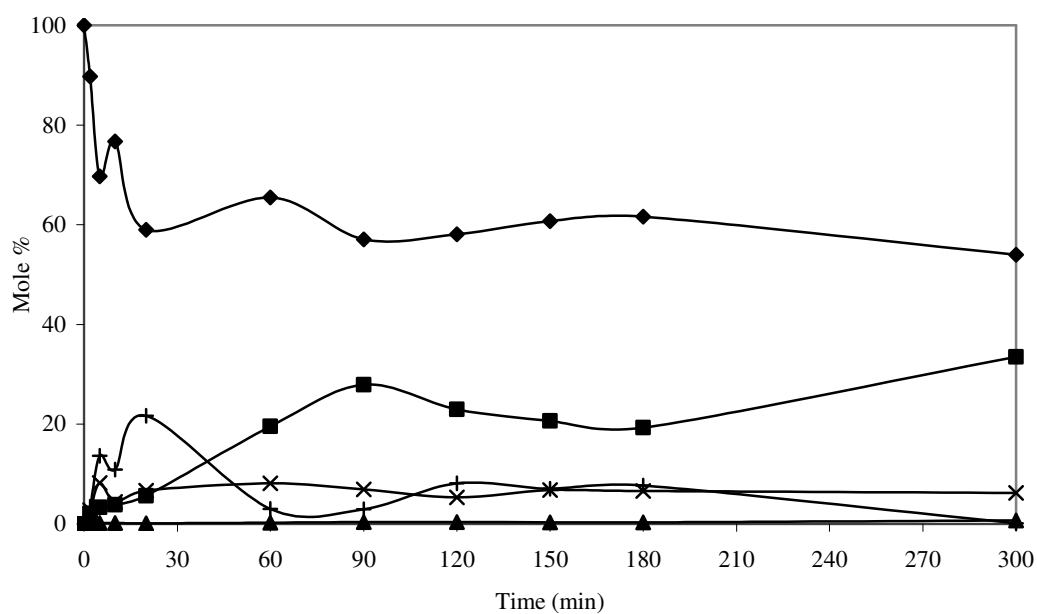
(a)



(b)



(c)



(d)

Figure 5.20. Product distribution of citral hydrogenation over Ni-Sn/Na-Y (0.02) (a), Ni-Sn/Na-Y (0.05) (b) and Ni-Sn/Na-Y (0.1) (c) and Ni-Sn/Na-Y(0.2) (d): (◆) Citral; (■) Citronellal; (▲) Citronellol; (●) Isopulegol; (×) Nerol; (+) Acetals; (○) Geraniol.

The change of acetal formation with respect to reaction time for the reaction performed over Ni-Sn/Na-Y(0.05) catalyst is given in Figure 5.21.

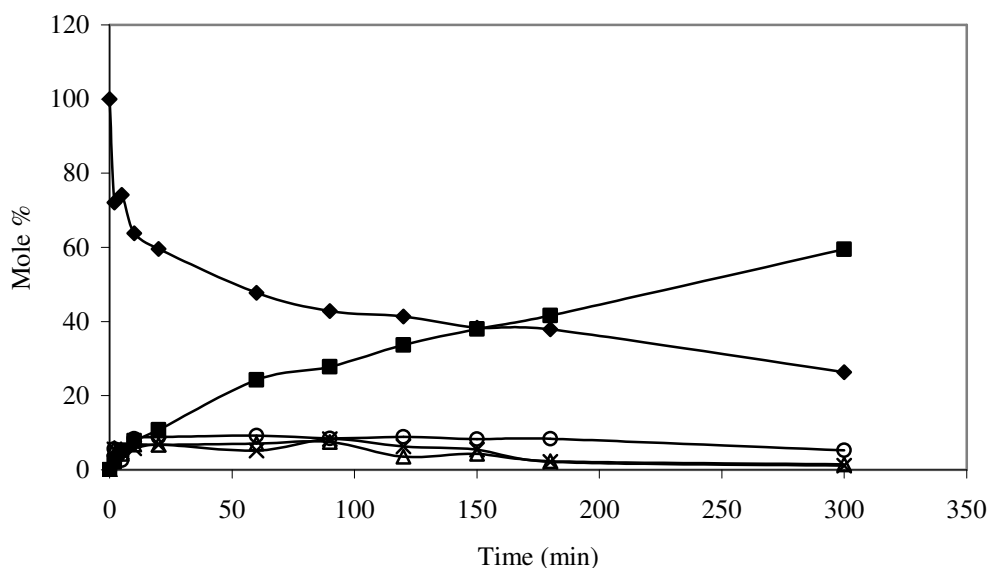


Figure 5.21. Change of acetal formation with respect to reaction time over Ni-Sn/Na-Y(0.05) catalyst. (◆) Citral; (■) Citronellal; (×) Acetal 1; (Δ) Acetal 2; (○) Acetal 3.

The acetal peaks at retention times of 22.44, 22.7 and 23.4 min were referred to as Acetal(1), Acetal(2) and Acetal(3). The main acetal observed in Figure 5.21 was Acetal(3). The amount of Acetal(1) decreased while the citronellal amount increased. Thus Acetal(1) can be the citronellal acetal.

The conversion of citral, selectivity to UOLs, citronellal and yield of these products in the hydrogenation of citral over monometallic and bimetallic catalysts are tabulated in Table 5.16.

Table 5.16. Conversion, selectivity and yield values with Ni/Na-Y and Ni-Sn/Na-Y catalysts (t=300 min).

Catalysts	Conversion	Selectivity		Yield	
		UOLs	Citronellal	UOLs	Citronellal
Ni/Na-Y	>99	<1	85.0	<1	85.0
Ni-Sn/Na-Y(0.02)	64.5	3.2	69.0	2.0	45.0
Ni-Sn/Na-Y(0.05)	74.0	6.0	80.0	4.5	59.0
Ni-Sn/Na-Y(0.1)	65.5	7.2	72.2	5.0	47.3
Ni-Sn/Na-Y(0.2)	46.0	14.00	73.0	6.2	34.0

The highest conversion (99 %) was obtained with the monometallic Ni/Na-Y catalyst but the selectivity to unsaturated alcohols was lower than that obtained from bimetallic catalysts. The highest citral conversion acquired with the bimetallic Ni-Sn/Na-Y(0.05) catalysts was 74 %. The most selective catalyst to the unsaturated alcohols was Ni-Sn/Na-Y(0.2) with the selectivity and yield of 14 % and 6.2 % respectively.

The changes in selectivity to unsaturated alcohols, nerol and geraniol, over bimetallic catalysts supported by Na-Y zeolite support can be seen on the selectivity versus Sn/Sn+Ni graph in Figure 5.22. Selectivity to nerol and geraniol increased with Sn content of the catalyst.

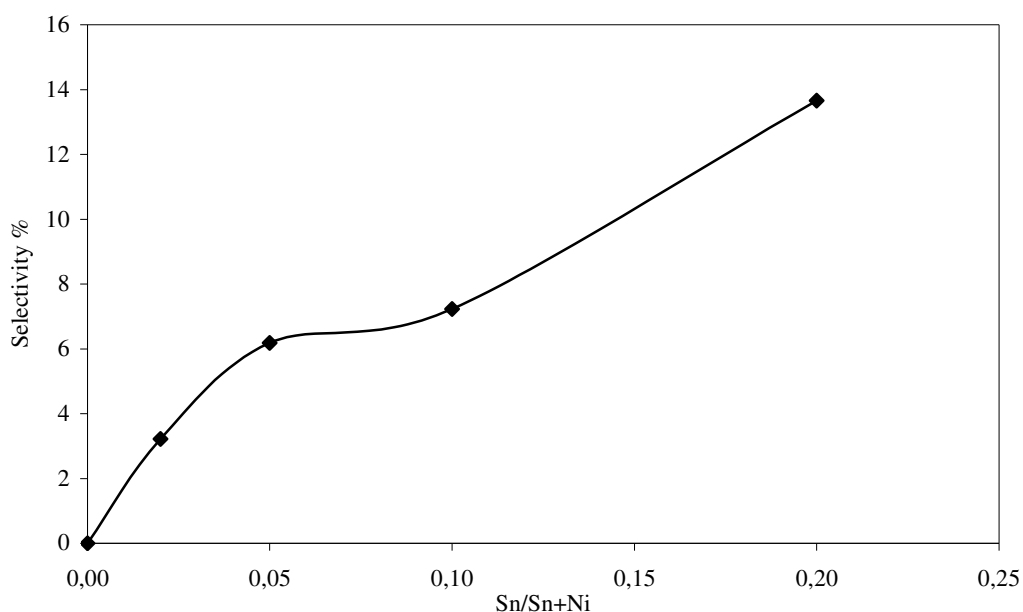


Figure 5.22. Selectivity to unsaturated alcohols as a function of Sn/Sn+Ni ratio.

### 5.2.2. Ni/Na- $\beta$ & Ni-Sn/Na- $\beta$ Catalysts

The Na- $\beta$  supported catalysts were Ni/Na- $\beta$  and Ni-Sn/Na- $\beta$ (0.2). Figure 5.23 represents the product distribution of citral hydrogenation over monometallic Ni/Na- $\beta$  catalyst.

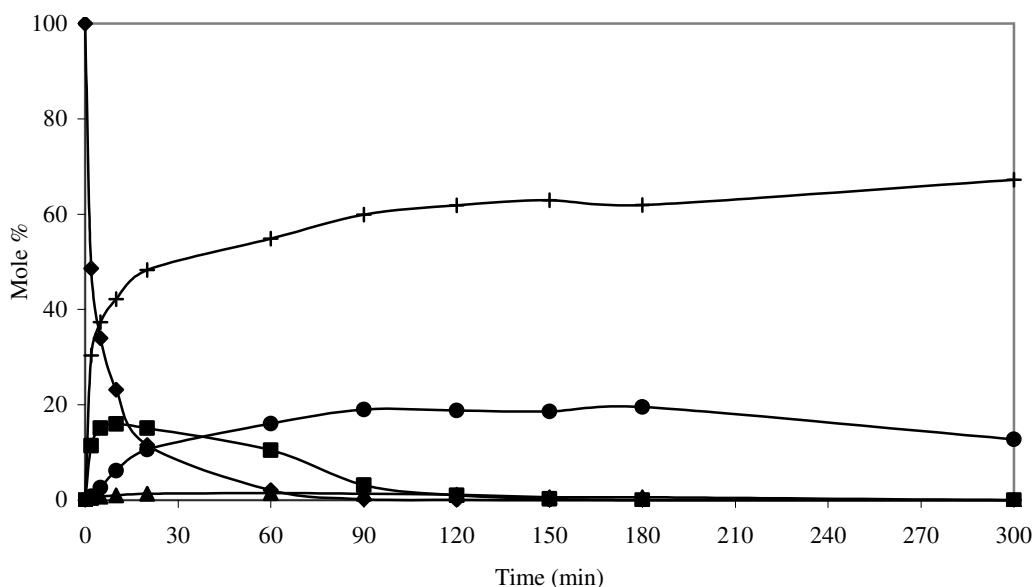


Figure 5.23. Product distribution of citral hydrogenation over monometallic Ni/Na- $\beta$  catalyst: (◆) Citral; (■) Citronellal; (▲) Citronellol; (●) Isopulegol; (+) Acetals.

The major product observed with monometallic catalyst was acetal. Citronellal formation was observed in the first 2 min of reaction and then it was almost all transformed to acetals. Another product produced was isopulegol. At the end of the reaction time of 300 min, reaction mixture contained 67 % acetal and 13 % isopulegol. Isopulegol is formed from the isomerization reaction (Figure 2.2). Isomerization reaction takes place on acid sites. Thus, the formation of isopulegol suggested that Ni/Na- $\beta$  catalyst had acid sites.

Similar product distribution was observed over bimetallic catalyst Ni-Sn/Na- $\beta$ (0.2) as it is shown in Figure 5.24. The main product was acetal again. At the end of the reaction 71 % of acetal, 4 % of isopulegol, 3 % of citronellol and small amounts of nerol and geraniol (<1 %) were observed. Sn loading decreased the catalyst activity and isopulegol formation. This showed the interaction of Sn with Ni and acid sites.

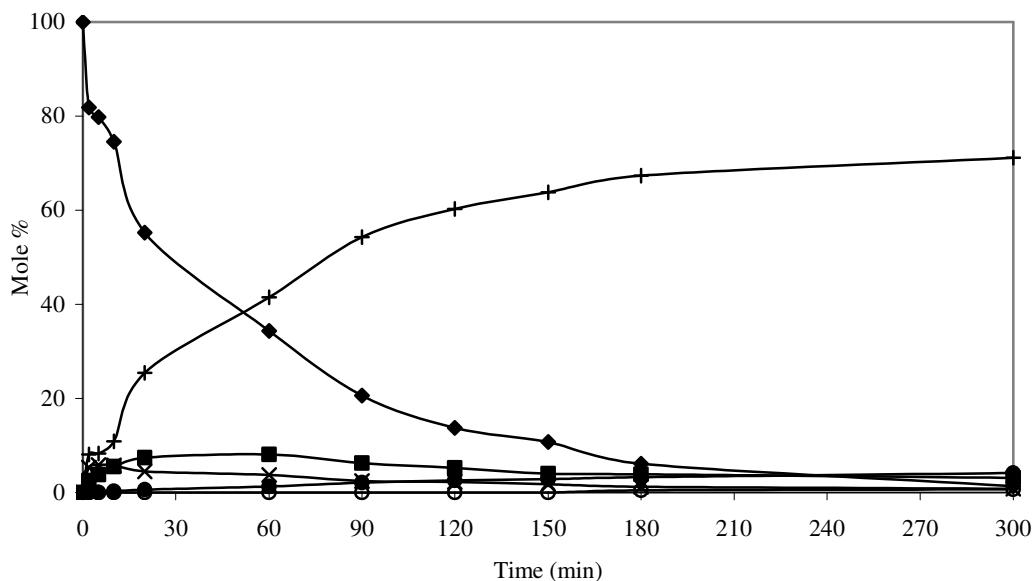


Figure 5.24. Product distribution of citral hydrogenation over bimetallic Ni-Sn/Na- $\beta$ (0.2) catalyst: (◆) Citral; (■) Citronellal; (●) Isopulegol; (×) Nerol; (+) Acetals; (○) Geraniol.

The change of acetal formation with respect to reaction time for the reaction performed over Ni-Sn/Na- $\beta$ (0.2) catalyst is given in Figure 5.25. The main acetal formed was Acetal(1).

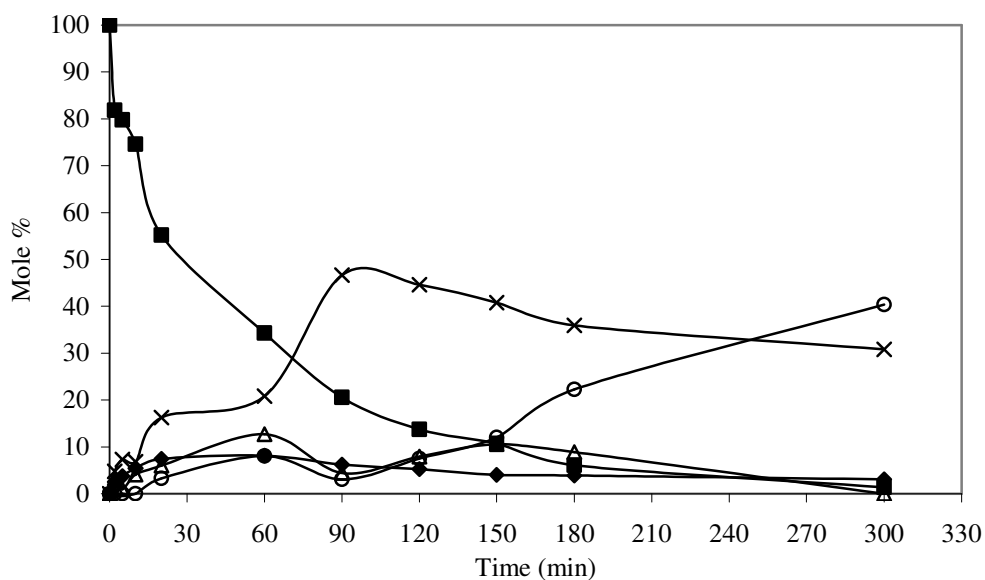


Figure 5.25. Change of acetal formation with respect to reaction time over Ni-Sn/Na- $\beta$ (0.2) catalyst. (◆) Citral; (■) Citronellal; (×) Acetal 1; (Δ) Acetal 2; (○) Acetal 3.

Conversion, selectivity and yield data over Ni/Na- $\beta$  and Ni-Sn/Na- $\beta$  catalysts are given in Table 5.17. Conversion of citral was very high both for monometallic and bimetallic catalysts. However, most of the citral was converted to the acetals giving very low selectivities to unsaturated alcohols and citronellal. Na- $\beta$  supported catalysts were not selective to desired products.

Table 5.17. Conversion, selectivity and yield values with different catalysts. (t=300 min)

Catalysts	Conversion	Selectivity		Yield	
		UOLs	Citronellal	UOLs	Citronellal
Ni/Na- $\beta$	100	0.0	0.0	0.0	0.0
Ni-Sn/Na- $\beta$ (0.2)	99.00	1.5	3.2	1.5	3.0

### 5.2.3. Ni/Na-Mordenite & Ni-Sn/Na-Mordenite Catalysts

The monometallic and bimetallic Mordenite supported catalysts tested in citral hydrogenation reaction were Ni/Mordenite, Ni-Sn/Mordenite(0.2), Ni-Sn/Mordenite (0.1), Ni-Sn/Mordenite (0.06) and Ni-Sn/Mordenite (0.02). The product distribution of citral over monometallic Ni/Mordenite catalyst up to the reaction time of 300 min is shown in Figure 5.26. Citral was converted to citronellal and acetal at the initial stage of the reaction. After 50 % of citral conversion, acetal concentration remained constant while citral was converted to citronellal. At the reaction time of 120 min acetal conversion to citronellal started. This suggested that acetal was probably citronellal acetal. Citral hydrogenation over monometallic catalyst gave 72 % citronellal, 15 % acetal, and small amount of citronellol (2.3 %) at the end of the reaction time.

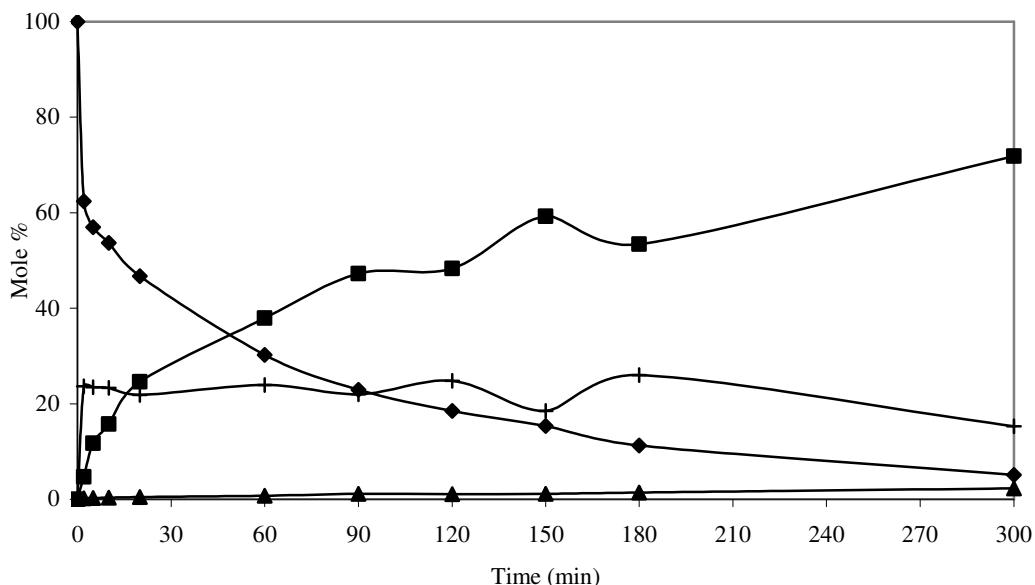


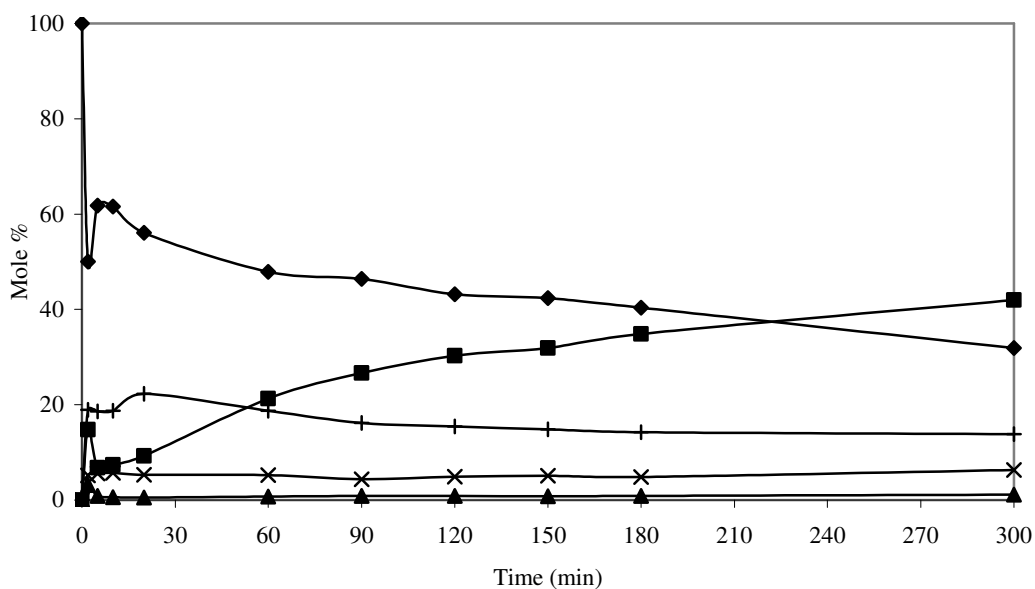
Figure 5.26. Product distribution of citral hydrogenation over monometallic Ni/Mordenite catalyst: (◆) Citral; (■) Citronellal; (▲) Citronellol; (+) Acetals.

The product distribution obtained by bimetallic catalysts is given in Figure 5.27. The major product was citronellal for all bimetallic catalysts. Nerol formation was also observed. This product formation could be due to the bimetallic nature of the catalysts, as discussed in Section 3.2.2. For the catalyst Ni-Sn/Mordenite(0.02), citral was converted to citronellal, acetal, nerol and citronellol. At the end of the reaction time, 42 % citronellal, 14 % acetal, 6.3 % nerol and small amount of citronellol were obtained in the reaction mixture.

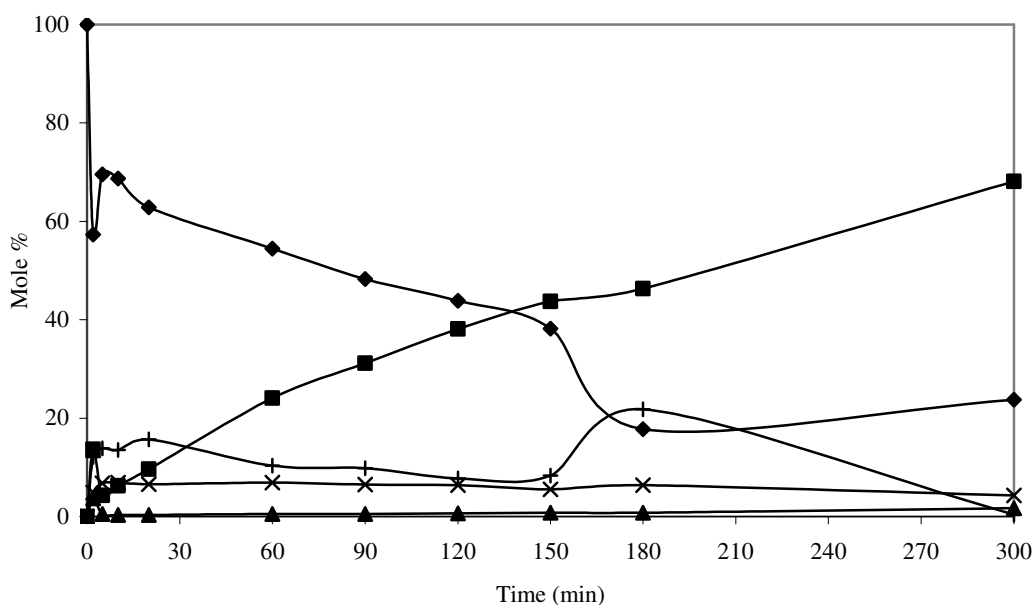
Figure 5.27 (b) shows that acetal formation decreased for the Sn/Ni+Sn ratio of 0.06. All of the acetal produced during 180 min was then converted to citronellal. Citronellal composition increased to 68 % while the nerol composition was 4.3 % at the end of 300 min.

For the catalyst Ni-Sn/Mordenite(0.1), most of the citral transformed to citronellal by giving small amounts of nerol and citronellol. Citronellal composition was found as 55 % while the amounts of nerol and citronellol were 5 % and 2.4 % respectively at the end of the reaction. Small amounts of acetal produced at the beginning of the reaction was converted to citronellal.

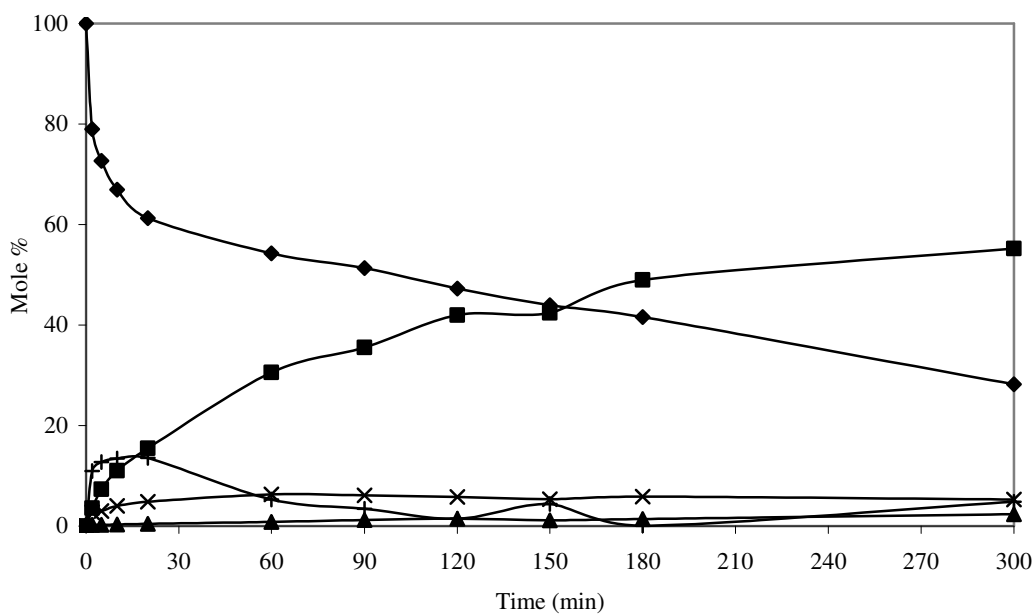
After the further addition of Sn, the acetal formation was almost eliminated over Ni-Sn/Mordenite(0.2) catalyst (Figure 5.27 (d)). Acetal was produced in the first 15 min and then converted to citronellal completely at the end of 60 min. Reaction mixture had 32 % citronellal and 6.6 % nerol at the end of the reaction time.



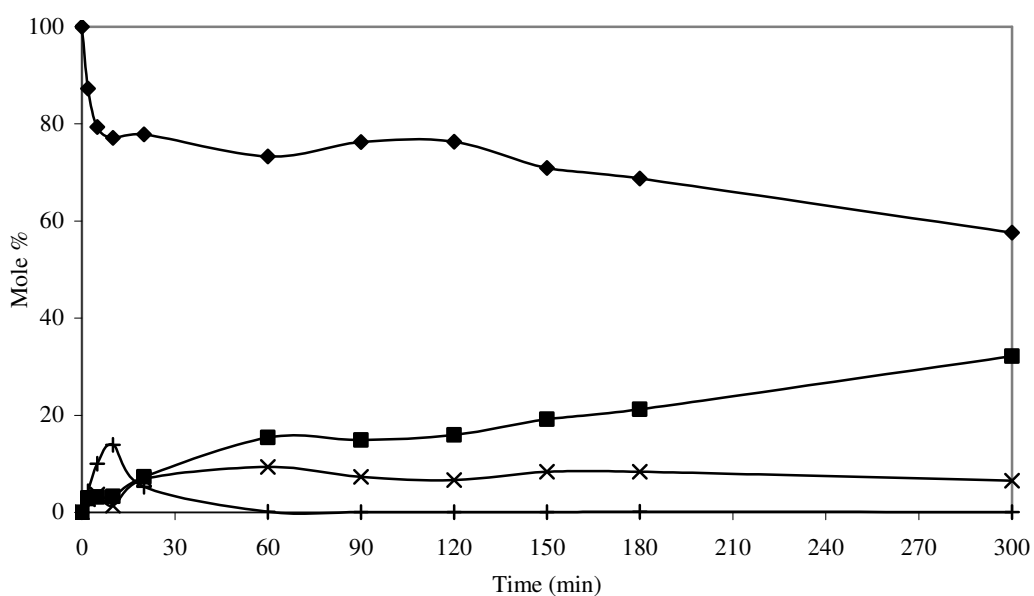
(a)



(b)



(c)



(d)

Figure 5.27. Product distribution of citral hydrogenation over Ni-Sn/Na-Mordenite (0.02) (a), Ni-Sn/Na-Mordenite (0.06) (b) and Ni-Sn/Na-Mordenite (0.1) (c) and Ni-Sn/Na-Mordenite (0.2) (d): (◆) Citral; (■) Citronellal; (▲) Citronellol; (●) Isopulegol; (×) Nerol; (+) Acetals.

The Ni catalyst activity decreased when promoted with Sn as it was observed in Figure 5.27. This could be due to deposition of Sn on active Ni metal sites. In addition, the formation of acetals dropped while the unsaturated alcohols, nerol and geraniol, production increased. The product distribution changed with different Sn/Ni+Sn ratio but not in a regular way.

Figure 5.28 shows the formation of acetals during the reaction over Ni/Na-Mordenite catalyst. The main acetal formed was Acetal(1). Citronellal and Acetal(1) converted one to another between 120 and 180 min and then Acetal (1) transformed to citronellal indicating that it was citronellal acetal.

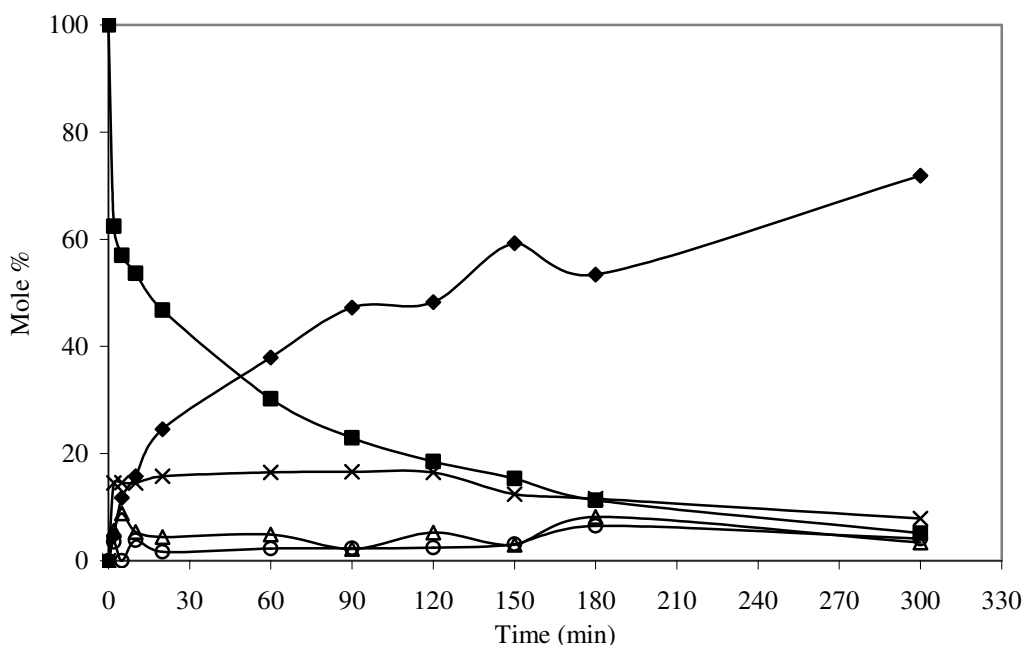


Figure 5.28. Change of acetal formation with respect to reaction time over Ni/Na-Mordenite catalyst. (◆) Citral; (■) Citronellal; (×) Acetal 1; (Δ) Acetal 2; (○) Acetal 3.

The conversion of citral, selectivity to citronellal, unsaturated alcohols geraniol and nerol, yield of citronellal and unsaturated alcohols are given in Table 5.18. The highest conversion of citral was obtained with the monometallic Ni/Na-Mordenite catalyst as 95 %. Among the bimetallic catalysts Ni-Sn/Mordenite(0.06) catalyst gave the maximum citral conversion (76.3 %). The most selective catalyst to unsaturated

alcohols nerol and geraniol was Ni-Sn/Mordenite(0.2) with selectivity of 16 % to unsaturated alcohols.

Table 5.18. Conversion, selectivity and yield values with Ni/MCM-41 and Ni-Sn/MCM-41 catalysts (t=300 min.)

Catalysts	Conversion	Selectivity		Yield	
		UOLs	Citronellal	UOLs	Citronellal
Ni/Mordenite	95.0	0.0	76.0	0.0	72.0
Ni-Sn/Na-Mordenite(0.02)	68.0	9.3	62.0	6.3	42.0
Ni-Sn/Na-Mordenite(0.06)	76.3	6.0	90.0	4.3	68.0
Ni-Sn/Na- Mordenite(0.1)	72.0	6.3	73.0	5.3	55.2
Ni-Sn/Na-Mordenite(0.2)	42.4	16.0	76.0	7.0	32.2

The changes in selectivity to unsaturated alcohols nerol, geraniol and citronellol over bimetallic catalysts supported by Na-Mordenite zeolite support can be seen on the selectivity versus Sn/Sn+Ni graph (Figure 5.29). Selectivity to unsaturated alcohols increased with the Sn/Sn+Ni ratio.

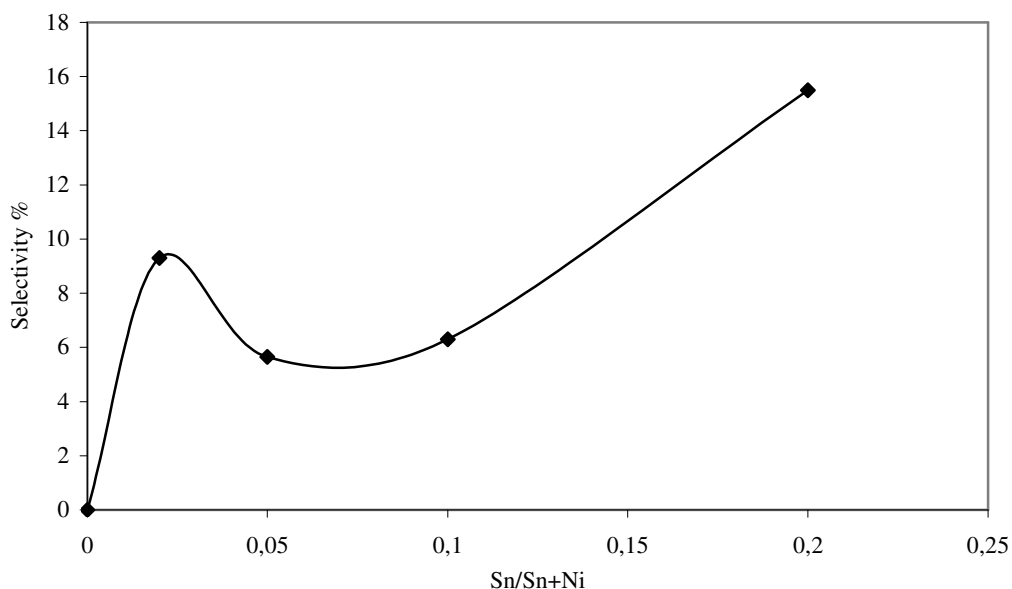


Figure 5.29. Selectivity to unsaturated alcohols as a function of Sn/Sn+Ni ratio.

#### 5.2.4. Ni/MCM-41 & Ni-Sn/MCM-41 Catalysts

The MCM-41 supported catalysts tested in citral hydrogenation reaction were, Ni/MCM-41, Ni-Sn/MCM-41(0.042), Ni-Sn/MCM-41(0.033). The product distribution over monometallic Ni/MCM-41 catalyst up to the reaction time of 300 min is shown in Figure 5.30.

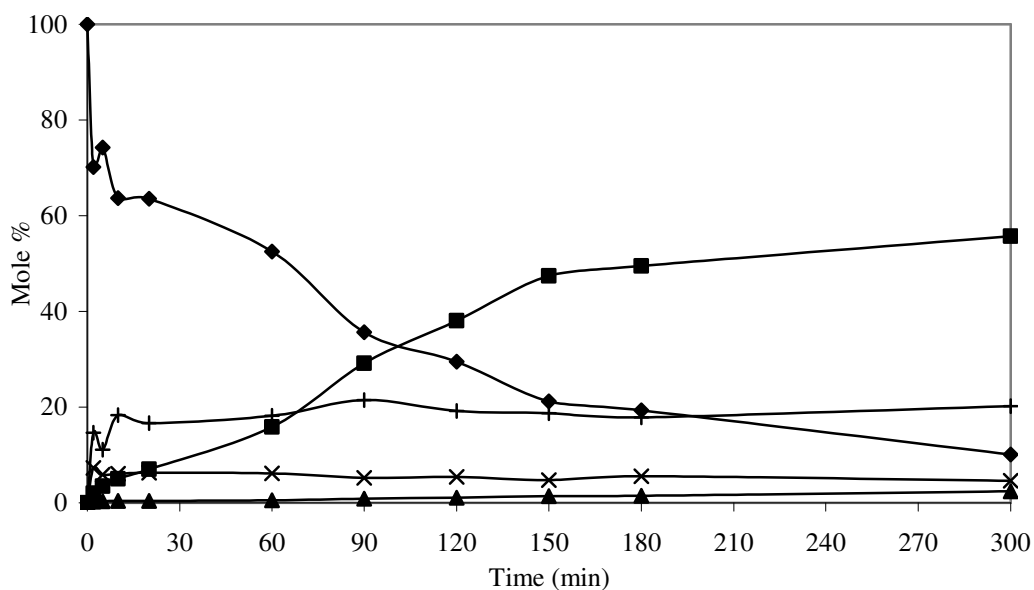
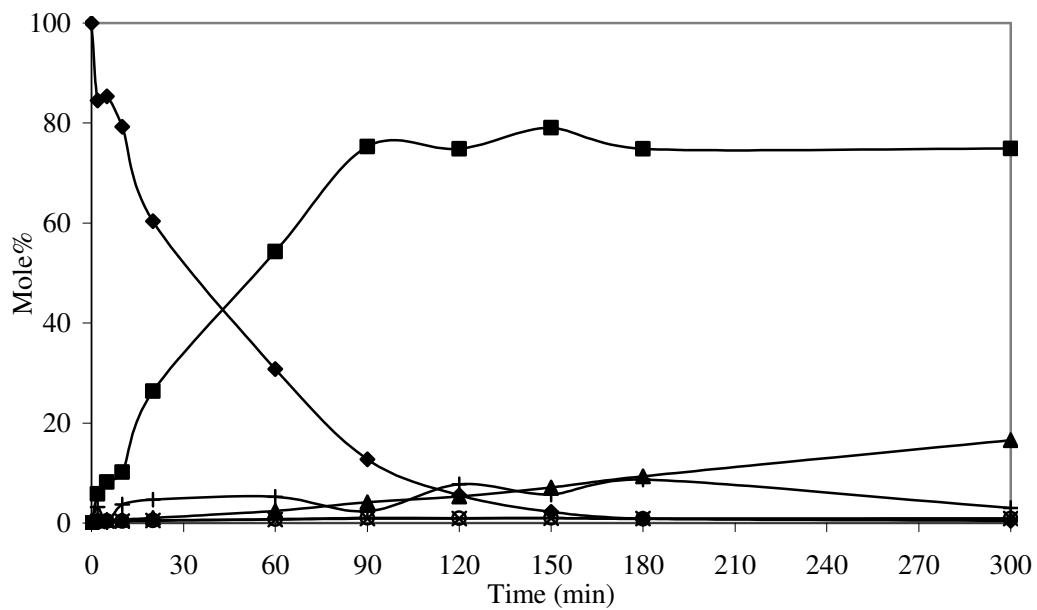


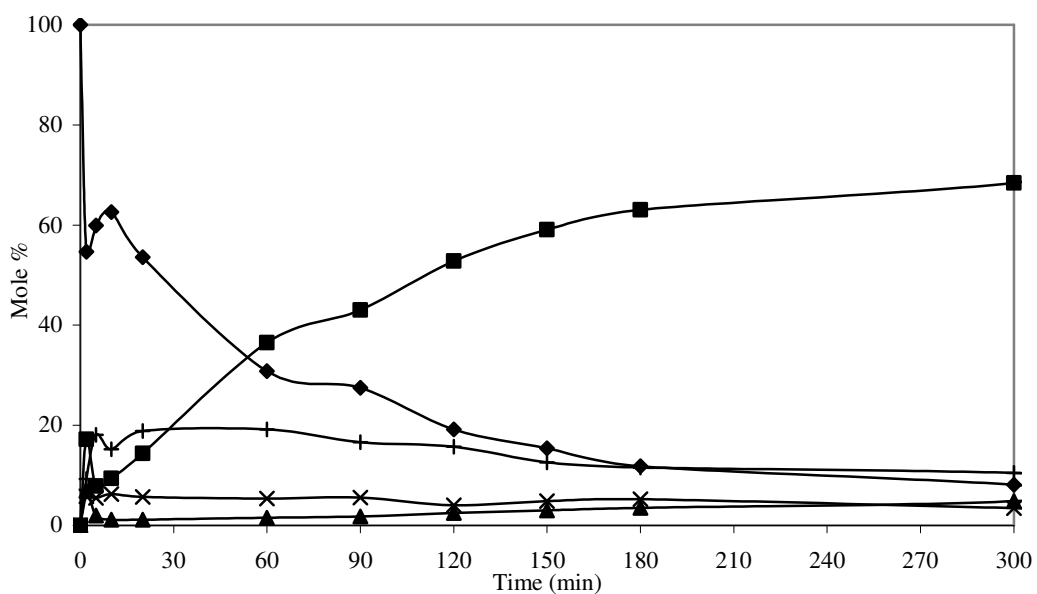
Figure 5.30. Product distribution of citral hydrogenation over monometallic Ni/MCM-41 catalyst: (◆) Citral; (■) Citronellal; (▲) Citronellol; (×) Nerol; (+) Acetals.

The main products obtained over monometallic Ni catalyst were again citronellal and acetal. In the first 15 min of the reaction acetal was formed and then its composition remained constant. At the end of the reaction time, the amount of citronellal was 55 %, amount of acetal was 20 %, nerol and citronellol compositions were 4.6 % and 2.3 % respectively.

Figure 5.31 shows the product distribution obtained over bimetallic catalyst Ni-Sn/MCM-41(0.042) and Ni-Sn/MCM-41(0.033).



(a)



(b)

Figure 5.31. Product distribution of citral hydrogenation over bimetallic NiSn/MCM-41(0.033) (a) and Ni-Sn/MCM-41(0.042) (b): (◆) Citral; (■) Citronellal; (▲) Citronellol; (×) Nerol; (+) Acetals; (○) Geraniol.

After addition of Sn (Sn/Sn+Ni mol ratio of 0.033), acetal formation decreased. Acetal produced transformed to citronellal after 180 min. Most of the citral was converted to citronellal. Besides, promoter addition increased the citronellol formation. At the end of the reaction time, the product distribution was as follows: 75 % citronellal, 16.5 % citronellol, 3 % acetal. Sn addition resulted in the hydrogenation of conjugated C=O bond to give citronellol as product.

In the case of Ni-Sn/MCM-41(0.042), citral was mostly converted to citronellal and acetal. After 60 min, acetal was also converted to citronellal. Higher amounts of Sn loading increased the nerol formation to 4 % and acetal formation to 10.5 %. In addition, citronellol and citronellal amounts were decreased to 5 % and 68 %, respectively at the end of the reaction time. These results indicated that there could be an optimum Sn loading for high catalyst selectivity.

The changes in the acetal formation during the reaction time of 300 min over Ni/MCM-41 catalyst are shown in Figure 5.32. the main acetal observed was Acetal(3). Its amount increased while the citral amount decreased. Citral converted to citronellal and Acetal(3). Thus, Acetal (3) can be citral acetal.

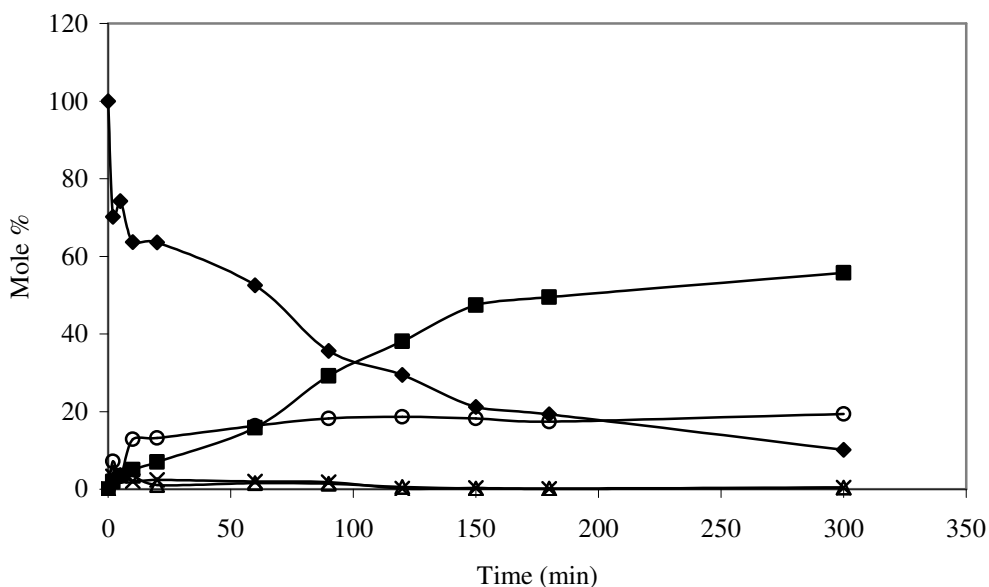


Figure 5.32. Change of acetal formation with respect to reaction time over Ni/MCM-41 catalyst. (◆) Citral; (■) Citronellal; (×) Acetal 1; (Δ) Acetal 2; (○) Acetal 3.

The conversion of citral, selectivity to nerol, geraniol and citronellal, yield of citronellal and unsaturated aldehydes nerol and geraniol are tabulated in Table 5.19. The most active catalyst was Ni-Sn/MCM-41(0.033) with the conversion of greater than 99 %, giving 75 % citronellal selectivity at the end of 300 min. However, the most selective catalyst to the unsaturated alcohols was Ni/MCM-41 with 5 % selectivity in contrast to the expectation that higher selectivity could be obtained by bimetallic catalysts.

Table 5.19. Conversion, selectivity and yield values with Ni/MCM-41 and Ni-Sn/MCM-41 catalysts. (t=300 min)

Catalysts	Conversion	Selectivity		Yield	
		UOLs	Citronellal	UOLs	Citronellal
Ni/MCM-41	90.0	5.0	62.0	5.0	56.5
Ni-Sn/ MCM-41(0.033)	>99	2.0	75.0	2.0	75.0
Ni-Sn/ MCM-41(0.042)	92.0	4.0	75.0	3.5	70.0

In contrast with other tested catalysts, Ni/MCM-41 catalyst activity increased by increasing the amount of promoter up to a known amount of Sn.

### 5.2.5. Ni/Clinoptilolite & Ni-Sn/Clinoptilolite Catalysts

Clinoptilolite supported catalysts tested in citral hydrogenation reaction were Ni/Clinoptilolite, Ni-Sn/Clinoptilolite(0.2). Product distribution obtained over monometallic catalyst is shown in Figure 5.33. The products observed over monometallic catalyst were citronellal, citronellol, nerol, isopulegol and acetal. In the first 10 min a sharp increase was observed in acetal formation and then it was converted to citronellal. After 180 min, small amount of citral was converted to citronellal and small amount of citronellal was converted to citronellol. At the end of the reaction time, the reaction solution had 75 % citronellal, 9.5 % citronellol, 2.3 % nerol and 6 % isopulegol.

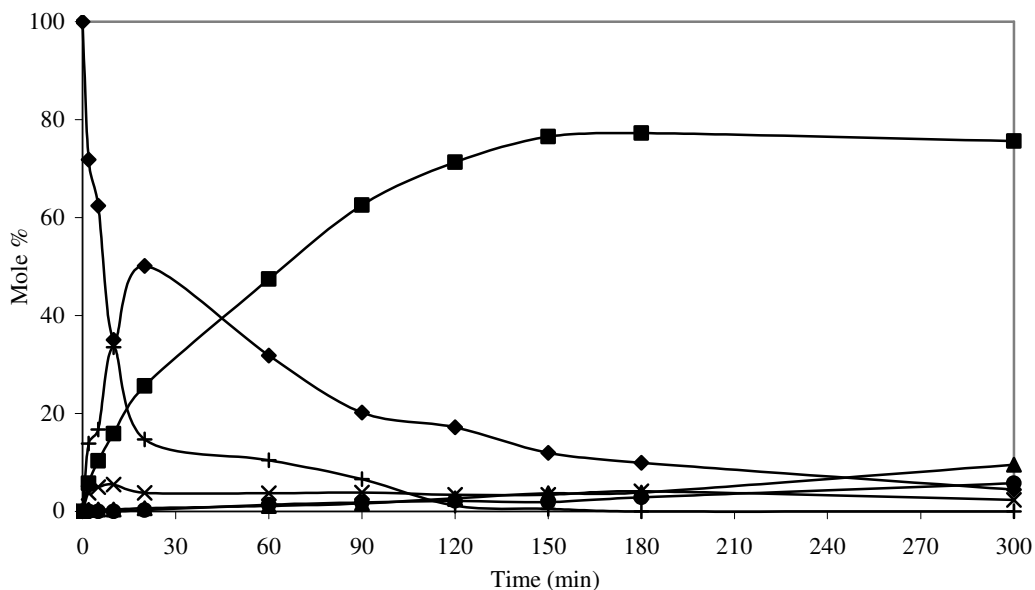


Figure 5.33. Product distribution of citral hydrogenation over monometallic Ni/Clinoptilolite catalyst: (◆) Citral; (■) Citronellal; (▲) Citronellol; (●) Isopulegol; (×) Nerol; (+) Acetals.

Figure 5.34 represents the product distribution over bimetallic Ni-Sn/Clinoptilolite(0.2) catalyst. Citral was mostly converted to citronellal. The acetal formed was also converted to citronellal after 10 min. The addition of Sn increased the formation of nerol to 6 % and decreased the formation of citronellal to 50 %.

The monometallic catalyst was much more active than bimetallic catalyst. This suggested that some of the active Ni sites were covered by Sn species. As a result, the reaction rate dropped. The amount of acetal formed decreased by bimetallic catalysts as observed with some of the previously discussed bimetallic catalysts. Initial formation rate of citronellal was much higher over catalyst Ni/Clinoptilolite than over Ni-Sn/Clinoptilolite(0.2).

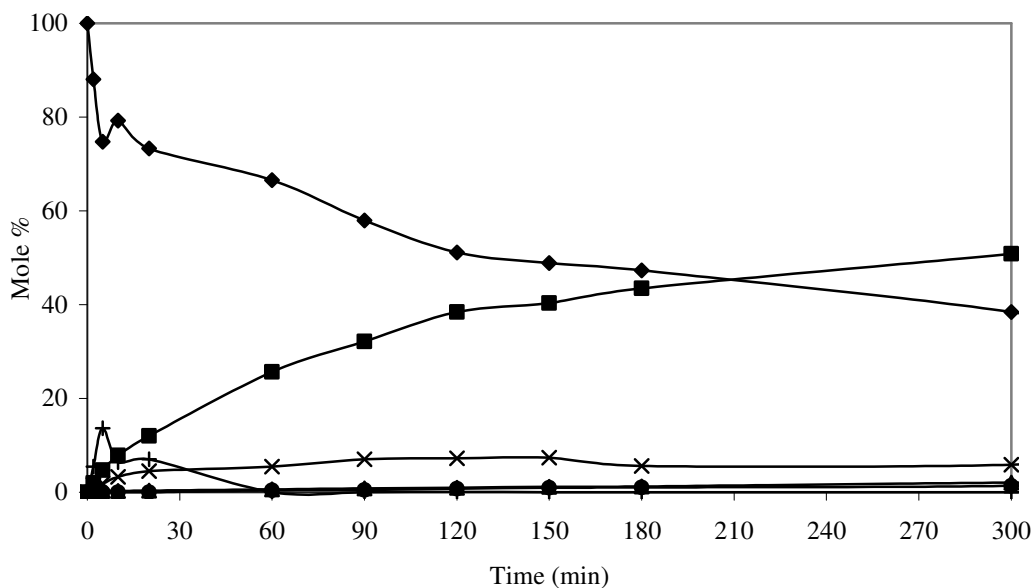


Figure 5.34. Product distribution of citral hydrogenation over bimetallic Ni-Sn/Clinoptilolite(0.2) catalyst: (◆) Citral; (■) Citronellal; (▲) Citronellol; (●) Isopulegol; (×) Nerol; (+) Acetals.

The conversion of citral, selectivity to nerol, geraniol and citronellal, yield of citronellal and unsaturated alcohols nerol and geraniol are tabulated in Table 5.20. The highest conversion (96 %) was observed with monometallic catalyst while the most selective catalyst to unsaturated alcohols is bimetallic one with selectivity of 10 %.

Table 5.20. Conversion, selectivity and yield values with Ni/Clinoptilolite and Ni-Sn/Clinoptilolite catalysts. (t=300 min.)

Catalysts	Conversion	Selectivity		Yield	
		UOLs	Citronellal	UOLs	Citronellal
Ni/Clinotilolite	96.0	2.5	79.2	2.4	76.0
Ni-Sn/Clinotilolite(0.2)	62.0	10.0	83.0	6.0	51.0

### 5.2.6. Pt/Na-Y Catalysts & Pt-Sn/Na-y Catalysts

The Pt loaded Na-Y catalysts tested in citral hydrogenation reaction were Pt/Na-Y and Pt-Sn/Na-Y(0.02). Figure 5.35 represents the product distribution of citral hydrogenation reaction obtained over monometallic Pt catalyst.

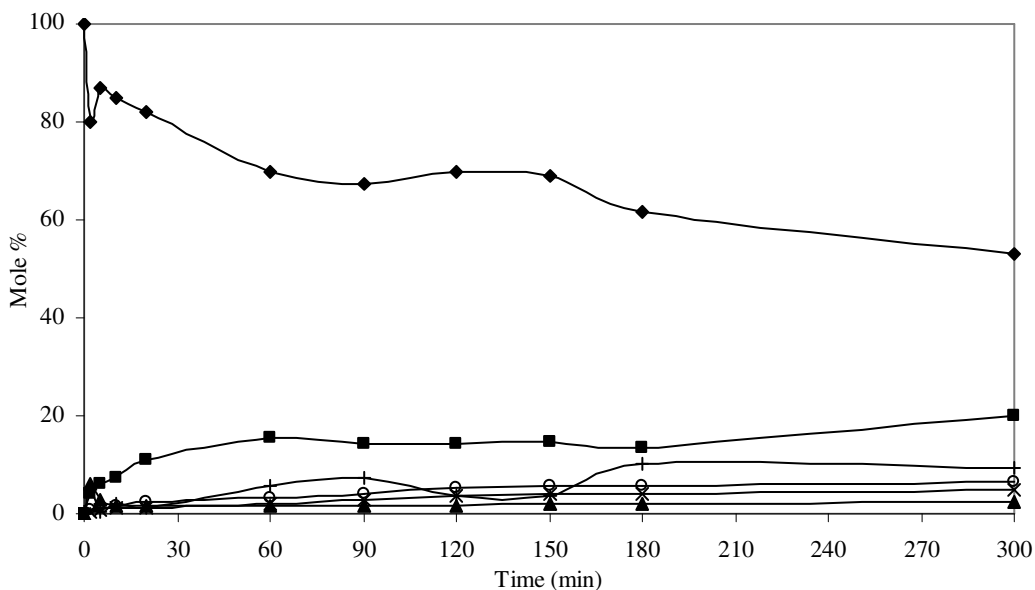


Figure 5.35. Product distribution of citral hydrogenation over monometallic Pt/Na-Y catalyst: (◆) Citral; (■) Citronellal; (▲) Citronellol; (×) Nerol; (+) Acetals; (○) Geraniol.

The monometallic catalyst showed low activity giving only 50 % citral conversion. The main product was citronellal (20 %). Pt/Na-Y catalyst led to the formation of unsaturated alcohols with a total amount of 11.5 %. At the end of the reaction time the amount of acetal and citronellol were 9 % and 3 % respectively.

Figure 5.36 shows the product distribution over bimetallic catalyst. Most of the citral was converted to citronellal. Sn loading increased the monometallic catalyst activity and changed the product distribution. Addition of promoter to the monometallic Pt catalyst decreased the unsaturated alcohol formation to 3 % in the contrary with the Sn promoted Ni catalysts. The final reaction mixture had 52.5 % citronellal, and 6.4 % citronellol. Acetal formation was very low for this catalyst (<1 %).

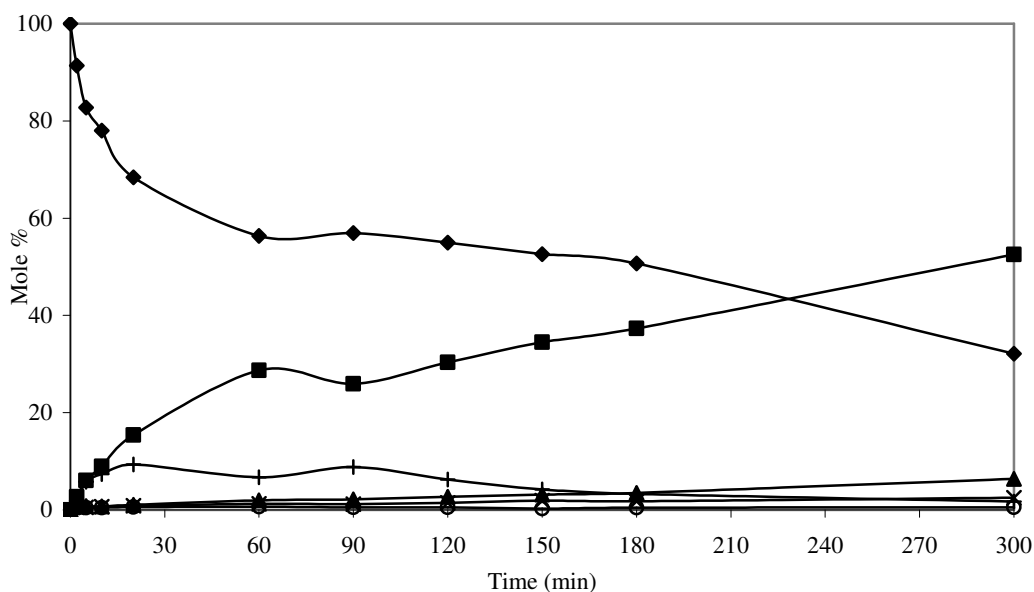


Figure 5.36. Product distribution of citral hydrogenation over bimetallic Pt-Sn/NaY(0.02) catalyst: (◆) Citral; (■) Citronellal; (▲) Citronellol; (×) Nerol; (+)Acetals; (○) Geraniol.

The conversion of citral, selectivity to nerol, geraniol and citronellal, yield of citronellal and unsaturated alcohols nerol and geraniol are tabulated in Table 5.21.

Table 5.21. Conversion, selectivity and yield values over Pt/NaY and Pt-Sn/NaY catalysts. (t=300 min)

Catalysts	Conversion	Selectivity		Yield	
		UOLs	Citronellal	UOLs	Citronellal
Pt/NaY	47.0	25.0	44.0	12.0	20.0
Pt-Sn/ NaY(0.02)	68.0	4.5	77.4	3.0	53.0

The highest conversion of citral (68 %) was achieved over Pt-Sn/Na-Y(0.02) catalyst but the most of the citral was converted to citronellal. The highest selectivity to unsaturated alcohols (25 %) was obtained over monometallic catalyst. This is in agreement with literature. It is reported that Pt catalyst is selective to unsaturated alcohols (Vilella et al. 2004; Blackmond et al. 1991; Malathi et al. 2001). The yields of unsaturated alcohols decreased while the yield of citronellal increased by the addition of promoter.

### 5.2.7. Pt/MCM-41 & Pt-Sn/MCM-41 Catalysts

The MCM-41 supported Pt catalysts tested in citral hydrogenation reaction were Pt/MCM-41 and Pt-Sn/MCM-41(0.02). The product distribution obtained over monometallic catalyst is given in Figure 5.37.

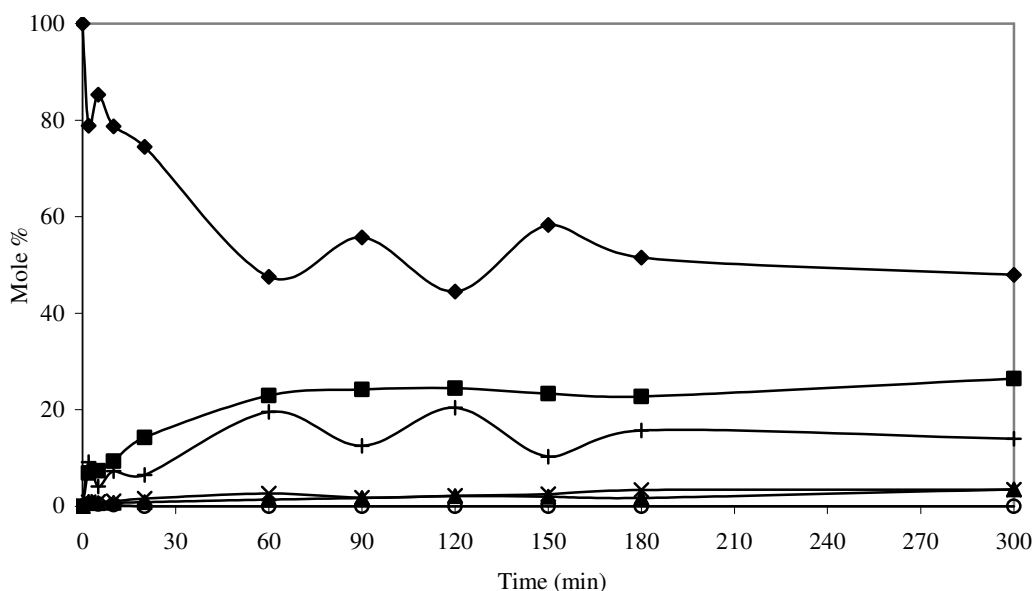


Figure 5.37. Product distribution of citral hydrogenation over Pt/MCM-41 catalyst: (◆) Citral; (■) Citronellal; (▲) Citronellol; (×) Nerol; (+) Acetals; (○) Geraniol.

Citral was mainly converted to acetal and citronellal. The catalyst showed low activity in citral conversion. Citral conversion rate was fast at some stage and at some stage it was slow. Between the reaction time of 60 and 180 min acetals were converted back to citral and then citral was again converted to acetal. This showed that there was a reversible reaction between citral and acetal. After 1 h of reaction, citral hydrogenation stopped; the catalyst was deactivated. At the end of 300 min, reaction mixture had 26.5 % citronellal, 14 % acetal, 3.5 % citronellol and 3.5 % nerol.

The product distribution over bimetallic Pt catalyst is given in Figure 5.38. Product distribution and catalyst activity was slightly different from that of the catalyst Pt/MCM-41. The citronellal and acetal were the main products. After 1h reaction time citral conversion stopped. This showed that the bimetallic Pt catalyst was also deactivated. Addition of Sn increased the unsaturated alcohol total composition to 7 %. Acetal amount (10 %) was smaller than that of monometallic catalyst. Citronellal

composition was 23.5 % while the amount of citronellol was smaller the 1 % at the end of reaction time.

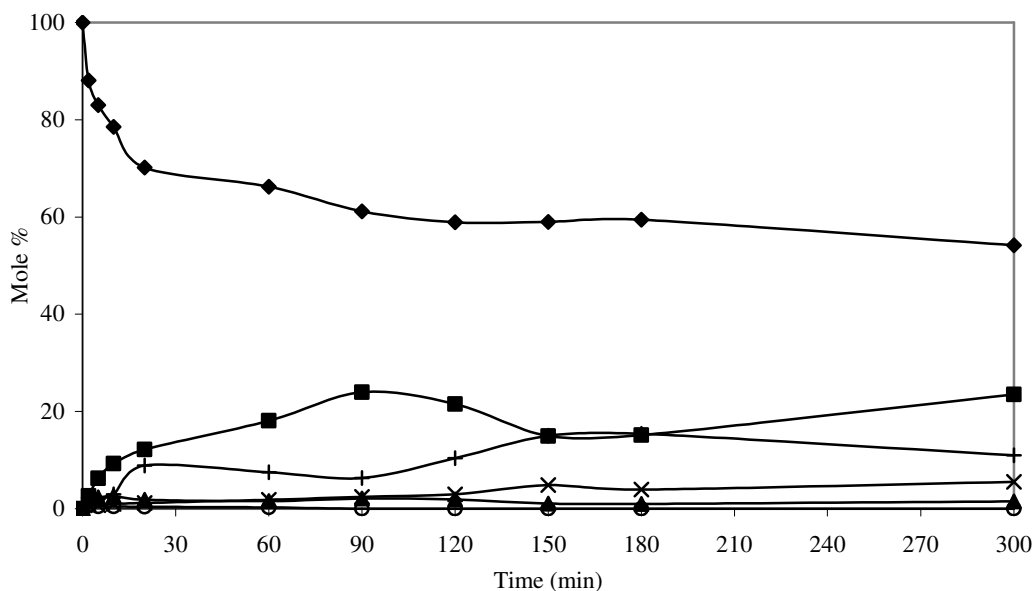


Figure 5.38. Product distribution of citral hydrogenation over Pt-Sn/MCM-41(0.02) catalyst: (◆) Citral; (■) Citronellal; (▲) Citronellol; (×) Nerol; (+) Acetals; (○) Geraniol.

The conversion of citral, selectivity to UOLs and citronellal, yield of UOLs and citronellal are given in Table 5.22. The expected promoter effect of Sn was observed from the selectivity values. For the bimetallic catalyst, the selectivity to unsaturated alcohols was twice as that obtained over monometallic catalyst while the conversion decreased from 52 % to 46 %.

Table 5.22. Conversion, selectivity and yield values of Pt/MCM-41 and Pt-Sn/MCM-41 catalysts (t=300 min.).

Catalysts	Conversion	Selectivity		Yield	
		UOLs	Citronellal	UOLs	Citronellal
Pt/MCM-41	52.0	7.0	51.0	3.5	26.5
Pt-Sn/ MCM-41(0.02)	46.0	12.0	51.0	5.5	23.5

### 5.2.8. Pt/Clinoptilolite & Pt-Sn/Clinoptilolite Catalysts

The clinoptilolite supported Pt catalysts tested in citral hydrogenation reaction were Pt/Clinoptilolite and Pt-Sn/Clinoptilolite (0.02). The product distribution obtained over Pt/Clinoptilolite catalyst is given in Figure 5.39.

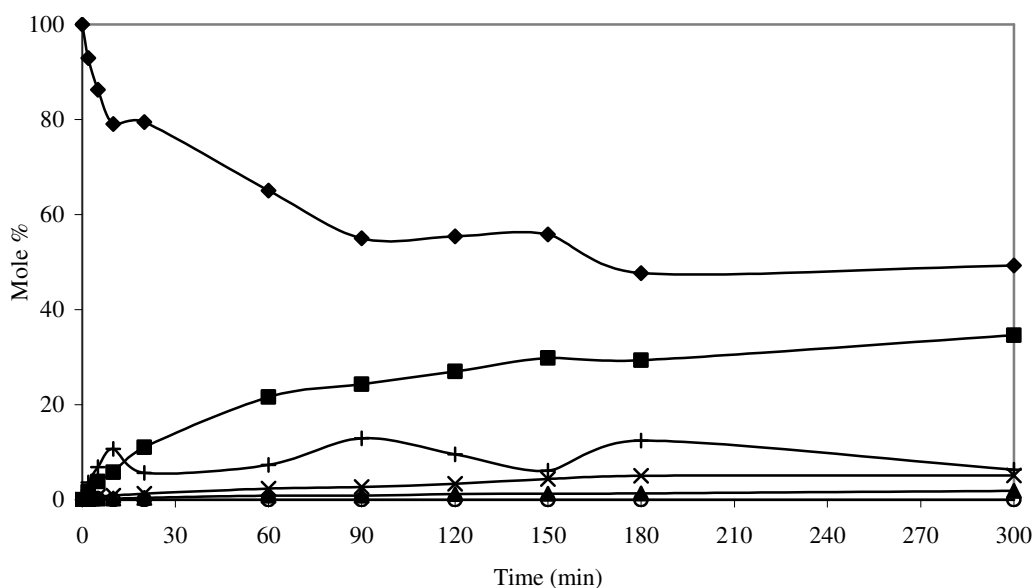


Figure 5.39. Product distribution of citral hydrogenation over Pt/Clinoptilolite catalyst: (◆) Citral; (■) Citronellal; (▲) Citronellol; (×) Nerol; (+) Acetals; (○) Geraniol.

Citral was initially converted mainly to citronellal and acetal. Between 90 and 180 min. reaction time, acetal and citral were converted to one and another reversibly. After 180 min, citral hydrogenation stopped and acetal was converted to citronellal.

This monometallic Pt/Clinoptilolite catalyst also deactivated. The reaction solution had 34.5 % citronellal while the nerol amount was 5 %.

Figure 5.40 shows the product distribution over Pt-Sn/Clinoptilolite catalyst. Initially the main products were citronellal and acetal. After 180 min, acetal started to convert to citronellal. The promotion of Pt catalyst by Sn increased the unsaturated alcohol formation up to 14.3 %. Compositions of citronellal and citronellol in solution also increased to 40 % and 10.5 % respectively at the end of 300 min. The acetal amount remained the same with that obtained over monometallic catalyst.

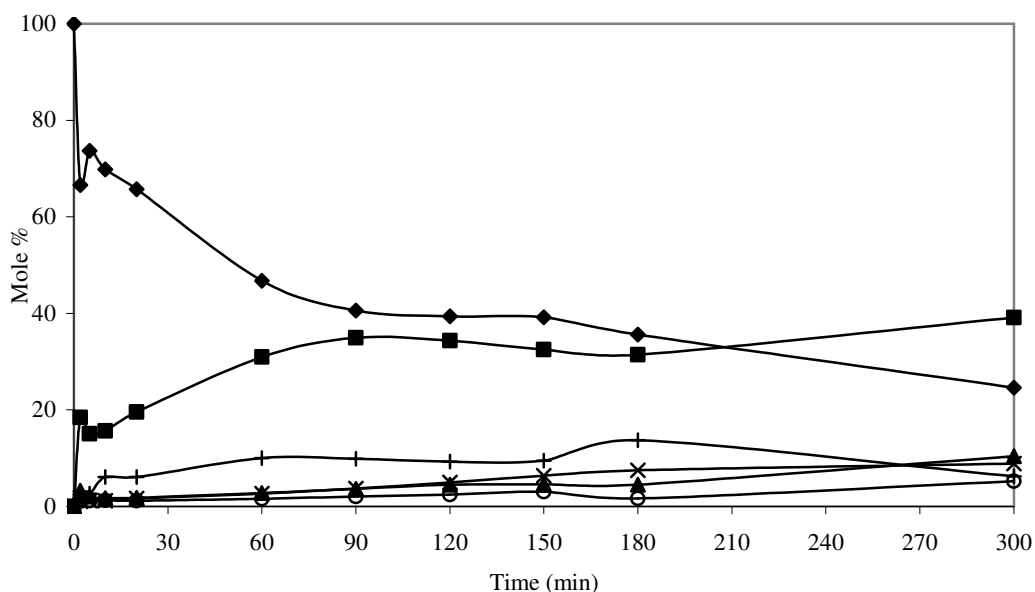


Figure 5.40. Product distribution of citral hydrogenation over Pt-Sn/Clinoptilolite(0.02) catalyst: (◆) Citral; (■) Citronellal; (▲) Citronellol; (×) Nerol; (+) Acetals; (○) Geraniol.

Figure 5.41 shows the formation of acetals during the reaction time of 300 min over Pt-Sn/Clinoptilolite(0.02) catalyst. Citral mainly converted to citronellal and Acetal(1). After 120 min reaction time Acetal(1) transformed to citronellal showing that it was citronellal acetal.

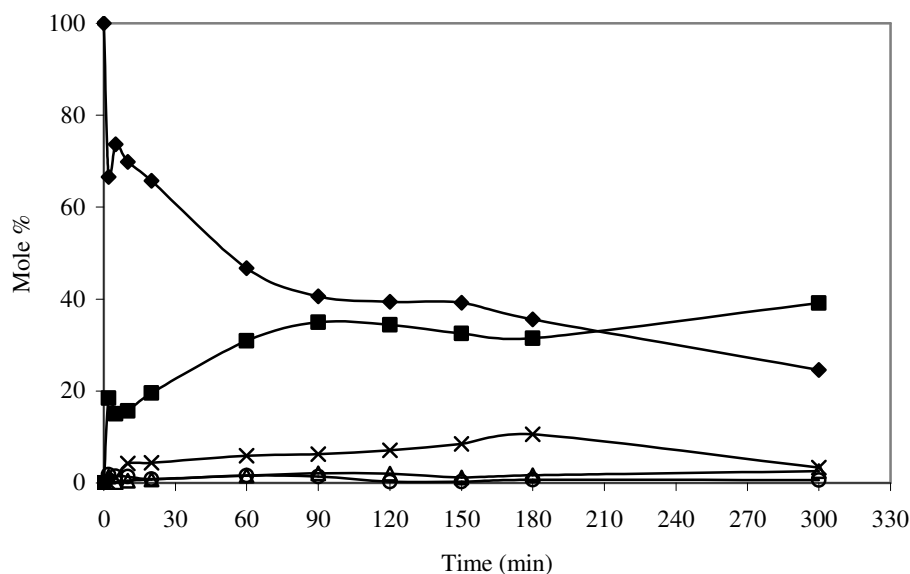


Figure 5.41. Change of acetal formation with respect to reaction time over Ni-Sn/Clinoptilolite(0.02) catalyst. (◆) Citral; (■) Citronellal; (×) Acetal 1; (Δ) Acetal 2; (○) Acetal 3.

The conversion of citral, selectivity to UOLs and citronellal, yield of UOLs and citronellal are given in Table 5.23. Bimetallic Pt-Sn/Clinoptilolite(0.02) catalyst gave the highest conversion (76 %), selectivity to unsaturated alcohols (19 %) and yield of unsaturated alcohol (14 %). The activity of bimetallic catalyst was higher than that of monometallic catalyst in contrary with the previous bimetallic Ni catalysts. The reason could be the fact that Sn species provided synergisms, so higher reaction rate and selectivity were obtained.

Table 5.23. Conversion, selectivity and yield values with Pt/Clinoptilolite and Pt-Sn/Clinoptilolite catalysts. (t=300 min)

Catalysts	Conversion	Selectivity		Yield	
		UOLs	Citronellal	UOLs	Citronellal
Pt/Clinoptilolite	51.0	10.0	68.0	5.0	35.0
Pt-Sn/Clinoptilolite	76.0	19.0	53.0	14.0	39.0

### 5.2.9. Comparison of Different Supports

The performances of different zeolite supports in citral hydrogenation reaction were investigated in terms of conversion of citral and yield of desired products nerol, geraniol, citronellol and citronellal. Figure 5.42 shows the changes in conversion and yield data with respect to time over monometallic Ni catalysts for different zeolite supports.

The most active catalyst was Ni/Na- $\beta$  with 100 % conversion of citral at the end of the reaction time of 300 min. However this catalyst gave the minimum yield to desired products. The main product obtained over this catalyst was acetal as it was discussed previously. Na- $\beta$  support has greater Si/Al ratio (12) among the other support materials used in this study as it is seen in Table 5.24. The high Si/Al ratio means lower amount of acid sites. But these acid sites are very strong that makes the catalyst very active. However they prefer the side reactions producing undesired products such as acetals.

The highest yield (85.4 %) to desired products was achieved over Ni/Na-Y catalyst. The activity of this catalyst was also as high as that of Ni/Na- $\beta$  catalyst (99.85 % conversion). The best interaction between the active metal and support material was achieved over Na-Y supported Ni catalyst among all Ni loaded monometallic catalysts. This catalyst had higher surface area and lower Si/Al ratio as it was shown in Table 5.24. Also Na-Y support material had the higher crystal size (Section 5.1.1).

The Pt loaded Na-Y, MCM-41 and Clinoptilolite catalysts are compared in Figure 5.43 in terms of citral conversion and yield of desired products. The maximum citral conversion (52 %) was achieved over MCM-41 supported Pt catalyst. However the yield to desired products was low. The citral conversion over Pt/Clinoptilolite catalyst was as high as Pt/MCM-41 catalyst. Besides, this catalyst led to the maximum yield of desired products (39.68 %).

The catalyst activities and selectivities were found to be affected by the support type. The selectivity and yield to desired products changed in the following order: Na-Y > Clinoptilolite > Mordenite > MCM-41 > Na- $\beta$ .

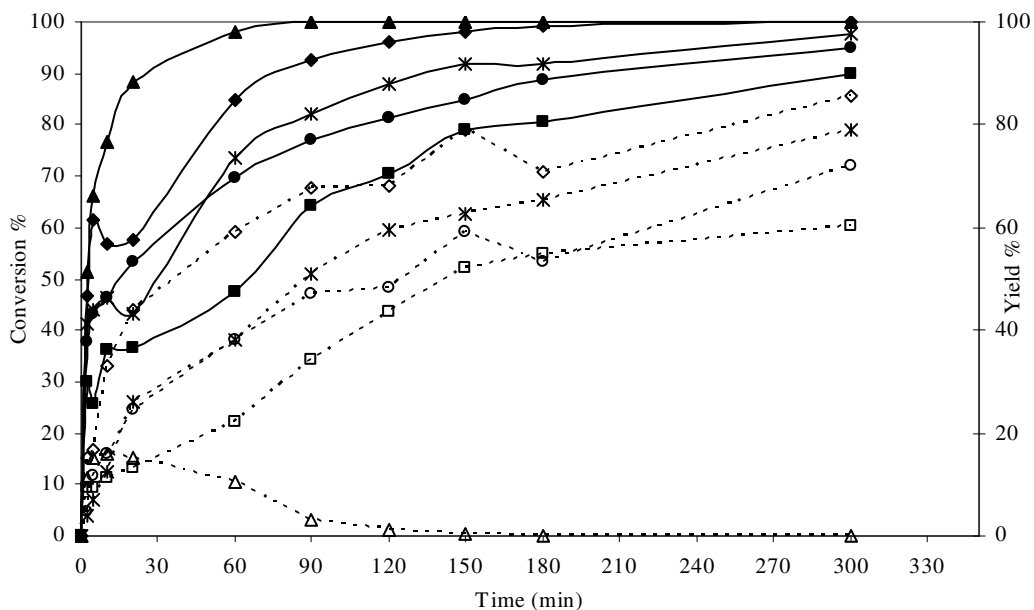


Figure 5.42. Conversion and Yield vs. Time for zeolite supported Ni catalysts: (◆) Ni-NaY Conversion; (▲) Ni/Na-Beta Conversion; (●) Ni/Mordenite Conversion; (■) Ni/MCM-41 Conversion; (✕) Ni/Clinontitolite Conversion; (◇) Ni-NaY Yield; (Δ) Ni/Beta Yield; (○) Ni/Mordenite Yield; (□) Ni/MCM-41 Yield; (✕) Ni/Clinoptilolite Yield.

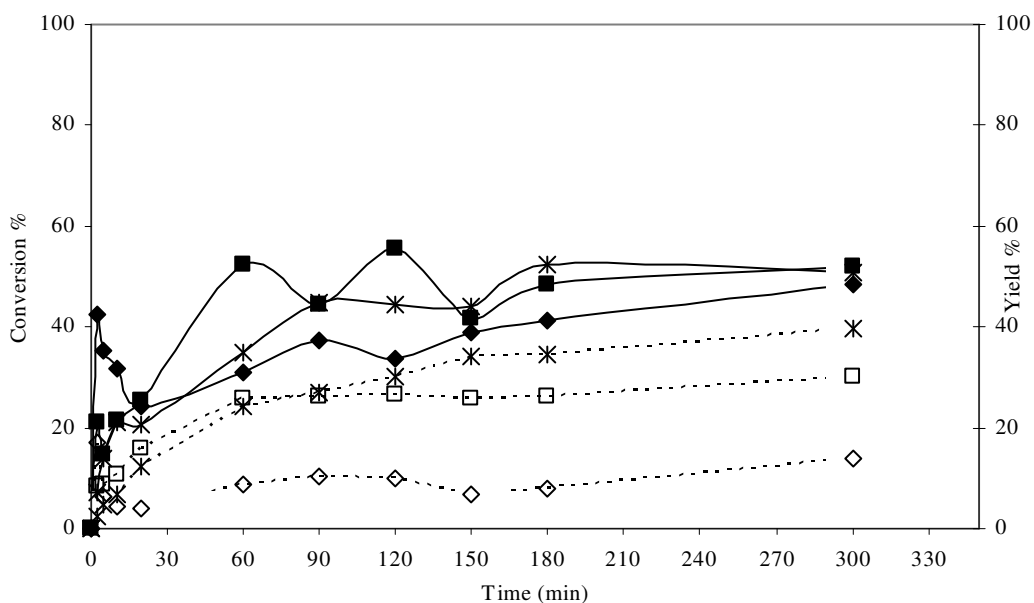
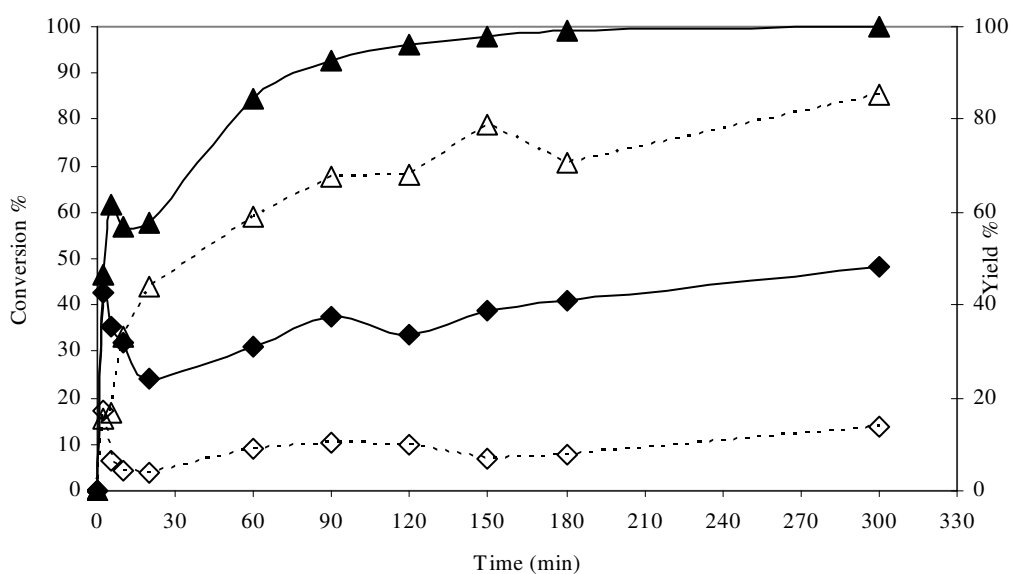


Figure 5.43. Conversion and Yield vs. Time for zeolite supported Pt catalysts: (◆) Pt/NaY Conversion; (■) Pt/MCM-41 Conversion; (✕) Pt/Clinontitolite Conversion; (◇) Pt/NaY Yield; (□) Pt/MCM-41 Yield; (✕) Pt/Clinoptilolite Yield.

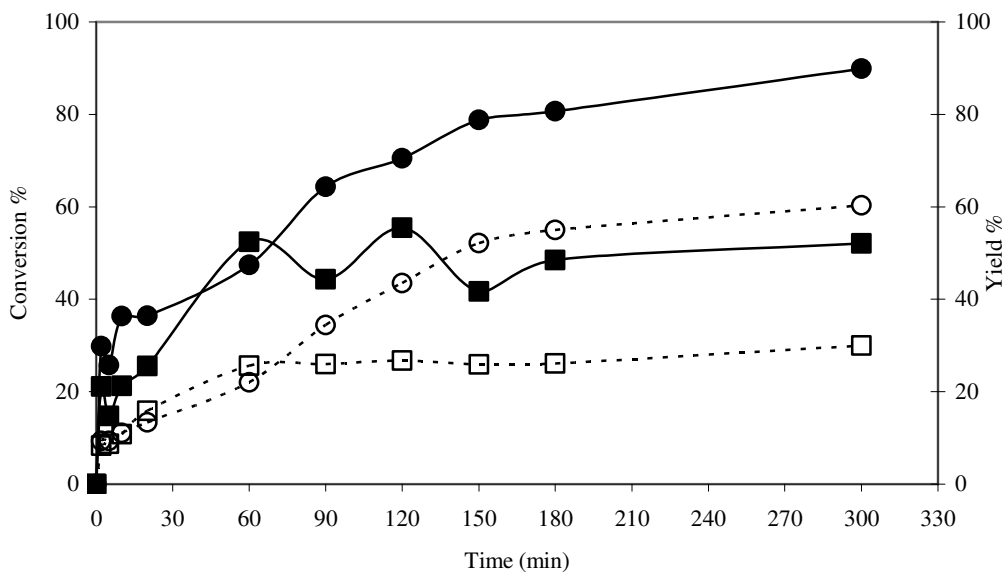
### 5.2.10. Comparison of Active Metals

The variation of conversion and yield to desired products for different active metals, Pt and Ni is given in Figure 5.44. Monometallic Ni catalyst gave better activity and yield to desired products when compared with monometallic Pt-catalyst.

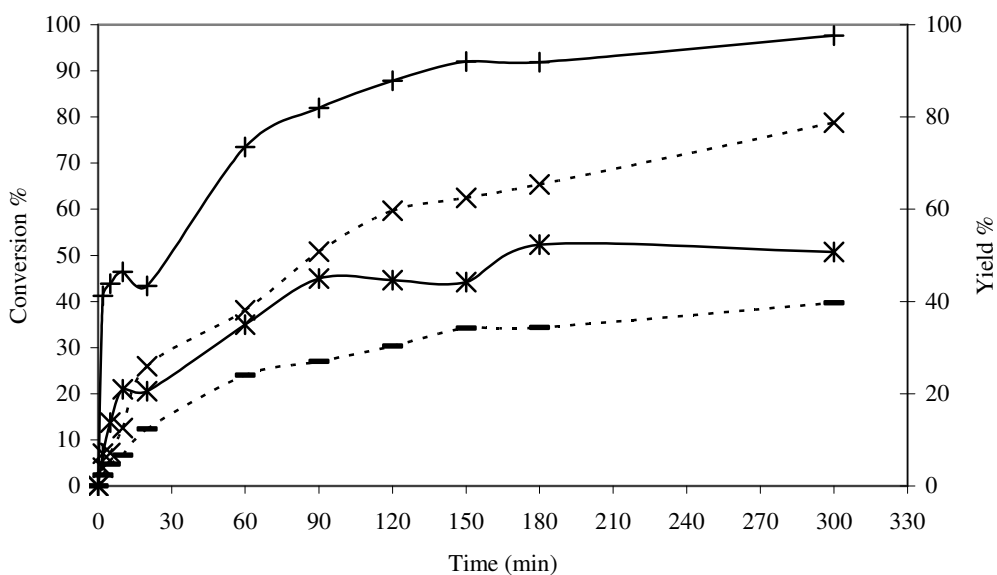
The maximum conversion and yield to desired products were achieved over Na-Y supported Ni catalyst. This suggested that Ni catalyst was more active and selective to desired products than Pt catalyst when it was supported by Na-Y zeolite. This could be due to better Ni dispersion and interaction with Na-Y zeolite. The higher surface area of Ni/Na-Y catalyst among the other microporous material supported monometallic catalysts could be the reason of better dispersion and interaction (Table 5.24). The conversion of citral was obtained as 99.85 % while the yield was 85.4 % for Ni/Na-Y catalyst at the end of 300 min.



(a)



(b)



(c)

Figure 5.44. Conversion and yield vs. time for NaY (a), MCM-41 (b) and Clinoptilolite (c) supported Pt and Ni catalysts: (◆) Pt/NaY Conversion; (▲) Ni/NaY Conversion; (■) Pt/MCM-41 Conversion; (●) Ni/MCM-41 Conversion; (+) Pt/Clinoptilolite Conversion; (x) Ni/Clinoptilolite Conversion; (◇) Pt/NaY Yield; (Δ) Ni/NaY Yield; (□) Pt/MCM-41 Yield; (○) Ni/MCM-41 Yield; (-) Pt/Clinoptilolite Yield; (x) Ni/Clinoptilolite Yield.

The similar result was observed for the MCM-41 and supported catalysts. Again the Ni loaded MCM-41 catalyst gave the highest conversion (89.89 %) and yield (60.33 %) values.

Clinoptilolite supported Ni catalyst had the maximum conversion (97.62 %) and yield (78.80 %) values as in the case of other supported Ni catalysts. For the monometallic catalysts, Ni showed much more activity and selectivity than Pt catalysts. Metal dispersion on the surface, and metal specificity itself could be the reasons for the results obtained.

### 5.2.11. Comparison of Bimetallic Catalysts

Activities and selectivities of MCM-41 and Na-Y supported Ni-Sn and Pt-Sn catalysts are compared in Figure 5.45.

In the case of bimetallic catalysts Pt and Ni active metals showed different behaviours in citral hydrogenation reaction. When Ni was promoted with Sn, the catalyst activity dropped. On the other hand, the Pt catalyst activity increased with Sn promoter.

Pt-Sn/Na-Y and Ni-Sn/NaY showed similar activities and selectivities. In case of MCM-41 support, a large difference between Pt-Sn and Ni-Sn catalyst was observed. Pt-Sn showed an activity almost two times higher than Ni-Sn. It also showed much higher yield to desired products. MCM-41 support was the best for the bimetallic catalyst.

Monometallic catalysts gave the highest yield to desired products. However, larger amount of unsaturated alcohols was produced by bimetallic catalyst. The amounts of unsaturated alcohols were not as much as reported in literature (Section 2.3.2.2). The reason could be the different types of support materials. The support materials used in literature were generally inert supports such as SiO<sub>2</sub>, Al<sub>2</sub>O<sub>3</sub>, etc. So the usage of these supports eliminates the SMSI effect. Also zeolite supports have acid sites in comparison to these inert supports. These acid sites could be the reason of differences in the product distribution and activity of the catalysts.

Table 5.24 shows the physico-chemical properties of all catalysts and citral conversion, product distribution and yield to desired products obtained over these catalysts.

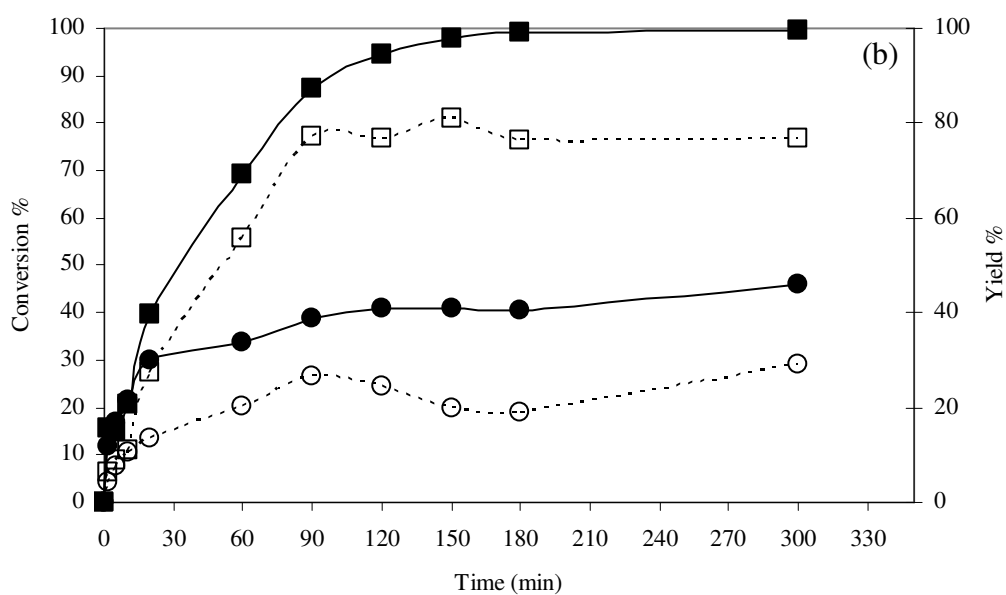
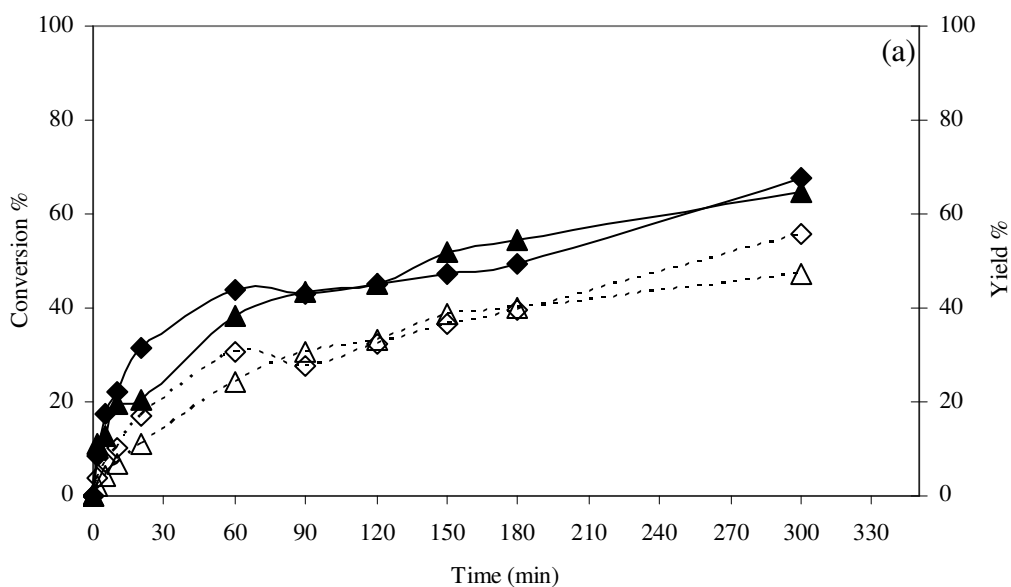


Figure 5.45. Conversion and yield vs. time for NaY (a) and MCM-41 (b) supported Pt-Sn and Ni-Sn bimetallic catalysts: (◆) Pt-Sn/NaY Conversion; (▲) Ni-Sn/NaY Conversion; (■) Pt-Sn/MCM-41 Conversion; (●) Ni-Sn/MCM-41 Conversion; (◇) Pt-Sn/NaY Yield; (Δ) Ni-Sn/NaY Yield; (□) Pt-Sn/MCM-41 Yield; (○) Ni-Sn/MCM-41 Yield.

**Table 5.24.** Physico-chemical properties, citral conversion, product distribution and yield to desired products obtained over all catalysts tested.

Catalysts	Surface Area (m <sup>2</sup> /g)	Si/Al	Conversion (%)	Citronellal (%)	Citronellol (%)	Nerol (%)	Geraniol (%)	Isopulegol (%)	Acetals (%)	Others (%)	Yield to UOLs	Yield to Desired Products
Na-Y	886.1	2.6										
Ni/Na-Y	785.7	2.6	>99	84.5	5.6	0.0	0.9	1.0	5.2	2.6	<1	86.0
Ni-Sn/Na-Y(0.025)	-	2.6	64.5	44.5	1.4	2.1	0.0	0.0	12.1	4.3	2.0	47.0
Ni-Sn/Na-Y(0.053)	-	2.6	74.0	58.7	1.5	4.5	0.0	0.4	5.6	3.0	4.5	63.5
Ni-Sn/Na-Y(0.1)	-	2.6	65.5	47.3	1.6	4.7	0.0	0.7	7.9	3.3	5.0	52.3
Ni-Sn/Na-Y(0.2)	-	2.6	46.0	33.5	0.7	6.2	0.0	3.1	0.1	2.3	6.2	40.2
Pt/Na-Y	-	2.6	47.0	19.4	4.0	6.5	7.8	0.0	8.1	3.3	12.0	32.0
Pt-Sn/Na-Y(0.02)	-	2.6	68.0	52.5	6.4	2.5	0.5	0.4	1.7	3.6	3.0	56.0
Na-β	558.8	12										
Ni/Na-β	549.2	12	100	0.0	0.0		0.0	12.9	84.8	<1	0.0	0.0
Ni-Sn/Na-β(0.2)	515.8	12	99.00	2.2	0.0	0.6	0.8	4.3	92.1	<1	1.5	4.5
Na-Mordenite	-	9										
Ni/Na-Mordenite	390.2	9	95.0	71.9	2.3	0.0	0.0	0.4	15.3	5.0	0.0	72.0
Ni-Sn/Na-	-	9	68.0	42.0	1.1	6.3	0.0	0.0	13.8	4.7	6.3	68.3
Ni-Sn/Na-	-	9	76.3	68.1	1.7	4.3	0.0	0.0	0.4	1.7	4.3	72.3
Ni-Sn/Na-Mordenite(0.1)	-	9	72.0	55.2	2.4	5.3	0.0	1.4	4.8	2.7	5.3	60.5
Ni-Sn/Na-Mordenite(0.2)	348.2	9	42.4	32.2	0.9	6.6	0.0	1.5	0.1	1.0	7.0	39.2
MCM-41	1449.0	-										
Ni/MCM-41	1074.2	-	90.0	55.7	2.4	4.6	0.0	0.0	20.2	4.8	5.0	61.5
Ni-Sn/ MCM-41 (0.033)	984.3	-	>99	74.9	16.6	0.9	0.9	0.0	3.0	3.2	2.0	77.0
Ni-Sn/ MCM-41 (0.042)	-	-	92.0	75.1	9.0	2.3	0.0	0.4	8.1	4.2	3.5	73.5
Pt/MCM-41	-	-	52.0	26.5	3.5	3.5	0.0	0.0	14.0	4.5	3.5	30.0
Pt-Sn/MCM-41(0.02)	-	-	46.0	23.5	1.5	5.5	0.0	0.0	11.0	4.2	5.5	29.0
Clinoptilolite	43.3	5.1										
Ni/Clinoptilolite	38.6	5.1	96.0	75.6	9.5	2.4	0.0	5.7	0.0	1.4	2.4	78.4
Ni-Sn/Clinoptilolite(0.2)	34.1	5.1	62.0	54.9	1.9	8.8	0.0	2.8	0.0	0.8	6.0	57.0
Pt-Sn/Clinoptilolite(0.02)	-	5.1	76.0	39.1	10.4	8.9	5.2	0.4	6.3	5.1	14.0	53.0

## CHAPTER 6

### CONCLUSIONS

Na-Y, Na-Beta, Na-Mordenite, MCM-41, and Clinoptilolite supports were found to have crystalline structure and high surface area. They had different morphologies with crystallite sizes changing from 100 nm to 5  $\mu\text{m}$ . All supports contained substantial amount of Al except Na-MCM-41. Their Si/Al ratios were determined as: 2.6 for Na-Y, 12.4 for Na-Beta, 9.0 for Na-Mordenite and 5.1 for Clinoptilolite.

The catalysts, monometallic (Ni and Pt) and bimetallic (Ni-Sn and Pt-Sn), showed characteristics peaks of the support in XRD diagrams. This indicated that the crystal structure of the supports was not affected by metal loading of Ni, Pt and Sn through impregnation and coimpregnation. Ni and Pt peaks were obtained in XRD spectra of the catalysts indicating that the metal loading processes were successful. Besides the Pt active metal peaks, the peaks of  $\text{PtSn}_2$  alloy were observed in XRD analysis for all bimetallic Pt catalyst. In the case of bimetallic Ni catalysts,  $\text{Ni}_4\text{Sn}$  alloy peaks were observed for the catalysts that have Sn/Ni+Sn ratio greater than 0.1. The active metal was found to be evenly distributed over the support surface.

The surface area of the support decreased by metal loading. This attributed to the blockage and narrowing of the pores of the support materials.

The activity and product distribution obtained over different monometallic catalysts was affected by the support. The main products of citral hydrogenation reaction over monometallic Ni and Pt catalysts were citronellal and acetal.

The highest yield (93.34 %) to desired products namely nerol, geraniol and citronellol and citronellal obtained with active Ni metal was over Na-Y support. A citral conversion of 99.85 % was achieved. The most selective monometallic Pt catalyst was found to be Pt /MCM-41 giving yield of desired products as 40 %. Thus, the best support differed for different active metal.

Ni and Pt metals showed different behavior when they were in bimetallic form. Sn loading affected the activity of the catalyst and yield of desired products. They were decreased or increased depending on the support. This was attributed to the coverage of

active metal by Sn and to the synergism formed between the metal by Sn which varied depending on the support.

The selectivity to unsaturated alcohols increased with increasing Sn/Sn+Ni ratio from 0.02 to 0.2 for bimetallic Ni catalysts except for MCM-41 supported Ni catalyst. Addition of Sn increased the formation of unsaturated alcohols over bimetallic Pt catalysts except for Na-Y supported one. The selectivity to desired products was found to be higher for monometallic Pt catalyst than the bimetallic Pt catalyst.

The promoter effect on reaction rate was affected by active metal type and the support. In general, it decreased monometallic Ni catalyst activity. However, it increased monometallic Pt catalyst activity.

Ni active metal gave higher yields to desired products compared to Pt. For monometallic catalyst, the best three catalyst were Ni/Na-Y, Ni/Clinoptilolite and Ni/Mordenite with total yields of desired products as 85, 82 and 72 % respectively. The best bimetallic catalyst was Ni-Sn/MCM-41. It gave yield of 80 %.

## REFERENCES

- Aramendia, M.A., Borau, V., Jimenez, C., Marinas, J.M., Porras, A. and Urbano, F.J. 1997. "Selective Liquid-Phase Hydrogenation of Citral over Supported Palladium", *Journal of Catalysis*. Vol. 172, p. 46–54.
- Mäki-Arvela, P., Tiainen, L.-P., Lindblad, M., Demirkan, K., Kumar, N., Sjöholm, R., Ollonqvist, T., Väyrynen, J., Salmi, T. and Murzin, D.Yu. 2003. "Liquid-phase Hydrogenation of Citral for Production of Citronellol: Catalyst Selection", *Applied Catalysis A: General*. Vol. 241, p. 271–288.
- Augustine, R., 1996. *Heterogeneous Catalysis for the Synthetic Chemist*, (Marcel Dekker, Inc.)
- Baeza, B.B., Guerrero-Ruiz, A., Wang, P. and Rodríguez, I. 2001. "Hydrogenation of Citral on Activated Carbon and High-Surface-Area Graphite-Supported Ruthenium Catalysts Modified with Iron", *Journal of Catalysis*. Vol. 204, p. 450–459. (a)
- Baeza, B., Rodríguez-Ramos I. and Guerrero-Ruiz, A. 2001. "Influence of Mg and Ce Addition to Ruthenium Based Catalysts Used in the Selective Hydrogenation of  $\alpha$ - $\beta$  Unsaturated Aldehydes", *Applied Catalysis A: General*. Vol. 205, p. 227-237.(b)
- Bhatia, S., 1990. *Zeolite Catalysis: Principles and Application*, (CRC Press, Inc.)
- Blackmond, G., Oukaci, I.R., Blanc, B. and Gallezot, P. 1991. "Geometric and Electronic Effects in the Selective Hydrogenation of  $\alpha$ - $\beta$  Unsaturated Aldehydes over Zeolite-Supported Metals", *Journal of Catalysis*. Vol. 131, p. 401-411.
- Breck, D.W., 1974 *Zeolite Molecular Sieves*, (Wiley-Interscience Publication)
- Chen, B., Dingerdissen, U., Krauter, J.G.E., Lansink Rotgerink, H.G.J., Möbus, K., Ostgard D.J., Panster, P., Riemeier, T.H. and Seebald, S. 2004. "New Developments in Hydrogenation Catalysis Particularly in Synthesis of Fine and Intermediate Chemicals", *Applied Catalysis A: General*. Vol. 280, p 17-46.
- Ciesla, U. and Schüth, F. 1999. "Ordered Mesoporous Materials" *Microporous and Mesoporous Materials*. Vol. 27, p. 131.
- Coupé, J.N., Jordão, E., Fraga, M.A. and Mendes, M.J. 2000 "A Comparative Study of SiO<sub>2</sub> Supported Rh–Sn Catalysts Prepared by Different Methods in the Hydrogenation of Citral", *Applied Catalysis A: General*. Vol. 199, p. 45–51.
- Eimer, G.A., Pierella, L.B., Monti, G.A. and Anunziata, O.A. 2003. "Preparation and Characterization of Aluminum-Containing MCM-41", *Catalysis Communications*. Vol. 4, p. 118-123.
- Ertl, G., Knözinger, H. and Weitkamp, J. 1999. *Preparation of Solid Catalysts*, (Wiley-VCH, Weinheim)

- Hernandez, M.A. 2000. "Nitrogen-Sorption Characterization of the Microporous Structure of Clinoptilolite-Type Zeolites", *Journal of Porous Materials*. Vol. 7, p. 443-454.
- Lafaye, G., Micheaud-Especel, C., Montassier, C. and Mare, P. 2002. "Characterization of Bimetallic Rhodium-Germanium Catalysts Prepared by Surface Redox Reaction", *Applied Catalysis A: General*. Vol. 230, p. 19–30.
- Lin, H.P., Cheng, S. and Mou, C.Y. 2002. *Microporous Matter*. p. 10-11.
- Malathi, R., Viswanath, R.P. 2001. "Citral Hydrogenation on Supported Platinum Catalysts", *Applied Catalysis A: General*. Vol. 208, p. 323–327.
- Michiels, P. and Herdt, O.C.E., 1987. *Molecular Sieve Catalysts*.
- Moulijn, J.A., van Leeuwen, P.W.N.M. and van Santen, R.A. 1994. "Catalysis-An Integrated Approach to the Homogeneous, Heterogeneous and Industrial Catalysis", *Applied Catalysis A: General*. Vol. 79, p. N14-N18.
- Noller, H. and Lin, W.M. 1984. "Activity and Selectivity of Ni-Cu/Al<sub>2</sub>O<sub>3</sub> Catalysts for Hydrogenation of Crotonaldehyde and Mechanism of Hydrogenation", *Journal of Catalysis*. Vol. 85, p. 25-30.
- Ponec, V. 1997. "On the Role of Promoters in Hydrogenations on Metals;  $\alpha$ ,  $\beta$ -Unsaturated Aldehydes and Ketones", *Applied Catalysis A: General*. Vol. 149, p. 27-48.
- Qye, G., Sjöblom, J. and Stöcker, M. 2001. "Synthesis, Characterization and Potential Applications of New Materials in the Mesoporous Range", *Advances in Colloid and Interface Science*. Vol. 89-90, p. 439-466.
- Reyes, P., Rojas, H., Pecchi, G. and Fierro, J.L.G. 2002. "Liquid-Phase Hydrogenation of Citral over Ir-Supported Catalysts", *Journal of Molecular Catalysis A: Chemical*. Vol. 179, p. 293–299.
- Ribeiro, F. R., et. al., ed. 1984. *Zeolites: Science and Technology*, (Martinus Nijhoff Publishers, The Hague)
- Salmi, T., Mäki-Arvela, P., Toukoniitty, E., Neyestanaki, A.K., Tiainen, L.P., Lindfors, L.E., Sjöholm, R. and Laine, E. 2000. "Liquid-Phase Hydrogenation of Citral Over an Immobile Silica Fibre Catalyst", *Applied Catalysis A: General*. Vol. 196, p. 93–102.
- Santori, G.F., Mónica L.C. and Osmar A.F. 2002. "Hydrogenation of Carbonyl Compounds Using Tin-Modified Platinum-Based Catalysts Prepared via Surface Organometallic Chemistry on Metals (SOMC/M)", *Journal of Molecular Catalysis A: Chemical*. Vol. 186, p. 223–239.

- Silva, A.M., Santos, O.A.A., Mendes, M.J., Jordão, E. and Fraga, M.A. 2003. "Hydrogenation of Citral over Ruthenium-Tin Catalysts", *Applied Catalysis A: General*. Vol. 241, p. 155–165.
- Simoncic, P. and Armbruster, T. 2005. "Cationic Methylene Blue Incorporated into Zeolite Mordenite-Na: A Single Crystal X-Ray Study", *Microporous and Mesoporous Materials*. Vol. 81, p. 87–95.
- Singh U.K. and Vannice, M.A. 2000. "Liquid-Phase Hydrogenation of Citral over Pt/SiO<sub>2</sub> Catalysts I. Temperature Effects on Activity and Selectivity", *Journal of Catalysis*. Vol. 191, p. 165–180.
- Singh, U.K. and Vannice, M.A. 2000. "Influence of Metal–Support Interactions on the Kinetics of Liquid-Phase Citral Hydrogenation", *Journal of Molecular Catalysis A: Chemical*. Vol. 163, p. 233–250.
- Sordelli, L., Psaro, R., Vlais, G., Cepparo, A., Recchia, S., Dossi, C., Achille, F., and Robertino, Z. 1999. "EXAFS Studies of Supported Rh–Sn Catalysts for Citral Hydrogenation", *Journal of Catalysis*. Vol. 182, p. 186–198.
- Tsitsishvili, G.V., Andronikashvili, T.G. and Kirov, G.N. 1992. *Natural Zeolites*, (Ellis Horwood Limited, 1<sup>st</sup> Edition, New York), p. 40.
- Uçar, Ş., Yılmaz, S., Artok, L., Ms. Thesis, "Investigation of Catalytic Activity and Selectivity of Pd and Ni Loaded Clinoptilolite Rich Natural Zeolite for Citral Hydrogenation", 2002.
- Yılmaz, S., Ucar, Ş., Artok, L., Güleç, H., "The Kinetics of Citral Hydrogenation over Pd Supported on Clinoptilolite Rich Natural Zeolite", *Catalysis A: General*, in press, 2005.
- van Druten, G.M.R. and Ponec, V. 2000. "Hydrogenation of Carbonylic Compounds Part I: Competitive Hydrogenation of Propanal and Acetone Over Noble Metal Catalysts", *Applied Catalysis A: General*. Vol. 191, p. 153–162.
- Vilella, I.M.J., de Miguel, S.R., de Lecea, C.S.M., Linares-Solano, Á. and Scelza, O.A. 2004. "Catalytic Performance in Citral Hydrogenation and Characterization of Pt-Sn Catalysts Supported on Activated Carbon Felt and Powder", *Applied Catalysis A: General*. Vol. 281, p. 247-258.

# APPENDIX A

## GC-MS CHROMATOGRAMS OF PRODUCTS

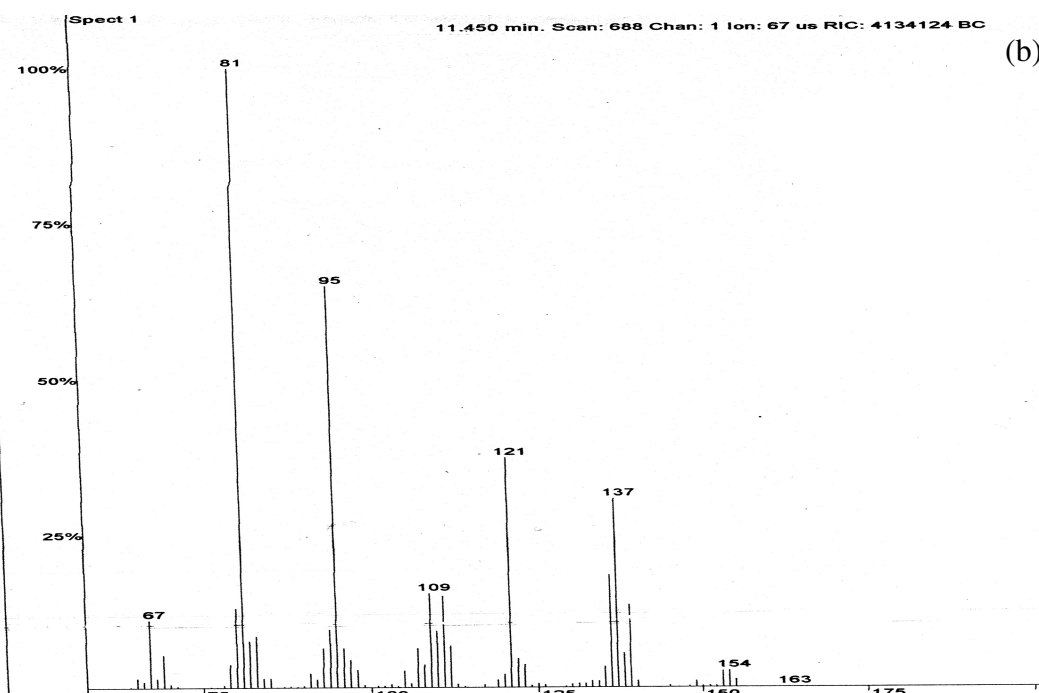
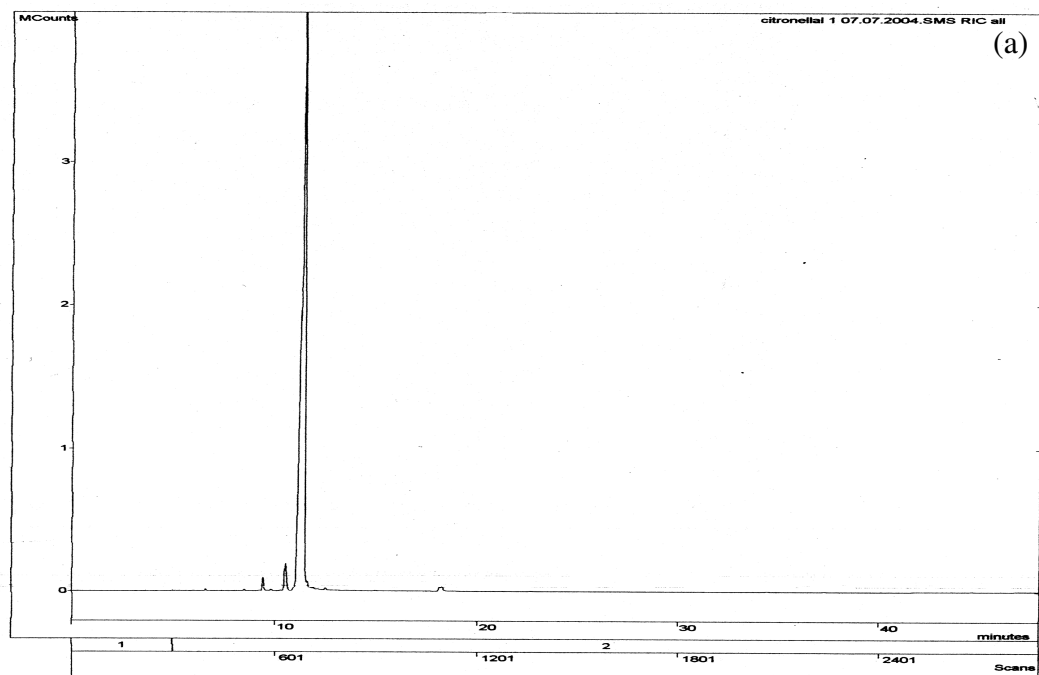


Figure A. 1. GC-MS chromatogram(a) and spectrum(b) of citronellal.

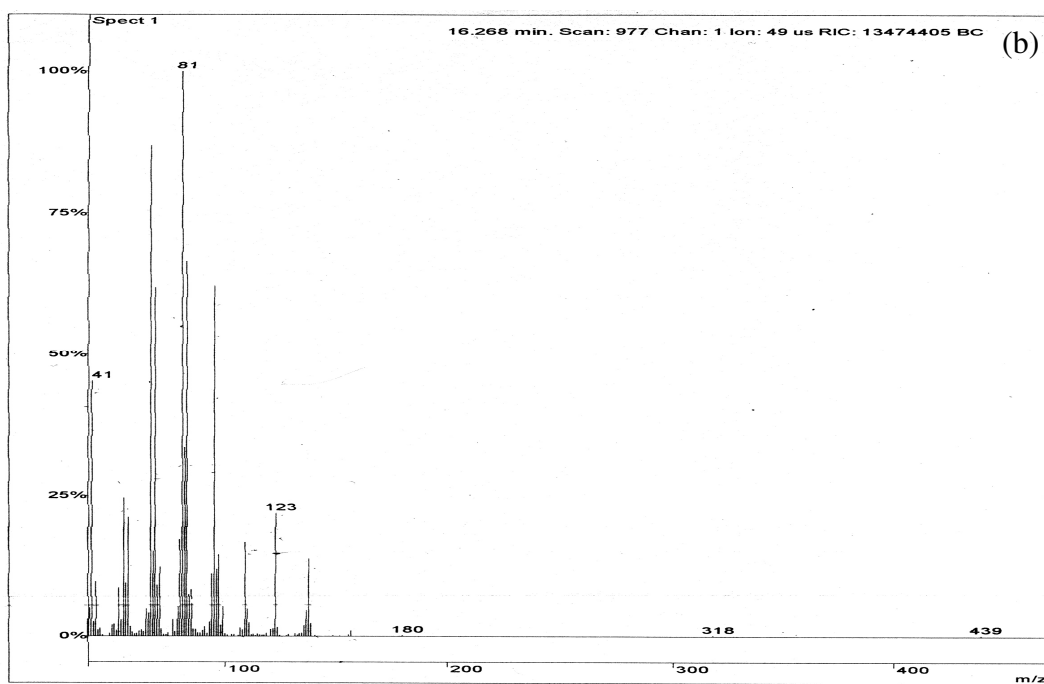
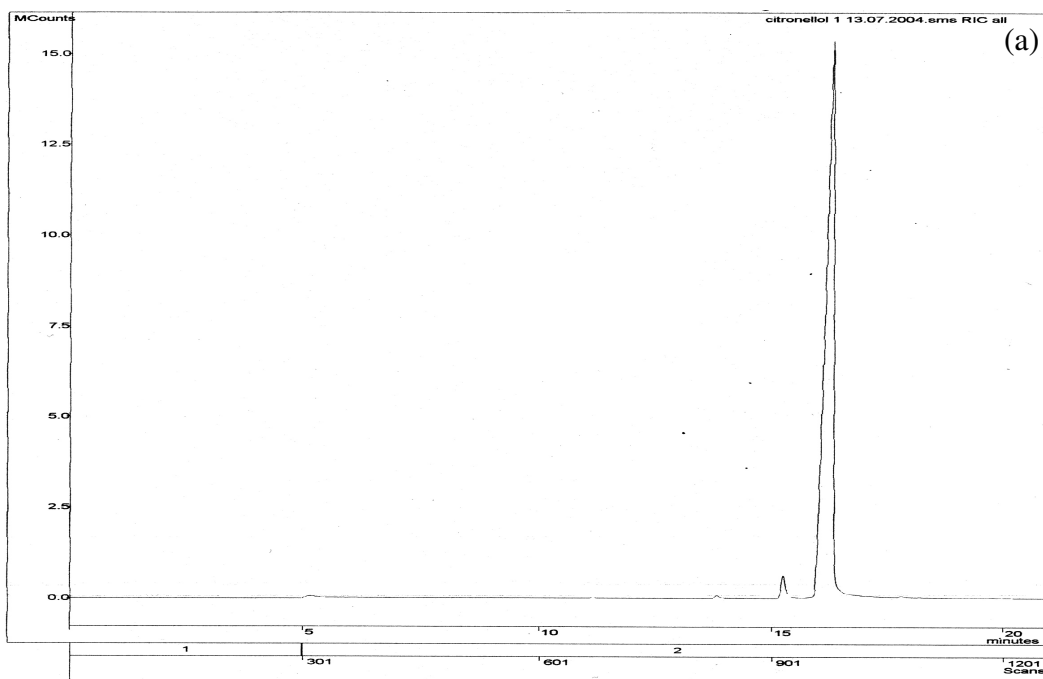


Figure A.2. GC-MS chromatogram(a) and spectrum(b) of citronellol.

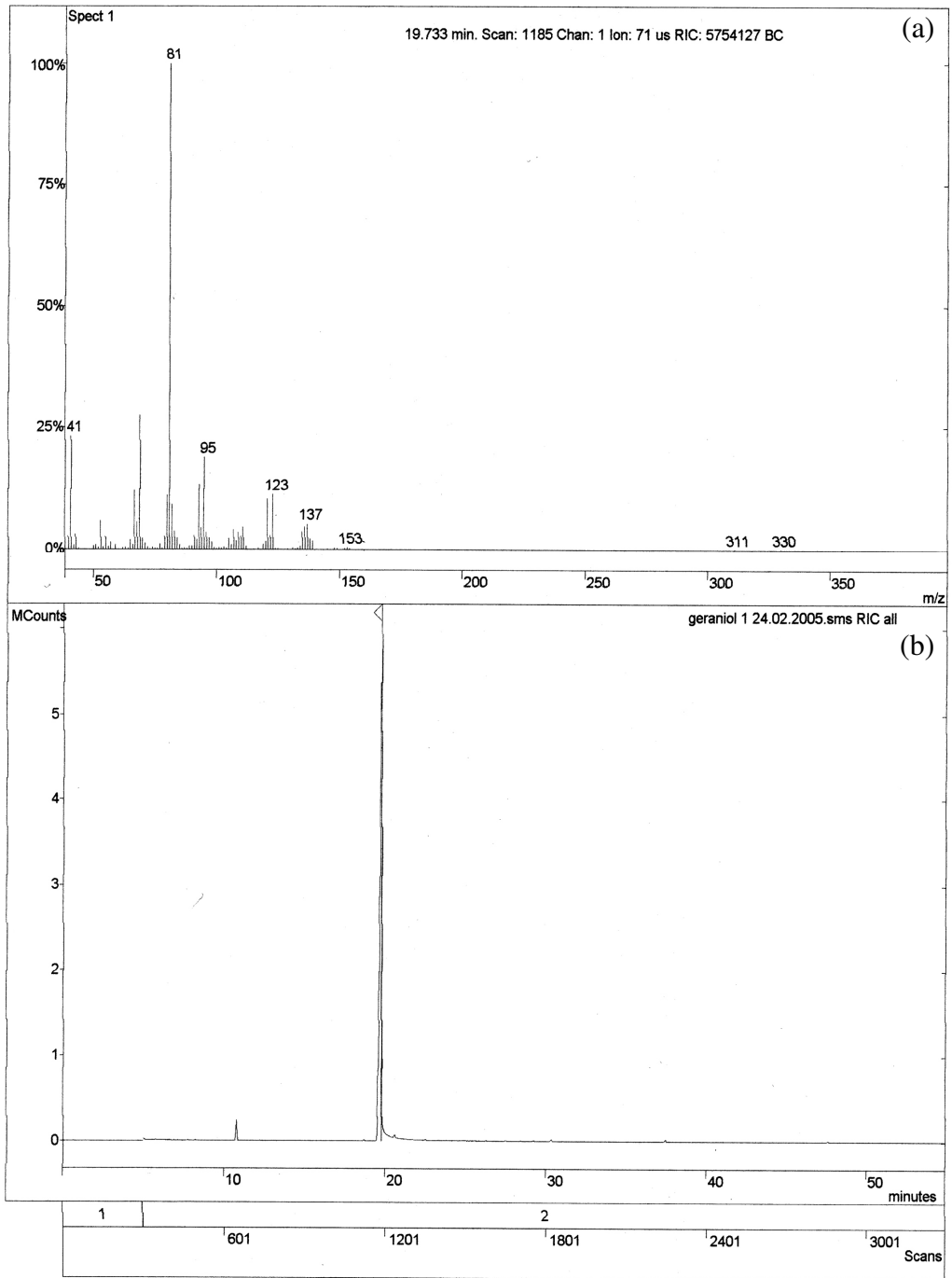


Figure A.3. GC-MS spectrum (a) and chromatogram (b) of geraniol.

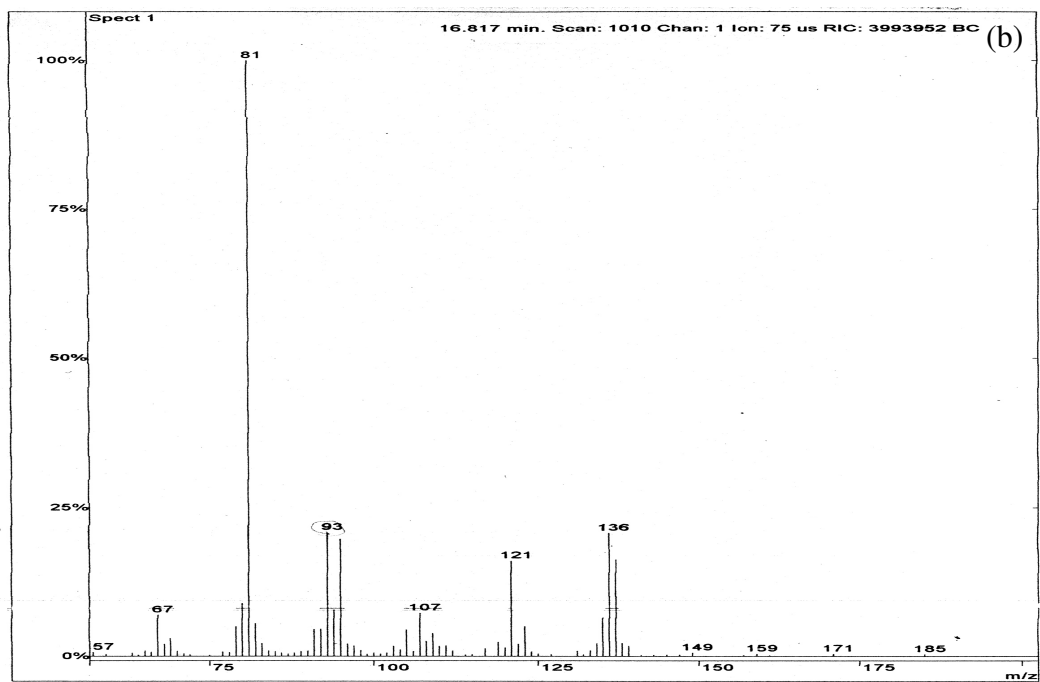
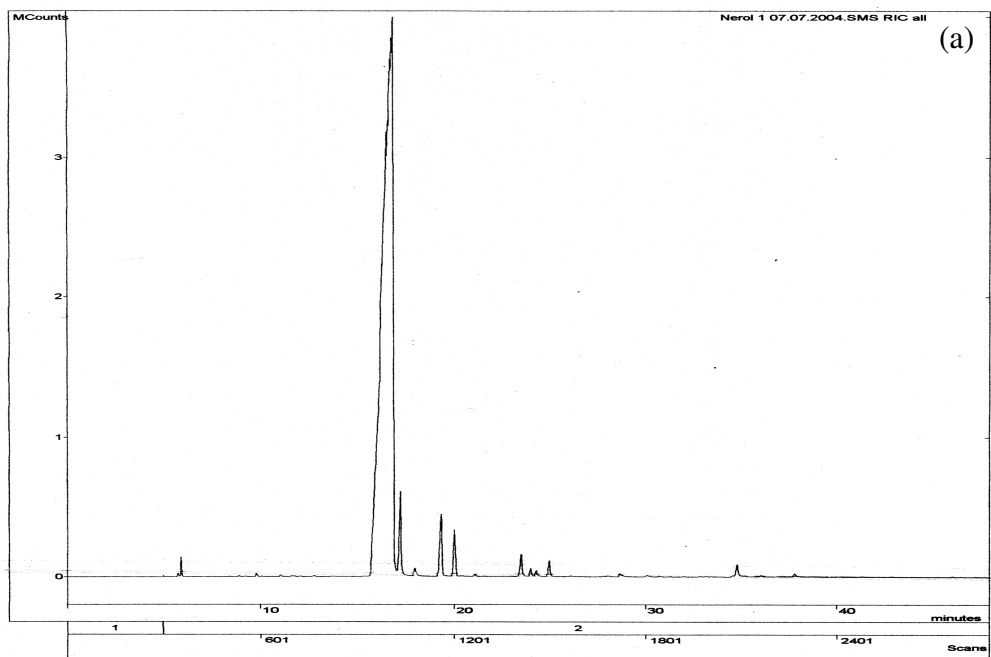


Figure A.4. GC-MS chromatogram (a) and spectrum (b) of nerol.

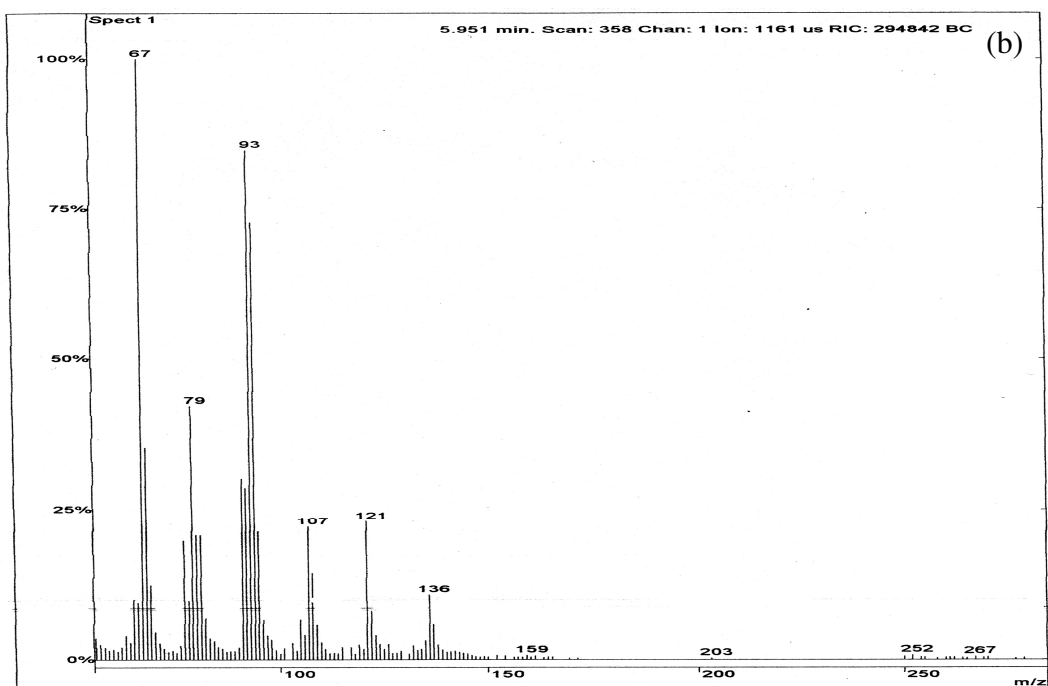
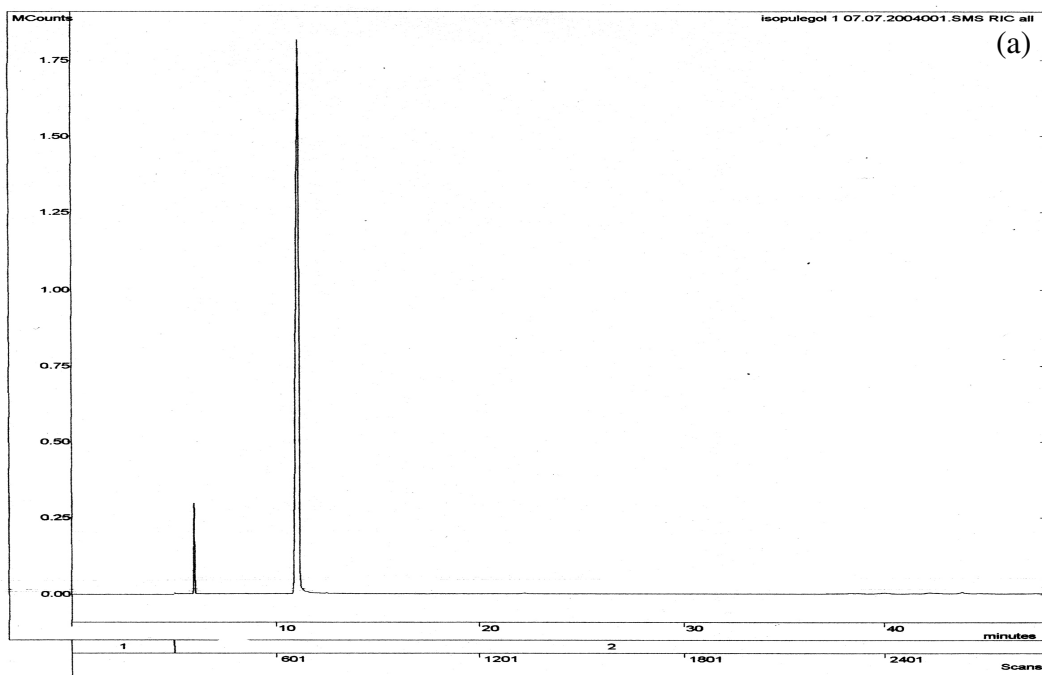


Figure A.5. GC-MS chromatogram (a) and spectrum (b) of isopulegol.

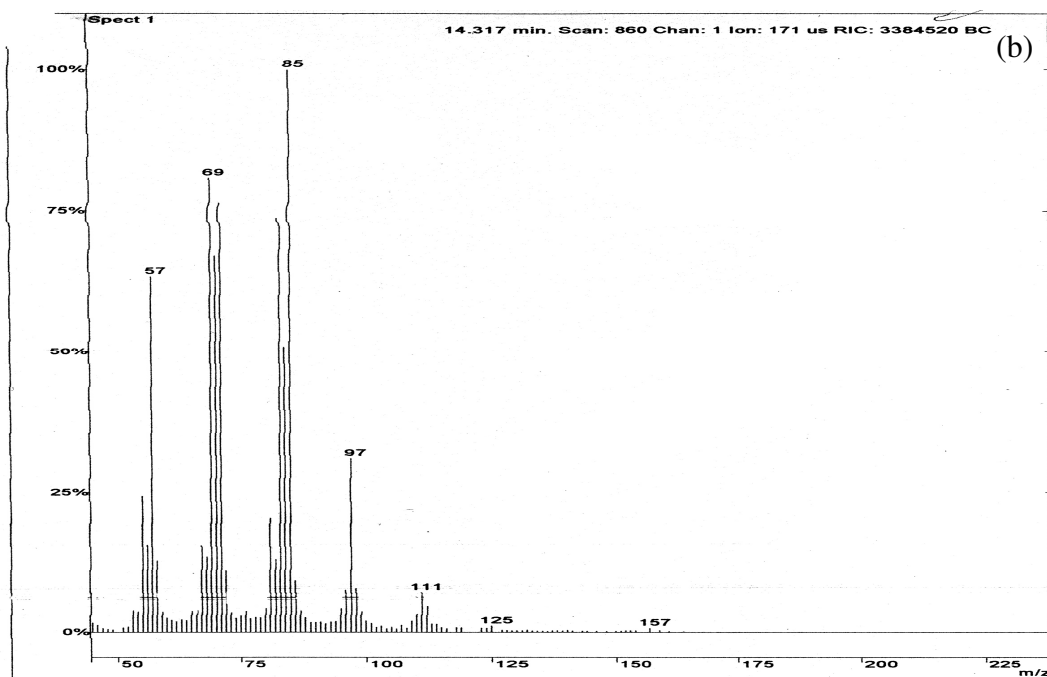
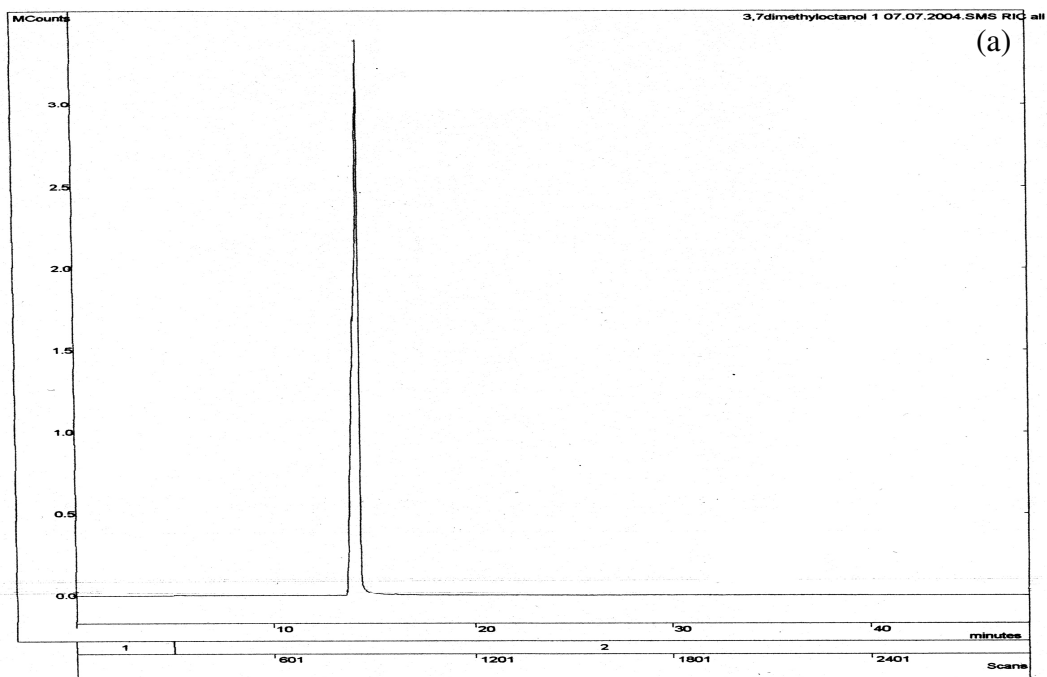


Figure A.6. GC-MS chromatogram (a) and spectrum (b) of 3,7 Dimethyl-1- octanol.

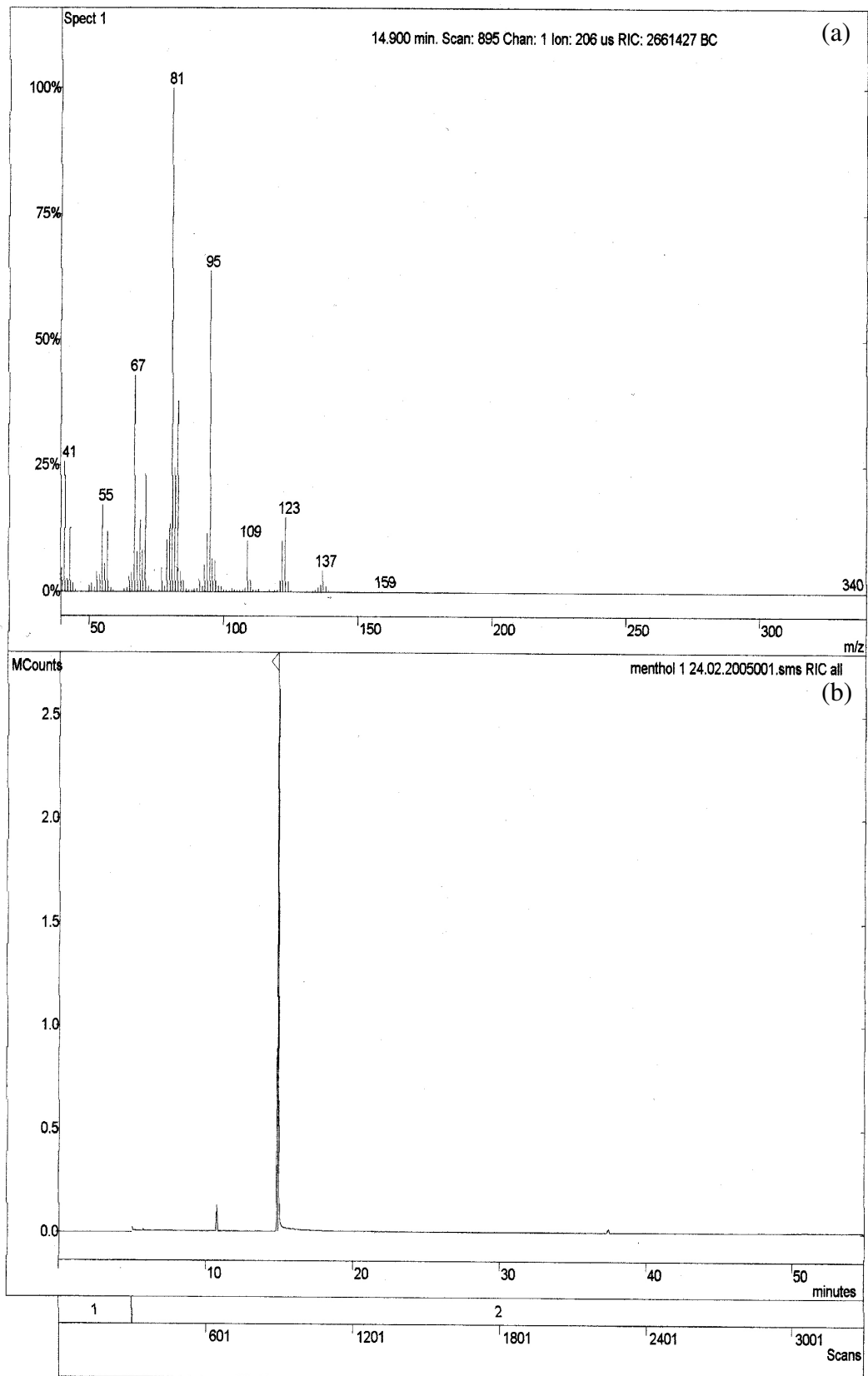
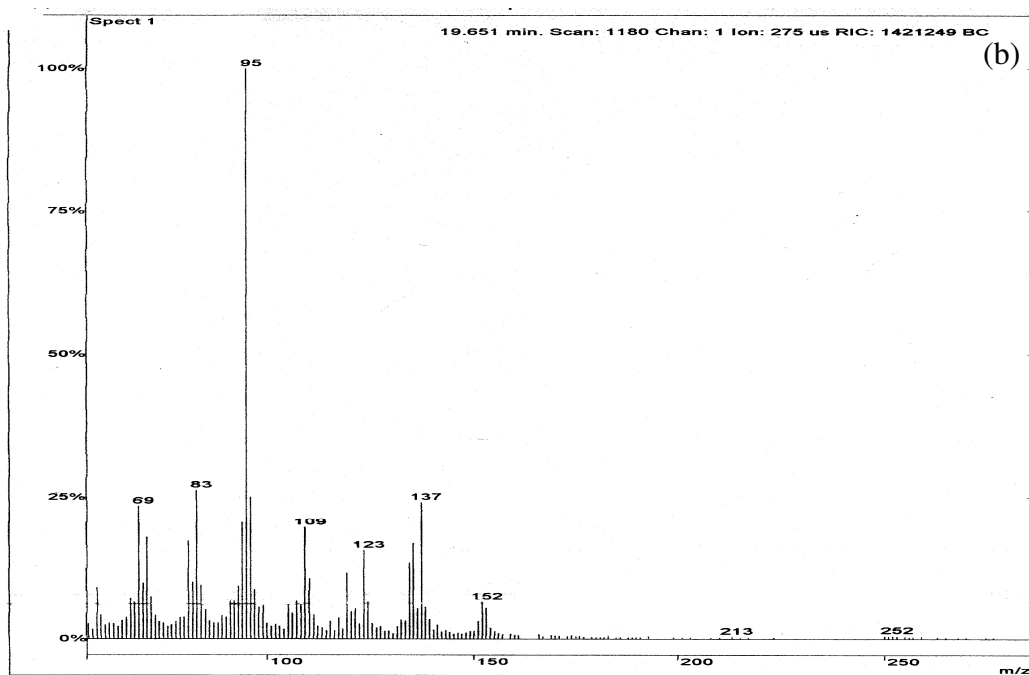
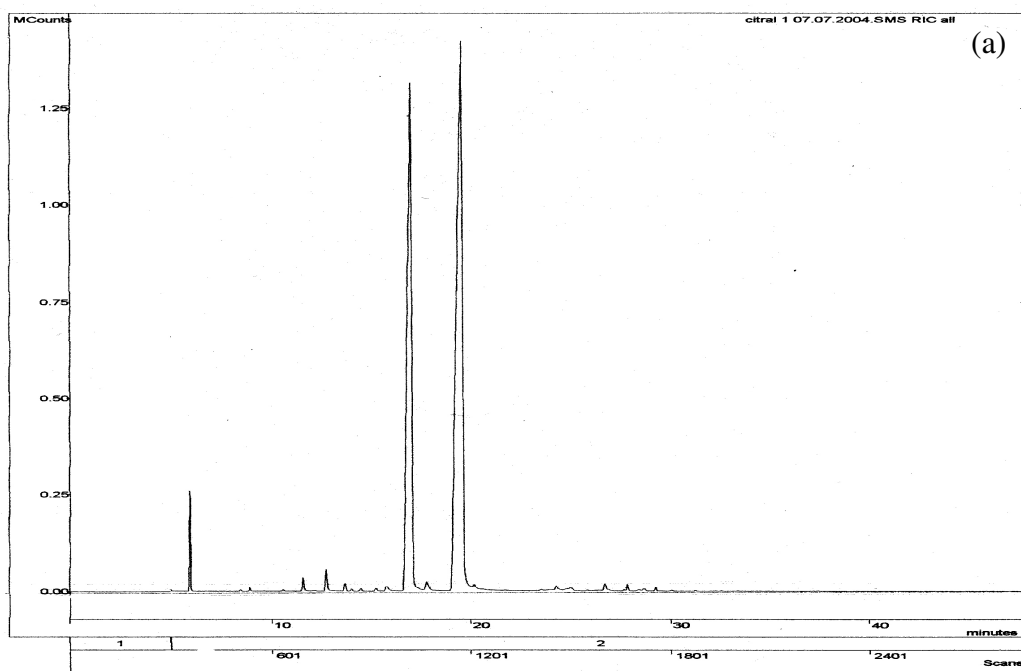


Figure A.7. GC-MS spectrum (a) and chromatogram (b) of menthol.



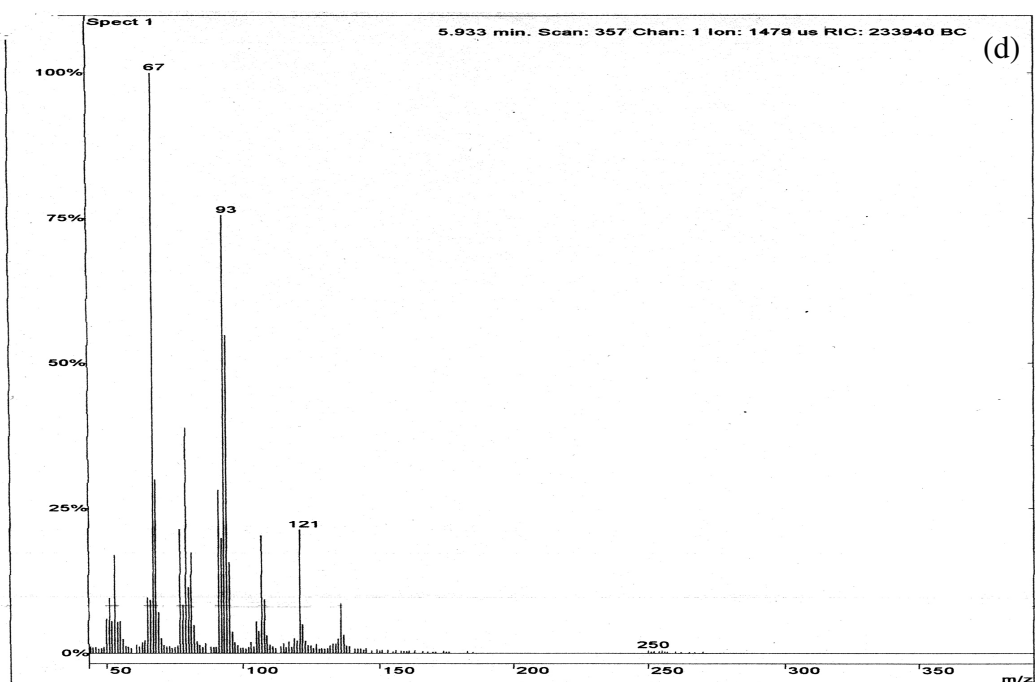
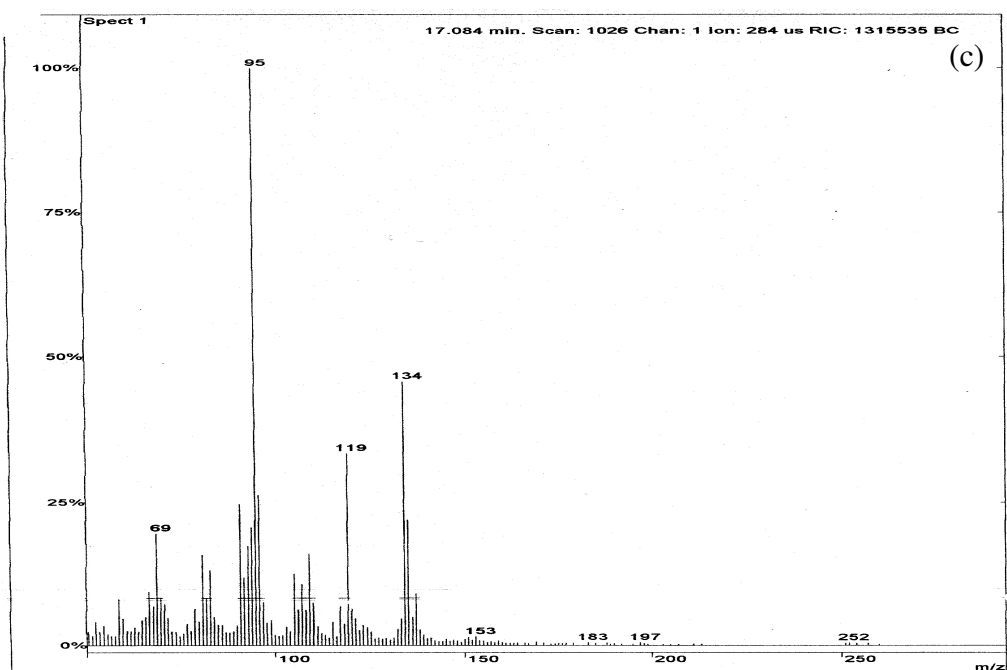


Figure A.8. GC-MS spectrum (a) and chromatograms (b), (c), (d) of citral.